LIFE IN THE RAIN SHADOW: UNDERSTANDING SOURCES OF RECHARGE, GROUNDWATER FLOW, AND THEIR EFFECTS ON GROUNDWATER DEPENDENT ECOSYSTEMS IN THE PANAMINT RANGE, DEATH VALLEY, CALIFORNIA, USA
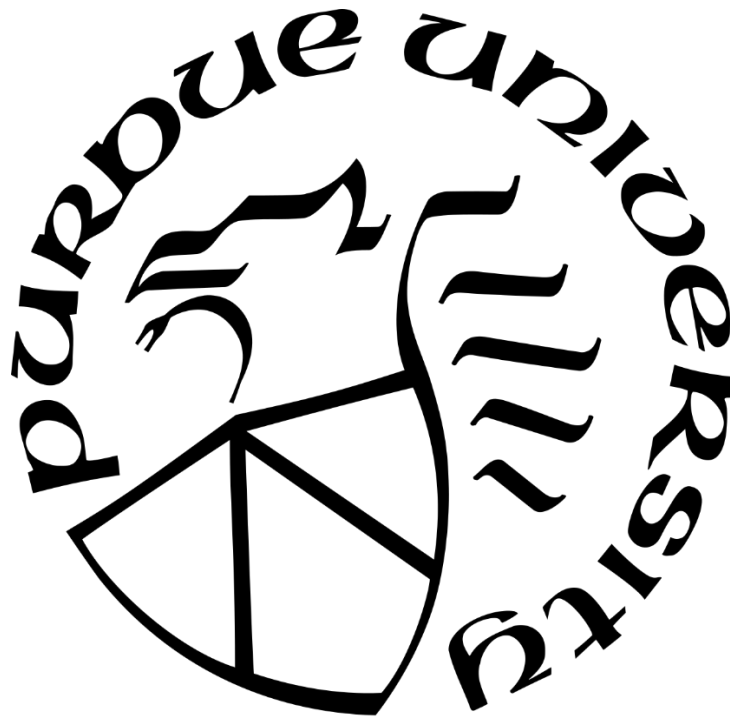
by

Carolyn L. Gleason

A Thesis

Submitted to the Faculty of Purdue University

In Partial Fulfillment of the Requirements for the degree of

Master of Science

Department of Earth, Atmospheric, & Planetary Sciences

West Lafayette, Indiana

December 2018

THE PURDUE UNIVERSITY GRADUATE SCHOOL
STATEMENT OF COMMITTEE APPROVAL

Dr. Nathaniel A. Lifton, Chair

      Department of Earth, Atmospheric, & Planetary Sciences, Purdue University

Dr. Marty Frisbee

      Department of Earth, Atmospheric, & Planetary Sciences, Purdue University

Dr. Laura Rademacher

      Geological and Environmental Sciences, University of the Pacific

Dr. Don W. Sada

      Division of Hydrologic Sciences, Desert Research Institute Reno

Dr. Kenneth Ridgway

      Department of Earth, Atmospheric, & Planetary Sciences, Purdue University

Approved by:

      Dr. Darryl Granger

         Head of the Graduate Program

For my loving husband, Christopher.

I never knew all that I could accomplish until I knew you.

"It's strange how deserts turn us into believers. I believe in walking in a landscape of mirages, because you learn humility. I believe in living in a land of little water because life is drawn together. And I believe in the gathering of bones as a testament to spirits that have moved on. If the desert is holy, it is because it is a forgotten place that allows us to remember the sacred. Perhaps that is why every pilgrimage to the desert is a pilgrimage to the self."

-Terry Tempest Williams

ACKNOWLEDGMENTS

TABLE OF CONTENTS

LIST OF TABLES

LIST OF FIGURES

ABSTRACT

Author: Gleason, Carolyn L. MS
Institution: Purdue University
Degree Received: December 2018
Title: Life in The Rain Shadow: Understanding Sources of Recharge, Groundwater Flow, and
   Their Effects on Groundwater Dependent Ecosystems in the Panamint Range, Death
   Valley, California, USA
Major Professor: Dr. Marty D. Frisbee

Despite its location in the rain shadow of the southern Sierra Nevada, the Panamint Range within

Death Valley National Park, CA hosts a complex aquifer system that supports numerous springs.

These springs, in turn, support unique groundwater-dependent ecological communities. Spring

emergences range in elevation from 2434 m above sea level (within the mountain block) to 77 m

below sea level (in the adjacent basins). Waters were collected from representative Panamint

Range springs and analyzed for environmental isotopes and geochemical tracers to address the

following questions: 1) What is the primary source of recharge for the springs? How much

recharge occurs on the Panamint Range? 2) What groundwater flowpaths and geologic units

support springflow generation? and 3) What are the residence times of the springs? The stable

isotopic composition (δ^{18}O and δ^2H) of spring water and precipitation indicate that localized high-

elevation snowmelt is the dominant source of recharge to these perennial springs, though recharge

from rainfall is not wholly insignificant. Geochemical evolution was evaluated using principle

component analysis to compare the concentrations of all major spring cations and anions in a

multidimensional space and group them according to dominant geochemical signatures. These

resulting geochemical groups are controlled primarily by topography. The Noonday Dolomite and

other carbonate units in the range are identified as the water-bearing units in the mountain block

based on the ^{87}Sr/^{86}Sr of spring waters and rock samples. These units also offer higher hydraulic

conductivities than other formations and are chemically similar. Radiocarbon- and ^{3}H derived

residence times of these spring waters range from modern to approximately 1840 years, with the shortest residence times at higher altitudes and Hanaupah Canyon and increasing residence times with decreasing altitude. This residence time-altitude relationship is likewise likely topography-driven though there are significant disparities in mountain block storage between the various canyons of the range resulting in variable residence times between drainages. Lower Warm Springs A and B, however, are the exceptions to this trend as they emerge at lower altitudes (750m above sea level) and are likely driven by the transport of groundwater to the surface along faults which increases both the temperature and groundwater residence times of waters from these springs. Benthic macroinvertebrates and benthic and planktonic microbes were also sampled for each spring studied. BMI and microbial community structure in the Panamint Range is likewise topography-controlled with more tolerant communities at lower elevations (within more chemically evolved waters) and less tolerant species in the unevolved waters at higher elevations.

INTRODUCTION

Motivation

Sustainable freshwater resources are necessary for the continued human habitation and ecosystem integrity of arid and semi-arid landscapes around the globe, yet significant knowledge gaps still exist in understanding the complex groundwater flow processes that provide water to these regions (Anderson and Woolsey, 2005). The recent and prolonged California drought (2011 – 2017) has added a sense of urgency to these concerns in the United States, especially in the Central Valley and inland deserts of southern California (Borsa, 2014). Hydrogeological information is especially sparse within the rain shadow of the southern Sierra Mountains of California including the mountain block of the Panamint Range and the surrounding basins of the southern Great Basin (Figure 1). Located within Death Valley National Park, CA between two of the largest cities in the southwestern United States (Los Angeles, CA and Las Vegas, NV), the Panamint Range hosts a geologically complex and poorly quantified groundwater flow system that delivers critical groundwater discharge to springs emerging in the mountain block and surrounding basins (Badwater Basin to the east and Panamint Valley to the west). However, the hydrogeologic processes and groundwater flowpaths that support springflow generation in the mountain block of the Panamint Range and their role in the generation of basin springs beyond the mountain front have not been quantified.

Despite being located in the rain shadow of the southern Sierra Nevada, the Panamint Range contains numerous springs ranging from high elevation (over 2433m above sea level) to basin springs (77m below sea level). Compared to the southern Sierra Nevada, the Panamint Range receives less snowfall and exhibits a less persistent snowpack and likely much higher evaporation/sublimation rates. This presents a challenging question; where does the recharge

come from that supports these springs? Unfortunately recharge sources and amounts of recharge have not been quantified in the Panamint Range to date.

Groundwater processes are often difficult to study because they are hidden from direct observation, but the presence of springs in this region provides a window through which these processes are observable. In this case, the geochemical and isotopic data of the spring waters can be used to indirectly quantify groundwater processes. By virtue of its isolated location, the spring emergences in the Panamint Range are unique compared to the springs of the Sierra Nevada to the west and Spring Mountains to the east because they are relatively unaltered by human development, non-native ungulates and diversion. Pristine springs, such as those found in the Panamint Range, are preferable for geochemical analyses because they are less likely to be impacted by anthropogenic contamination (Bullen and Kendall, 1998). An analysis of these springs therefore informs our understanding of groundwater flow in the mountain block and hydrogeological connections between the mountain block and the surrounding basins to the east and west of the mountain block: Panamint Valley and Badwater Basin (respectively).
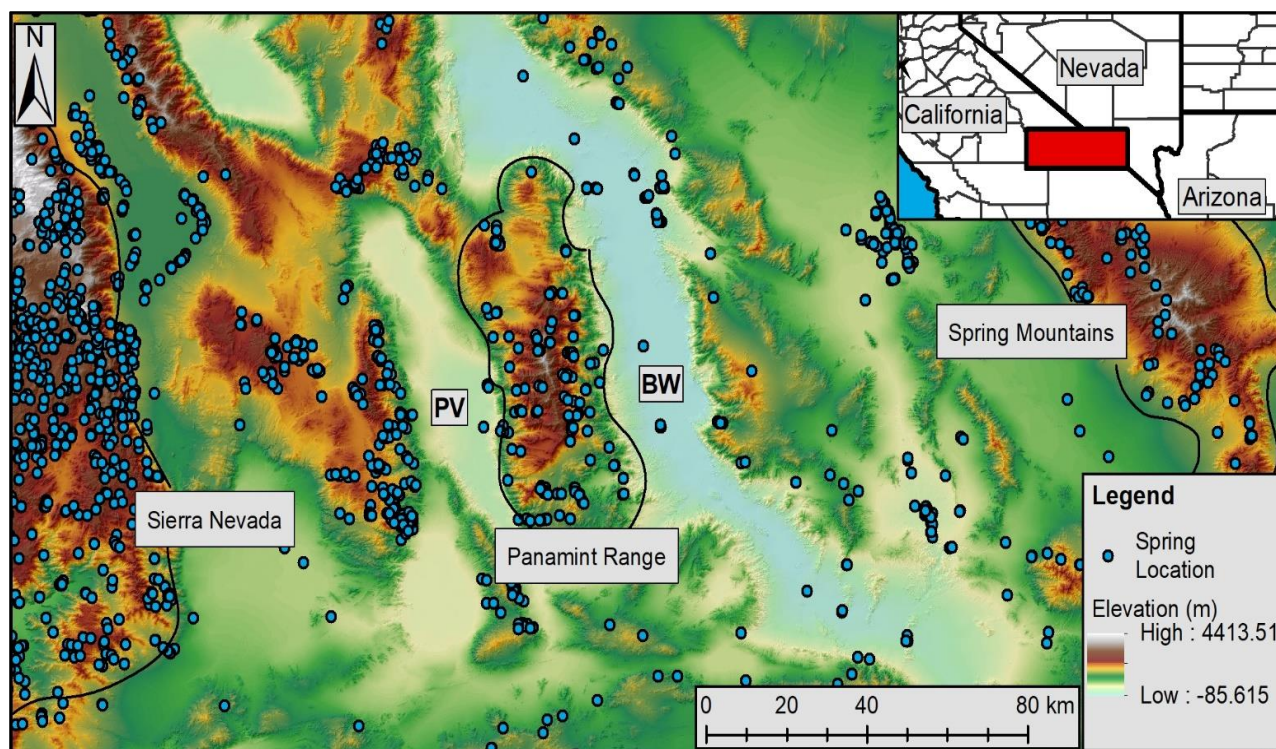
Figure 1. Elevation map of the Panamint Range and surrounding mountain ranges and their spring locations in the area depicted by the red box in the upper right-hand corner. Basins labeled using abbreviations such that BW= Badwater Basin and PV= Panamint Valley. Spring location information taken from the USGS National Hydrography Database (*https://nhd.usgs.gov*).

The following research was funded by the National Science Foundation, Integrated Earth Systems program and conducted in collaboration with universities across the country on an interdisciplinary project entitled: "Collaborative Research: Tectonic and climatic forcing of hydrological systems in the southern Great Basin: Implications for ancient and future aquatic system resilience" EAR 1516127 and EAR 1516698. The goals of this project are to quantify the processes responsible for spring generation across the southern Great Basin, and to build a model combining tectonic, climatic and paleohydrological data to track changes in this hydrological system over the last 14 million years. The ultimate goal is to better understand the principles governing spring resilience and vulnerability over geologic and climate change timescales. The hydrologic model will be calibrated to the investigation of the geochemical, microbial, and ecological processes of the modern springs present throughout the study area. The Panamint Range

springs fill a spatial gap and knowledge gap within the project study are in the larger southern Great Basin.

Since very little data has been collected in the Panamint Range, many first-order questions remain unanswered about the hydrogeological functioning of the mountains. For example, the presence of numerous perennial springs in the Panamint Range (Figure 1) seem to suggest that the mountains receive plentiful recharge. However, the extreme aridity of Death Valley and paucity of precipitation within the rain shadow of the Sierra Nevada argue against this inference. Therefore, there must be sufficient mountain block storage to maintain flow throughout the year at these springs despite low amounts of recharge inferred from its location (Ajami et al., 2011). In this thesis, I address the following questions:

1) What is the source of mountain block recharge in the Panamint Mountains? More specifically, is mountain block recharge sourced primarily from snowmelt, rainfall, or a combination of both? How much recharge occurs in the Panamint Range?

2) How and over what time scale is the water held in storage and subsequently circulated through the mountain block (i.e. what are the groundwater residence times of springs)?

3) What flowpaths and/or geologic units support flow to local- and regional-scale springs? How do these flowpaths and geologic units impact the geochemistry and residence times of these springs?

These hydrogeological questions have exciting implications for the Panamint Range and surrounding basins as they relate to the paleohydrologic story of the southern Great Basin.

While understanding the hydrologic functioning of these springs is fundamental to this study, it is also critical to address higher-order questions regarding the impact of hydrogeology on ecological processes. Desert springs often support diverse ecosystems. In fact, multiple studies

have shown that the springs in this region are critical to the aquatic ecosystems since they provide the only surface water resources to many bird, mammal, and insect species, both migratory and resident (Chambers et al., 2004; Sada et al., 2005; Hannah et al., 2007). They even host springsnails and pupfish: key endangered species of aquatic biota in the western United States (Hershler et al., 2014). But how does the hydrogeologic framework of these springs affect ecological diversity? What factors control resistance and vulnerability in spring ecosystems within this mountain system? How does benthic macroinvertebrate (BMI) abundance and diversity and microbiome abundance and diversity change as a function of the geochemistry and residence time of springs? This question will be addressed in the final chapter of this thesis.

The broader human implications of this research are also relevant to the past and continued habitation of the southern Great Basin. This study will provide new opportunities for groundwater resource conservation in the under-served rural desert communities surrounding this range. These communities include the ancestral homelands of the Timbisha-Shoshone Native American Tribe, their 313 acres of reservation lands within Death Valley National Park, and an even larger demographic of disadvantaged peoples in the Furnace Creek and Homewood Canyon-Valley Wells regions where mean annual incomes only fall within 23 and 42 percent of the mean annual income for the rest state of California (Alpert et al., 2014). By providing these communities with information on the groundwater flow processes that supply the limited freshwater resources around the Panamint Range, the sustainability of these resources becomes more feasible through cooperation with local water managers, regardless of any financial barriers within these communities that may have inhibited this kind of study in the past.

Site Description

The Panamint Range is a north/south trending mountain range located on the western side

of Death Valley National Park between two basins: Panamint Valley to the west and Death Valley to the east. These public lands are administered by the U.S. Bureau of Land Management (Ridgecrest office) and the U.S. National Parks Service (Death Valley National Park). The Panamint Range is a terrain of extremes in both elevation and climate, with spring emergences occurring at a variety of locations along its length (Figure 2). Its highest point (Telescope Peak) reaches an elevation of 3366 m (11,043 ft) while the lowest point in the region is Badwater Basin (on the eastern flank of the range) at an elevation of -77 m (-252 ft) – pronounced relief with extremes separated by only 17 km (Figure 2).
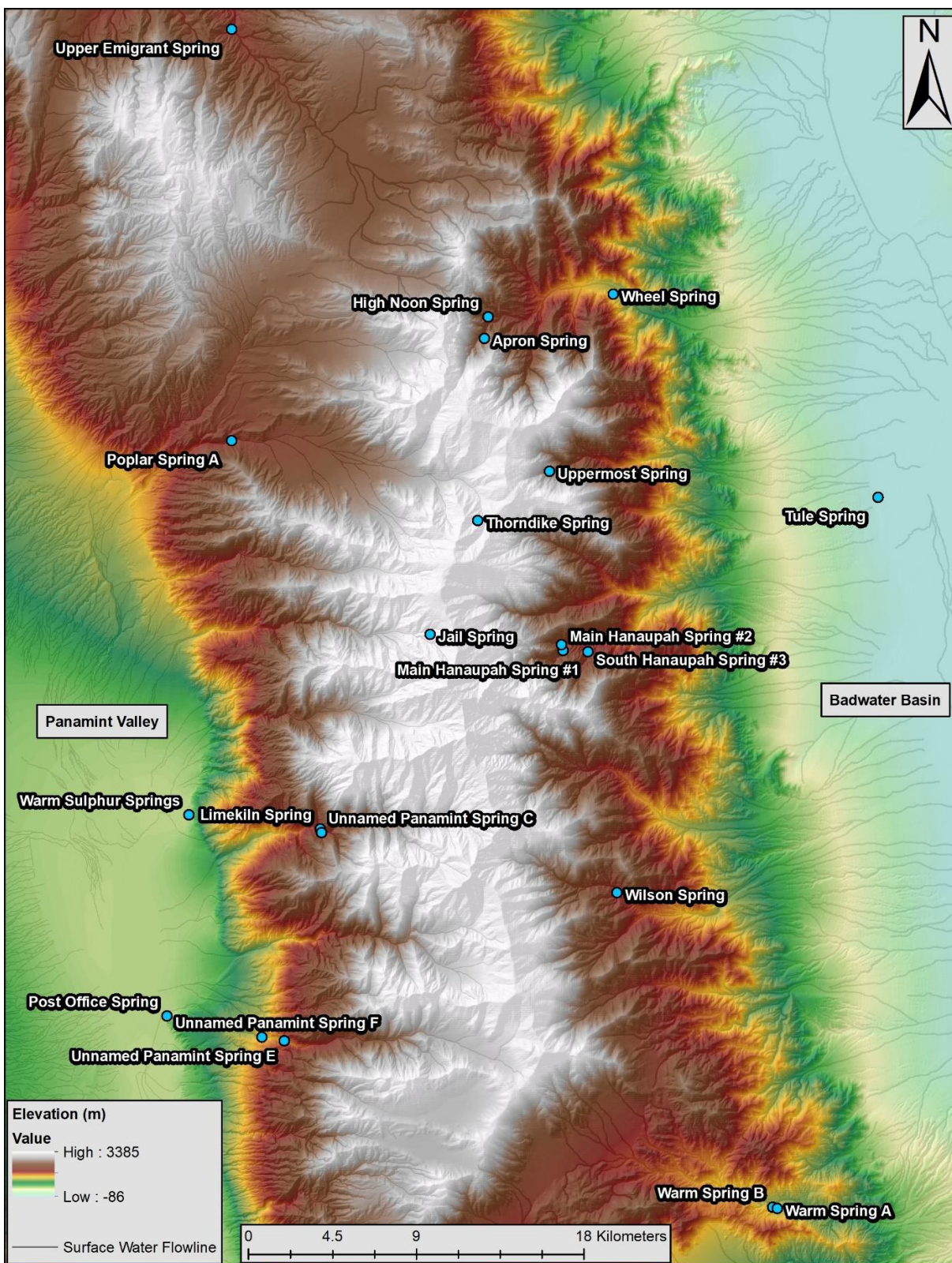
Figure 2. Elevation map of study area with relevant spring locations. Credit: USGS NED (https://lta.cr.usgs.gov/NED).

Geologic Setting

The Panamint Range represents a unique tectonic history in North America because of its location within a zone of extreme Cenozoic extension of heavily metamorphosed strata that were transported by Mesozoic folding and thrusting within a belt of Cordilleran metamorphic core complexes (Miller, 1987). The mountain block is composed primarily of Proterozoic sedimentary rock with several phases of granitic intrusive bodies that were emplaced between the Triassic period and Miocene epoch (Workman et al., 2002). Additionally, there are windows into metamorphosed Precambrian crystalline basement rock in the southern end of the range that can also be found in the Black Mountains across Death Valley (Stewart, 1983; Norton, 2011). The range is cut by steep ephemeral channels draining to both Panamint Valley and Badwater Basin, as emphasized by the flowlines in Figure 2. Observed fault planes within the mountain block dip 20-30 degrees eastward toward Death Valley (Maxson, 1950; Miller, 1987).

There are two primary theories on the emplacement of the Panamint Range. The first and most prevalent theory is that the Panamints are the result of the late Cenozoic transportation of the fault block from above or east of, the Black Mountains along a low-angle detachment fault during the formation of the Death Valley pull-apart basin (Stewart, 1983). This motion would have transported the Panamint Range 40 km northwestward from its original position as Basin and Range extension was occurring throughout the region (Stewart, 1983). The second and less broadly accepted theory suggests that the Panamint Range could instead be a large metamorphic core complex formed by a combination of Miocene Basin and Range extension and Pliocene strike-slip deformation (Armstrong, 1982; Norton, 2011).

These competing models offer different limitations to the maximum circulation depth for waters moving through the mountain block. If the mountain block is in fact a large metamorphic core complex, as the second theory would suggest, then the theoretical maximum circulation depth

for waters moving through that system would be shallower than that of the first theory. This difference is a direct result of the absence of deep set faulting seen in allochthonous slabs of sedimentary rock that would increase the secondary porosity of the mountain block (Schwartz and Zhang, 2003; Price et al., 2007). The metamorphic core complex would also theoretically have a lower primary porosity when compared to the sedimentary rocks that compose the allochthons of the region however, due to the high grade of metamorphism of the mountain block as a whole, it is difficult to quantify and defend these differences. Further study into the hydraulic conductivity of the Proterozoic basement rock versus the Paleozoic extensional allochthons and the hydraulic conductivity of the transitional zone between these units in both models is necessary in order to make such estimates and evaluate these interpretations (Norton, 2011).

Figure 3 displays the dominant surficial geologic facies present across the Panamint Range. While commonly mapped as singular sedimentary units based on age, the Workman et al. (2018) geologic map in combination with the 2011 study by Petterson et al. provide new insights into the hydrogeologic impacts of changes in formation within the Precambrian strata of the Panamint Range. The key Precambrian formations surrounding spring emergences within the range are (in order of increasing age): the Stirling Quartzite (Stirling Formation), the Johnnie Formation, the Noonday Dolomite (Noonday Formation), the Kingston Peak Formation, and the Beck Spring Dolomite (Beck Spring Formation). Additional units of hydrogeologic importance include the Cambrian Carrara and Bonanza King Formations and the felsic intrusive bodies located throughout the mountain block that range from Triassic to Miocene in age. Both the igneous activity that formed these bodies and the multiple faults of variable depth and orientation located throughout the Panamint Range result from the incipient rifting of western North America during the Cenozoic and can act either as barriers or conduits to groundwater flow within the mountain block (Miller,

1987; Bense et al., 2013).

Primary aquifers within the range are likely constrained to the Precambrian sedimentary strata because of the prevalence of more conductive carbonate rocks throughout these units. This inference is supported by field observations noting the proximity of the spring emergences to contacts between dolomitic units, such as the Noonday or Beck Spring Dolomites, and formations associated with marine regression, such as the Johnnie Formation and the Kingston Peak formation. Chemical weathering in the carbonate units and subunits has potentially enhanced porosity and pathways for groundwater within the mountain block along these relevant contacts. In comparison, the upper greenschist to lower amphibolite-grade metamorphism of the Precambrian rock likely limit hydraulic conductivity and deep circulation in these units (Miller, 1987). Due to the importance of contacts within the Precambrian sedimentary units, the stratigraphic column developed by Petterson et al. (2011) is provided as Figure 4 for easy reference. These formations are described in greater detail in the following section.
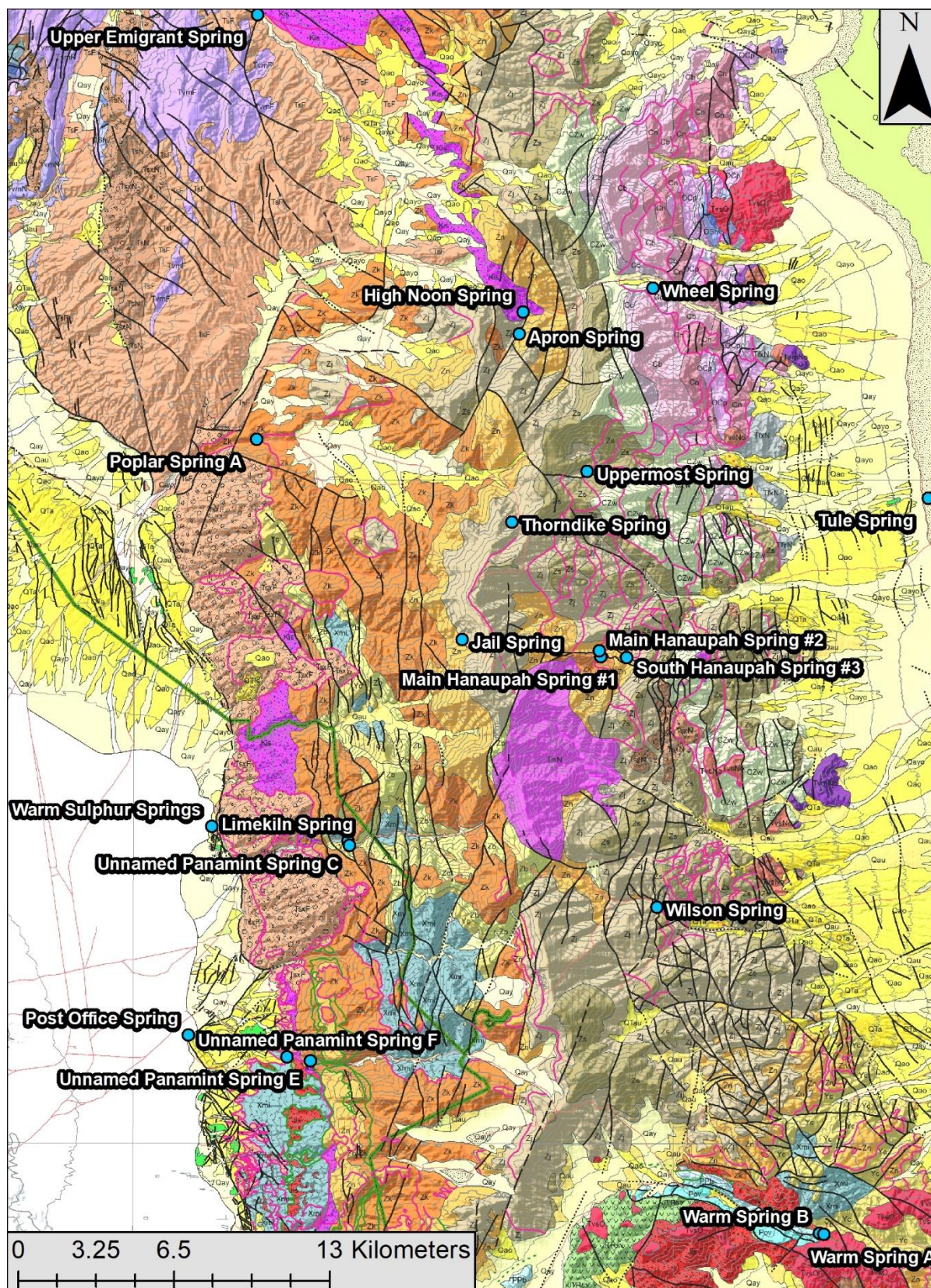
Figure 3. Geologic map of the Panamint Range with faults – map sourced from Workman et al. (2018). Full legend with descriptions of each geologic unit continued on the next page.

QUATERNARY AND TERTIARY SURFICIAL DEPOSITS (implied — left column)

Qayy	Youngest alluvium along active channels (Holocene)
Qay	Young alluvium (Holocene to latest Pleistocene?)
QTau	Undifferentiated alluvium (Holocene to latest Tertiary)
Qau	Undifferentiated younger alluvium (Holocene to middle Pleistocene)
Qayf	Young fine-grained alluvium (Holocene to latest Pleistocene?)
Qayo	Intermediate-age alluvium (middle Holocene to latest Pleistocene?)
Qao	Old alluvium (late to middle Pleistocene)
QTa	Oldest alluvium (middle Pleistocene to late Tertiary)

MASS WASTING DEPOSITS

QTls	Landslide block (Holocene to late Tertiary)

FINE-GRAINED DEPOSITS

Qe	Eolian deposits (Holocene to middle Pleistocene)
Qp	Playa and (or) salt pan deposits (Holocene)
QTd	Deposits associated with modern or past ground-water discharge (Holocene to late Tertiary)
QTp	Old paludal or lacustrine deposits (Pleistocene to late Tertiary)
Ql	Old lacustrine deposits (late to middle Pleistocene)

CENOZOIC IGNEOUS ROCKS

VOLCANIC DEPOSITS

QTvmB	Mafic volcanic deposits of the Badwater assemblage (Holocene to Pliocene)
TvsF	Silicic volcanic deposits of the Furnace Creek assemblage (Pliocene to Miocene)
TvmF	Mafic volcanic deposits of the Furnace Creek assemblage (Pliocene to Miocene)
TvsNy	Younger silicic volcanic deposits of the Navadu assemblage (Miocene)
TvsN	Silicic volcanic deposits of the Navadu assemblage (Miocene)
TvmNy	Younger mafic volcanic deposits of the Navadu assemblage (Miocene)
TvmN	Mafic volcanic deposits of the Navadu assemblage (Miocene)
TvsNo	Older silicic volcanic deposits of the Navadu assemblage (Miocene)
TvmNo	Older mafic volcanic deposits of the Navadu assemblage (Miocene)
TvsO	Silicic volcanic deposits of the Owlshead assemblage (Miocene)
TvmO	Mafic volcanic deposits of the Owlshead assemblage (Miocene)
TvsH	Silicic volcanic deposits of the Hells Gate assemblage (Miocene)
TvmH	Mafic volcanic deposits of the Hells Gate assemblage (Miocene)

INTRUSIVE ROCKS

TisF	Silicic intrusive rocks of the Furnace Creek assemblage (Miocene)
TimF	Mafic intrusive rocks of the Furnace Creek assemblage (Pliocene to Miocene)
TisN	Silicic intrusive rocks of the Navadu assemblage (Pliocene to Miocene)
TimN	Mafic intrusive rocks of the Navadu assemblage (Pliocene to Miocene)
TisO	Silicic intrusive rocks of the Owlshead assemblage (Pliocene to Miocene)
TimO	Mafic intrusive rocks of the Owlshead assemblage (Pliocene to Miocene)

CENOZOIC TECTONIC MÉLANGES

TfxF	Tectonic mélange of the Furnace Creek assemblage (Pliocene to Miocene)
TfxN	Tectonic mélange of the Navadu assemblage (Miocene)
TfxT	Tectonic mélange of the Titus Canyon assemblage (Miocene to Eocene)

CENOZOIC BASIN-FILL DEPOSITS

QTs	Post-basin-range sedimentary basin-fill deposits (Pleistocene to Pliocene)
QTsx	Post-basin-range rock-avalanche breccia deposits (Pleistocene to Pliocene)
QTsB	Sedimentary basin-fill deposits of the Badwater assemblage (Holocene to Pliocene)
TsF	Sedimentary basin-fill deposits of the Furnace Creek assemblage (Pliocene to Miocene)
TsvF	Sedimentary and volcanic basin-fill deposits of the Furnace Creek assemblage, undifferentiated (Pliocene to Miocene)
TsxF	Rock-avalanche breccia deposits of the Furnace Creek assemblage (Pliocene to Miocene)
TxF	Rock-avalanche breccia deposits and tectonic mélange of the Furnace Creek assemblage, undifferentiated (Pliocene to Miocene)
TsN	Sedimentary basin-fill deposits of the Navadu assemblage (Miocene)
TsvN	Sedimentary and volcanic basin-fill deposits of the Navadu assemblage, undifferentiated (Miocene)
TsxN	Rock-avalanche breccia deposits of the Navadu assemblage (Miocene)
TsO	Sedimentary basin-fill deposits of the Owlshead assemblage (Miocene)
TsH	Sedimentary basin-fill deposits of the Hells Gate assemblage (Miocene)
TsvH	Sedimentary and volcanic basin-fill deposits of the Hells Gate assemblage, undifferentiated (Miocene)
TsT	Sedimentary basin-fill deposits of the Titus Canyon assemblage (Miocene to Oligocene?)
TsxT	Rock-avalanche breccia deposits of the Titus Canyon assemblage (Miocene to Oligocene?)

MESOZOIC SEDIMENTARY AND VOLCANIC ROCKS

JTRsv	Sedimentary and volcanic rocks, undivided (Jurassic and Triassic)

MESOZOIC INTRUSIVE ROCKS

Kis	Younger Mesozoic silicic intrusive rocks (Cretaceous)
Jis	Older Mesozoic silicic intrusive rocks (Jurassic)
JTRis	Oldest Mesozoic silicic intrusive rocks (Jurassic to Triassic)

PALEOZOIC AND PROTEROZOIC SEDIMENTARY ROCKS

Pzu	Sedimentary rocks, undivided (Paleozoic)
PSu	Sedimentary rocks, undivided (Permian to Silurian)
Pov	Owens Valley Group (Lower Permian)
PIPb	Bird Spring Formation (Lower Permian and Pennsylvanian)
PIPkc	Keeler Canyon Formation (Lower Permian to Middle Pennsylvanian)
IPt	Tihvipah Limestone (Middle to Lower Pennsylvanian)
Mu	Sedimentary rocks, undivided (Upper and Lower Mississippian)
Dlb	Lost Burro Formation (Upper and Middle Devonian)
DShv	Hidden Valley Dolomite (Lower Devonian and Silurian)
OCu	Sedimentary rocks, undivided (Ordovician and Upper Cambrian)
Oes	Ely Springs Dolomite (Upper Ordovician)
Oe	Eureka Quartzite (Upper and Middle Ordovician)
OCp	Pogonip Group (Middle and Lower Ordovician and Upper Cambrian)
Cnbc	Nopah (Upper Cambrian), Bonanza King (Upper and Middle Cambrian), and Carrara Formations (Middle and Lower Cambrian), undivided
Cn	Nopah Formation (Upper Cambrian)
Cb	Bonanza King Formation (Upper and Middle Cambrian)
Cm	Monola Formation (Middle Cambrian)
Cc	Carrara Formation (Middle and Lower Cambrian)
Cms	Mule Spring Limestone (Lower Cambrian)
Csv	Saline Valley Formation (Lower Cambrian)
Cz	Zabriskie Quartzite (Lower Cambrian)
Ch	Harkless Formation (Lower Cambrian)
CZws	Wood Canyon Formation (Lower Cambrian and Neoproterozoic) and Stirling Quartzite (Neoproterozoic), undivided
CZw	Wood Canyon Formation (Lower Cambrian and Neoproterozoic)
Cpo	Poleta Formation (Lower Cambrian)
	Campito Formation (Lower Cambrian and Neoproterozoic)
Ccam	Montenegro Member (Lower Cambrian)
CZcaa	Andrews Mountain Member (Lower Cambrian and Neoproterozoic)
Zd	Deep Spring Formation (Neoproterozoic)
Zs	Stirling Quartzite (Neoproterozoic)
Zr	Reed Dolomite (Neoproterozoic)
Zw	Wyman Formation (Neoproterozoic)
Zj	Johnnie Formation (Neoproterozoic)
ZYp	Noonday Dolomite (Neoproterozoic) and Pahrump Group (Neoproterozoic to Mesoproterozoic), undivided
Zn	Noonday Dolomite (Neoproterozoic)
Zk	Kingston Peak Formation (Neoproterozoic)
Zb	Beck Spring Dolomite (Neoproterozoic)
Zh	Horse Thief Springs Formation (Neoproterozoic)
Yc	Crystal Spring Formation (Mesoproterozoic)

PALEOPROTEROZOIC CRYSTALLINE ROCKS

Xmi	Metamorphic and igneous rocks, undifferentiated (Paleoproterozoic)

———	Contact
———	Fault—Solid where certain; dashed where approximately located or inferred; dotted where concealed
———	Low-angle normal fault—Solid where certain; dashed where approximately located or inferred; dotted where concealed
———	Thrust fault—Solid where certain; dashed where approximately located or inferred; dotted where concealed

Figure 3(continued). Legend of mapped geologic units sourced from Workman et al. (2018).
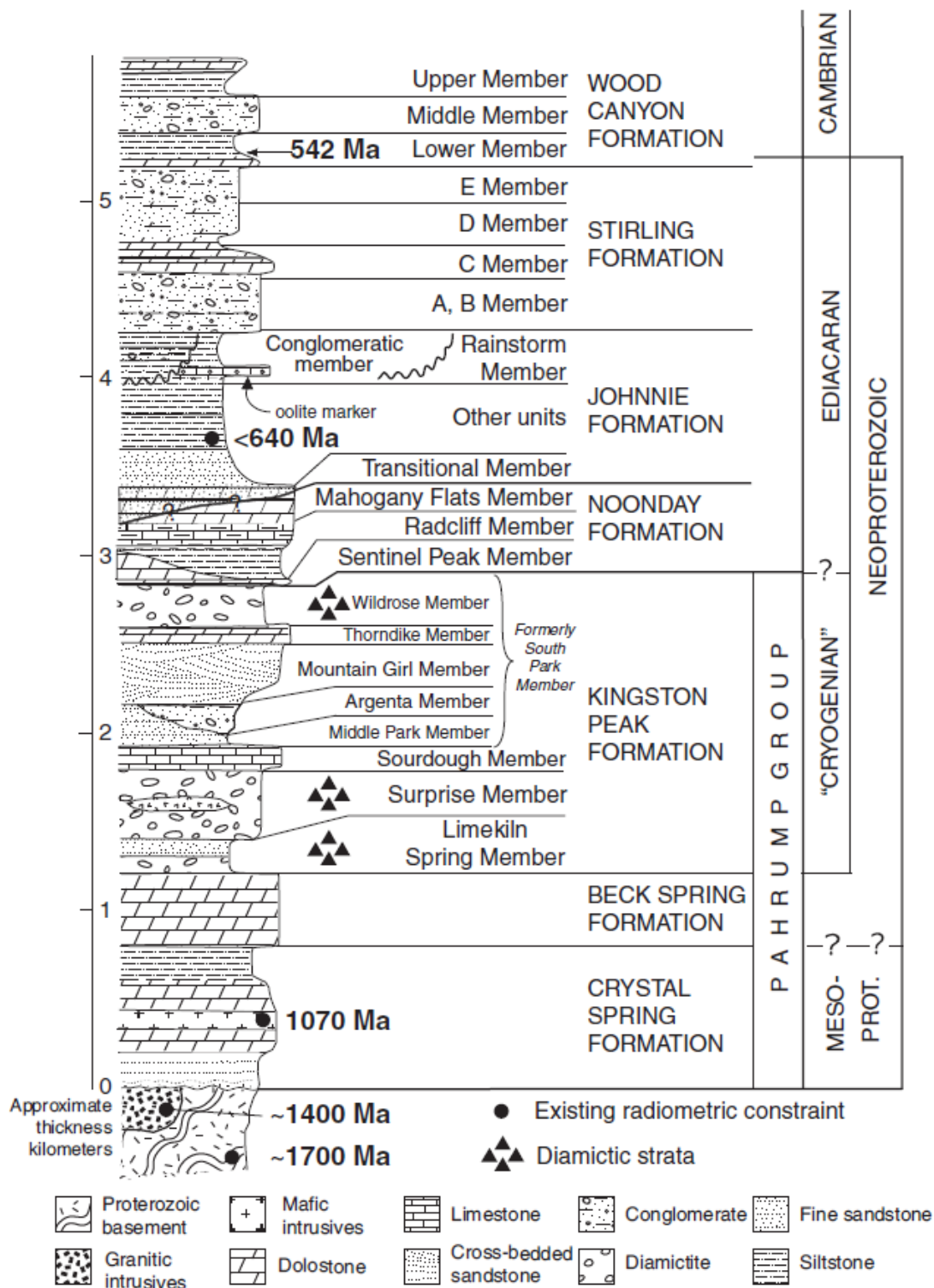
Figure 4. Stratigraphic column of the relevant strata of the Panamint Range (Source: Petterson et al., 2011). Composite age data modified from Stewart (1970), Wright et al. (1974), Labotka et al. (1980), and Heaman and Grotzinger (1992).

Table 1. Representative hydraulic conductivity values for the upper Proterozoic clastic and carbonate rock types of Death Valley National Park. Values were taken from Bedinger and Harrill (2012) and given an index letter for referencing complex formations with multiple rock types.

Rock Type	Conductivity Index Letter	Hydraulic Conductivity (meters/day)
Unfractured Shale	A	1×10^{-8} to 1×10^{-1}
Unfractured Quartzite	B	1×10^{-5} to 1×10^{0}
Unfractured Carbonate	C	1×10^{-4} to 1×10^{0}
Fractured Carbonate	D	1×10^{-2} to 1×10^{3}

<u>Precambrian Sedimentary Formation Descriptions (Oldest to Youngest)</u>

Crystal Spring Formation (Mesoproterozoic): This formation is the oldest of the three formations that comprise the Pahrump Group and can be separated into four sequences within the study area (Roberts, 1974; Miller, 1987). These sequences from bottom to top are 1) a marble with chert nodules, 2) a micaceous quartzite, 3) a garnet, chlorite and biotite-rich schist, and 4) a quartzite conglomerate (Albee et al., 1981). This formation varies in thickness but, with the exception of Tuber Canyon in the west central part of the Panamint Range where the unit is over 1,000 m thick, it is generally 200 – 300 m thick within the study area (Albee et al., 1981). Diabase sills up to 30 m thick are also present in the Manly Peak region of the range overlying the conglomerate (Miller, 1987). This formation contains type A, B, and D rocks (Table 1) which can, in principle, allow groundwater flow, but is not likely a primary aquifer.

Beck Spring Dolomite (Neoproterozoic): This is the middle unit within the Pahrump Group and consists of 200 – 300 m of massive siliceous dolomite that has been metamorphosed into marble in some places (Albee et al., 1981). As an ancient platform carbonate sequence, this unit also contains stromatolites, grainstones, and cryptalgal laminites (Tucker, 1983). This is primarily a

type C unit near spring emergences (Table 1; Figure 3) and is likely a good aquifer within the Panamint Range.

Kingston Peak Formation (Neoproterozoic): This formation is comprised of four members which form the upper section of the Pahrump Group (Miller, 1987). The first member is the Limekiln Spring Member, named for Limekiln Spring in Surprise Canyon (Albee et al., 1981). This member varies in thickness from 50 – 500 m and consists of argillite, schist, metamorphosed conglomerate with basement rock clasts, quartzite, and dolomite (Albee et al., 1987). The next member is the Surprise Member, a 250 – 1000 m diamictite unit with marble and pillowed or amygdaloidal basalts in some places (Miller, 1987). The third member is the Sourdough Limestone Member consisting of 5-30 m of thinly laminated micaceous limestone (Albee et al., 1981). The final member, the South Park Member, consists of 130 m of argillite overlain by 35 m of quartzite conglomerate, 70 m of feldspathic quartzite, and 30 m of pebbled argillite (Albee et al., 1981). This formation primarily contains type B and C sediments (Table 1) and is not likely to be a good aquifer in the Panamint Range.

Noonday Dolomite (Neoproterozoic): This unit consists of three members; The Sentinel Peak Member is the lowest member and consists of 200 m of thinly laminated dolostone with tube structures (Petterson et al., 2011). The next highest member is the 100 – 200 m Radcliff Member which consists of arkosic and feldspatic sandstone, argillite, and limestone (Petterson et al., 2011). The final member is the Mahogany Flats Member which consists of 200 m of fine gray dolostone and contains stromatolites, microbial mound structures, and sandstone fill behind these structures (Petterson et al., 2011). This is a type D unit (Table 1) and is likely a good aquifer in this range.

Johnnie Formation (Neoproterozoic): Consists of two members; the first is a lower 150 – 300 m sandy dolomite layer with interbedded quartzite, marble and andalusite-staurolite-biotite schist

(Albee et al., 1981). The upper member has recently been renamed the Rainstorm Member and consists of 700 m of a distinctive green calcareous argillite that also contains micas and limestone or dolomite layers (Albee et al., 1981; Petterson et al., 2011). This formation contains type A, B, and D rocks (Table 1) and is a possible aquifer for the Panamint Range.

Stirling Formation (Neoproterozoic): This formation is 500 m thick and contains quartzite, siltstone, and silty dolomite (Albee et al., 1981). It also exhibits thin purple argillite layers that contain scattered andalusite porphyroblasts (Albee et al., 1981). This formation contains type A, B, and C rocks (Table 1) which can conduct groundwater flow, but is likely not an important aquifer.

Hydrogeological Setting

It is difficult to provide information on annual rainfall in the Panamint Range due to a lack of continuous precipitation and temperature data, a consequence of the remote and difficult terrain. The orographic effect likely leads to increases in the amount of annual precipitation with increasing elevation, decreases in mean annual temperatures, and more snow than rain at higher elevations (Roe 2005). The exact amount of annual precipitation along the crest of the Panamint Range, however, remains poorly quantified. The California Department of Water Resources (1964) lists rainfall averages between 8 cm and 10 cm per year along the western Panamint Valley floor and an average rainfall of less than 5 cm per year on the eastern Badwater Basin side of the range. Average precipitation on the upper peaks of the Panamint Mountains, however, can only be estimated using modeled estimates. In this case, the PRISM climate dataset can be referenced to estimate precipitation in the high elevations of the Panamint Range and records an average annual precipitation rate of 486 mm per year (PRISM, 2004).

The majority of precipitation in the Panamint Range is likely focused at elevations above

approximately 2000 m above sea level due to increasing temperatures and evaporation rates with decreasing altitudes in the region. The dry adiabatic lapse rate in the Panamint Range is approximately -7.8 ⁰C per 1000 m and the wet adiabatic lapse rate is approximately -12 ⁰C per 1000 m (modified from Walker and Landau, 2018). Though these climatic conditions are similar to those in other ranges the southern Great Basin, it is likely that the evaporation and sublimation losses are higher in the Panamint Range because of its higher mean annual temperatures compared to the Sierra Nevada or Spring Mountains (DWR 1964). Summer temperatures in the greater Death Valley basin range from 30 – 46 ⁰C on average with winters between 4 and 19 ⁰C (Stachelski, 2013). Panamint Valley, however, is at a higher elevation than Death Valley (Figure 2) and exhibits correspondingly somewhat milder temperatures. According to the US National Oceanic and Atmospheric Administration (NOAA) Climate Data Online (2018) estimates of average annual summer temperatures from nearby Trona, CA range from 22 – 40 ⁰C with winter averages between 2 and 16 ⁰C. The only data available within the Panamint Range proper is from a NOAA site in Wildrose Canyon, a mid-elevation (1225 m) canyon that leads up toward the peaks within the mountain block. These data show average annual summer temperatures between 17 and 34 ⁰C and winter temperatures between 0 and 12 ⁰C.

Springs were selected for this study to achieve a broad spatial distribution across the Panamint Range, and in a variety of geologic settings (Figure 3). The springs therefore represent a variety of spring emergences and groundwater flow processes. This approach also captures the variety of climatic conditions that would be present at springs throughout the range and their associated differences in recharge and evaporation rates (Linacre, 1977). Geology, however is highly variable throughout the range and must be considered in the discussion of these springs. Since spring source areas are not known and very difficult to quantify, it is assumed that all

geologic units higher than a spring emergence can host flowpaths to an individual spring unless hydraulic data (

Table 1) suggest otherwise.

Definitions of Terms

Due to the interdisciplinary nature of this project, a few additional definitions are required. A *spring* is classically defined as a point in the landscape where groundwater emerges at the land surface through natural processes and not including artesian wells (Meinzer, 1927; Freeze and Cherry, 1979). Several types of springs are present in the Panamint Range. These types are defined by the proximity of the spring emergence to major geologic features and include contact springs, fault springs, and basin springs (Fetter, 1994; Manga, 2001; Springer and Stevens, 2008). A few of these springs contribute sufficient flow to support streams that flow out of the mountain block and onto the apex of a bajada or alluvial fan. The short reach of sustained flow down-gradient of the spring emergence is called a *spring run*. These features can be very ecologically important and often encapsulate multiple habitats; eucrenal habitats (near the spring emergence) and hypocrenal habitats (within the spring run) that each have their own associated species (Odum, 1953; Hynes, 1970; McCabe, 1998). Across scientific disciplines, spring runs may also be referred to as springbrooks, or *brook runs* (Williams and Hogg, 1988; McCabe, 1998). In this study, however, brook runs will only refer to streams with spring-supported perennial low-order streamflow.

In some cases, spring runs may flow a short distance down-gradient from the emergence only to re-infiltrate and potentially recharge the alluvium. This behavior occurs more commonly in mountainous semiarid watersheds. Earman et al. (2006) called this process *re-recharge* while others may call it groundwater *daylighting*. Based on satellite imagery, several springs located in channels in the Panamint Range appear to daylight multiple times down one drainage after the

point of emergence at the highest elevation. Groundwater daylighting can reset the radioisotopic clock of tracers like radiocarbon.

Groundwater *recharge* has an explicit definition; this is water that has infiltrated the soil, percolated below the rooting depth, and entered the fully saturated porous media below the water table (Freeze and Cherry, 1979). The rate of groundwater turnover from one point to another, most commonly the time it takes water to flow from the point of recharge to the point of discharge in an aquifer flow system is broadly referred to as the groundwater *residence time* (Loaiciga, 2004). Conversely, *age* in terms of groundwater is the average time elapsed since water recharged the subsurface (Bethke and Johnson, 2002). Groundwater samples are commonly comprised of waters of variable ages that can be determined using radiometric dating but it is the integration of these individual ages that accurately describes groundwater residence time (Bethke and Johnson, 2002). Flow characteristics and the landscape placement of springs can be used to broadly characterize recharge processes although they do not provide information on the definitive source of groundwater recharge (*i.e.,* rain versus snowmelt). These large-scale mountain recharge processes include: mountain block recharge (MBR), mountain front recharge (MFR), and mountain system recharge (MSR).

Mountain block recharge *(MBR)* is recharge which occurs at the highest elevations of the mountain block and primarily circulates within the mountain block, commonly intercepting faults or flowing into alluvial fans located along the front of mountain ranges (Manning and Solomon, 2003; Wilson and Guan, 2004; Bresciani et al., 2018). Mountain block springs typically source their discharge from MBR. In comparison, basin springs likely source their recharge from either mountain front recharge (*MFR*) or mountain system recharge (*MSR*). MFR is recharge which occurs when surface water flows from the mountain block and recharges alluvial sediments located

beyond the faulted mountain front (Manning and Solomon, 2003; Bresciani et al., 2018). The combination of MBR and MFR is collectively known as mountain system recharge (MSR) and can contribute significant amounts of water to surrounding basin aquifers because there is disproportionately more precipitation at high elevations due to orographic effects than there is in the basin itself (Wilson and Guan, 2004; Bresciani et al., 2018). The most prominent orographic effect in this setting is precipitation at high elevations during the winter that commonly exceed evapotranspiration rates, leading to enhanced recharge with elevation. Recharge in the basin in climatic conditions like those found in Death Valley is likely negligible because evaporation is much larger than precipitation at such low elevations.

Chapter Outlines

Chapter 2 addresses the following questions: 1) what is the source of mountain block recharge in the Panamint Mountains, and 2) how much recharge is occurring in the Panamint Mountains? The questions are addressed by analyzing stable isotope data from precipitation collectors and springs in the Panamint Range. I also frame the stable isotopic composition of springs in the Panamint Range relative to the southern Sierra Nevada and Spring Mountains wising data collected at other springs in the study area and previously published data.

Chapter 3 addresses the following questions: 1) what are the groundwater residence times of springs in the Panamint Range? and 2) What flowpaths and/or geologic units support flow to local- and regional-scale springs? A multi-tracer approach is used to determine the residence times of the spring waters, the groundwater flowpaths to the spring, and geochemical and kinetics along those flowpaths. This methodology is necessary because of the expected high variability of residence times in the mountain block. I also use inverse geochemical modeling from precipitation to identify dominant geochemical processes and understand how geologic facies and residence

times affect geochemistry. I then build a conceptual framework for spring permanence and variability using these data.

Building off the hydrologic framework of chapter 3, chapter 4 correlates spring chemistry and residence time with spring ecology metrics. This a collaborative chapter where the dominant geochemical processes are compared to trends in benthic macroinvertebrate and microbiome species diversity and abundance from the Panamint Range springs. Statistical relationships between these three datasets is accomplished using multivariate visualization tools. These relationships are used to describe spring geochemistry and residence times as controls on spring ecology in the Panamint Range.

References

Ajami, H., P.A. Trouch, T. Maddock III, T. Meixner, & c. Eastoe (2011). Quantifying mountain block recharge by means of catchment-scale storage-discharge relationships. *Water Resources Research*, 47, W04504, doi:10.1029/2010WR009598.

Albee, A.L., T.C. Labotka, M.A. Lanphere, & S.D. McDowell (1981). Geologic Map of Telescope Peak Quadrangle, California. *U.S. Geological Survey*. Map of GQ-1532.

Alpert, H., R. Kattelmann, M. Drew, J. Hatfield, & H. Crall (2014). Disadvantaged Communities of the Inyo-Mono Integrated Regional Water Management Program. *Inyo-Mono Integrated Regional Management Program Final Report*. http://inyo-monowater.org/our-work/dac/findings/

Anderson, M.T., & L.H. Woolsey (2005). Water Availability for the Western United States- Key Scientific Challenges. *U.S. Geological Survey Circular,* 1261, 85.

Armstrong, R.L. (1982). Cordilleran metamorphic core complexes from Arizona to southern Canada. *Annual Reviews: Earth and Planetary Sciences*, 10, 129-154.

Bedinger, M.S. & J.R. Harrill (2012). Groundwater Geology and Hydrology of Death Valley National Park, California and Nevada. *Natural Resource Technical Report NPS/NRSS/WRD/NRTR,* 652.

Bense, V.F., T. Gleeson, S.E. Loveless, O. Bour, & J. Scibek (2013). Fault zone hydrogeology. *Earth Science Reviews*, 127, 171-192.

Bethke, C.M. & T.M. Johnson (2002). Paradox of groundwater age. *Geology*, 30(2), 107-110.

Borsa, A.A., D.C. Agnew & D.R. Cayan (2014). Ongoing Drought-Induced Uplift in the Western United States. *Science*, 345(6204), 1587-1590.

Bresciani, B., R.H. Cranswick, E.W. Banks, J. Batlle-Aguilar, P.G. Cook, & O. Batelaan (2018). Using hydraulic head, chloride and electrical conductivity data to distinguish between mountain front and mountain block recharge to basin aquifers. *Hydrology and Earth System Sciences,* 22, 1629-1648. https://doi.org/10.5194/hess-22-1629-2018

Bullen, T.D., & C. Kendall (1998). Tracing of Weathering Reactions and Water Flowpaths: A Multi- Isotope Approach. In *Isotope Tracers in Catchment Hydrology*, Kendall C, McDonnell KK (eds). Elsevier Science B.V: Amsterdam; 611-646.

California Dept. of Water Resources (DWR) (1964). Ground Water Occurrence and Quality Lahontan Region. *Bulletin* No. 106(1), 439.

Chambers, J.C., J.R. Miller, J.A. MacMahon & Society for Ecological Restoration International (2004). Great Basin riparian areas: ecology, management and restoration. *Island Press*: Washington, DC.

Earman, S., A.R. Campbell, F.M. Phillips, & B.D. Newman (2006). Isotopic exchange between snow and atmospheric water vapor: Estimation of the snowmelt component of groundwater recharge in the southwestern United States. *Journal of Geophysical Research*, 111, D09302. doi:10.1029/2005JD006470.

Fetter, C.W. (1994). *Applied hydrogeology*. Upper Saddle River, New Jersey: Prentice-Hall, inc.

Freeze, R.A., and J.A. Cherry (1979). *Groundwater*. Englewood Cliffs, NJ: Prentice-Hall, inc.

Hannah, D.M., L.E. Brown, A.M. Milner, A.M. Gurnell, G.R. McGregor, G.E. Petts, B.P.G. Smith, & D.L. Snook (2007). Integrating climate-hydrology-ecology for alpine river systems. *Aquatic Conservation: Marine Freshwater Ecosystems*, 17, 636-656.

Heaman, L.M., & J.P. Grotzinger (1992). 1.08 Ga diabase sills in the Pahrump Group, California- Implications for development of the Cordilleran miogeocline. *Geology*, 20, 637-640.

Hershler, R., H.P. Liu, & J. Howard (2014). Springsnails: A New Conservation Focus in Western North America. *BioScience*, 64 (8), 693-700.

Hynes, H.B.N. (1970). The ecology of flowing waters in relation to management. *Journal (Water Pollution Control Federation)*, 42(3), Part 1, 418-424.

Labotka, T.C., A.L. Albee, M.A. Lanphere, & S.D. McDowell (1980). Stratigraphy, structure, and metamorphism in the central Panamint Mountains (Telescope-Peak Quadrangle), Death Valley area- California Summary. *Geological Society of American Bulletin*, 91, 125-129.

Linacre, E.T. (1977). A simple formula for estimating evaporation rates in various climates, using temperature data alone. *Agricultural Meteorology,* 18(6), 409-424.

Loaiciga, H.A. (2004). Residence time, groundwater age, and solute output in steady-state groundwater systems. *Advances in Water Resources*, 27, 681-688.

Manga, M. (2001). Using springs to study groundwater flow and active geologic processes. *Annual Review of Earth and Planetary Sciences*, 29, 201-228.

Manning, A.H., & D.K. Solomon (2003). Using noble gases to investigate mountain front recharge. *Journal of Hydrology*, 275, 194-207. doi: 10.1016/S0022-1694(03)00043-X

Maxson, J.H. (1950). Physiographic Features of the Panamint Range, California. *Bulletin of the Geological Society of America*, 61, 99-114.

McCabe, D.J. (1998). Biological communities in springbrooks. *Studies in Crenobiology: The Biology of Springs and Springbrooks*, Backhuys Publishers, Leiden, The Netherlands, 221-228

Meinzer, O.E. (1927). Large springs in the United States. *Water Supply Paper 557*, US Geological Survey.

Miller, J.M.G. (1987). Tectonic Evolution of the Southern Panamint Range Inyo and San Bernadino Counties. *California Geology* 40(9), 212-222.

Norton, I. (2011). Two-stage formation of Death Valley. *Geosphere*, 7(1), 171-182, doi: 10.1130/GES00588.1.

Odum, E.P. (1953). *Fundamentals of ecology*. Philadelphia, PA: W.B. Saunders Company.

Petterson, R., A.R. Prave, B.P. Wernicke, & A.E. Fallick (2011). The Neoproterozoic Noonday Formation, Death Valley region, California. *GSA Bulletin*, 123(7/8), 1317-1336. doi: 10.1130/B30281.1

Price, R.A., J.W. Sears, T.A. Harms, & C.A. Evenchick (2007). Whence the mountains? : inquiries into the evolution of orogenic systems: a volume in honor of Raymond A. Price. *Geological Society of America*, 433.

PRISM Climate Group (PRISM) (2004). [Recent years annual precipitation dataset] *Oregon State University*, http://prism.oregonstate.edu

Roberts, M.T. (1974). Stratigraphy and Depositional Environments of the Crystal Spring Formation, Southern Death Valley Region, California. *California Division of Mines and Geology*, Special Report 106, Geologic Features-Death Valley, California.

Roe, G.H. (2005). Orographic Precipitation. *Annual Review of Earth and Planetary Sciences*, 33, 645-671. doi: 10.1146/annurev.earth.33.092203.122541.

Sada, D.W., E. Fleishman, & D.D. Murphy (2005). Associations among spring-dependent aquatic assemblages and environmental and land use gradients in a Mojave Desert mountain range. *Diversity and Distributions*, 11, 91-99.

Schwartz, F.W., & H. Zhang (2003). Fundamentals of Groundwater. *John Wiley & Sons Inc* (1).

Springer, A.E. & L.E. Stevens (2009). Spheres of discharge of springs. *Hydrogeology Journal*, 17, 83. https://doi.org/10.1007/s10040-008-0341-y

Stachelski, C. (2013). A Century of Weather in Death Valley, CA: 1911-2011. *NOAA Technical Memorandum* NWS WR-289.

Stewart, J.H. (1970). Upper Precambrian and Lower Cambrian strata in the Southern Great Basin, California and Nevada. *U.S. Geological Survey Professional Paper*, 620, 206.

Stewart, J.H. (1983). Extensional tectonics in the Death Valley area, California: Transport of the Panamint Range structural block 80km northwestward. *Geology*, 11, 153-157.

Tucker, M.E. (1983). Diagenesis, Geochemistry, and Origin of a Precambrian Dolomite: the Beck Spring Dolomite of Eastern California. *Journal of Sedimentary Petrology*, 53(4), 1097-1119.

Walker, L.R., & F.H. Landau (2018). *A Natural History of the Mojave Desert*, University of Arizona Press, Tucson, AZ, 44-47.

Williams, D.D., & D.I. Hogg (1988). Ecology and production of invertebrates in a Canadian coldwater spring brook. *Holarctic Ecology*, 11, 41-54.

Wilson, J. L. & H. Guan (2004). Mountain-block Hydrology and Mountain-front Recharge. *Groundwater Recharge in a Desert Environment: The Southwestern United States*. American Geophysical Union. https://doi.org/10.1029/009WSA08

Workman, J.B., C.M. Menges, C.J. Frindrich, & R.A. Thompson (2018). Geologic map of Death Valley National Park, Nevada and California (Unpublished geologic map). *U.S. Geological Survey*, Denver, CO.

Wright, L.A., B.W. Troxel, E.G. Williams, M.T. Roberts, & P.E. Diehl (1974). Precambrian sedimentary environments of the Death Valley region, eastern California. *Death Valley Region, California and Nevada, Guidebook: Shoshone, California, Death Valley Publishing Co,* 27-36.

**IDENTIFYING THE SOURCES OF MOUNTAIN BLOCK RECHARGE TO THE
PANAMINT RANGE SPRINGS USING STABLE ISOTOPES**

Introduction

The spring emergences of the Panamint Range are unique; there are numerous springs despite the location within the rain shadow of the southern Sierra Nevada. Seasonal snow packs in the southern Sierra Nevada reach 2.5 – 4 m annually (Barbour et al., 1991). While snow packs are likely much thinner in the Panamint Range, the sources of groundwater recharge supporting these springs have not been quantified. In fact, this is the first study to date that has been conducted to identify the sources of recharge for the Panamint Range springs. Understanding the sources of groundwater recharge is particularly important in the Panamint Range because its springs should not exist in this arid environment without substantial recharge.

In examining the sources of recharge to the Panamint Springs, it is also important to discuss the possible mechanisms of recharge to the spring emergences. Groundwater recharge commonly occurs through three different mechanisms (or a combination of these mechanisms): 1) mountain block recharge (MBR), 2) mountain front recharge (MFR), or 3) the combination of MBR and MFR collectively known as mountain system recharge (MSR). MSR can contribute significant amounts of water to surrounding basin aquifers because there is disproportionately more precipitation at high elevations due to orographic effects than there is in the basin itself (Wilson and Guan, 2004; Bresciani et al., 2018).

The paucity in precipitation in the southern Great Basin combined with the perennial nature of spring flow throughout the range suggests that these springs are primarily supported by mountain block groundwater rather than seasonal precipitation (Ajami et al., 2011). There is evidence of the perennial nature of multiple springs in the Panamint Range both as zones of historical human development (i.e. mining camps, Native American farmlands and ranches) and

as persistent landscape features in satellite imagery over multiple decades (Wallace, 1980; White, 2006; Google Earth, 2015). The type of mountain block flow is specific to the landscape position of a spring. For example, basin springs likely source water from mountain system recharge (MSR) whereas mid-to-high elevation springs receive just mountain block recharge (Manning and Solomon, 2003). To determine the source of recharge for the Panamint Mountain block an investigation into the distribution of water stable isotopes (^{18}O, ^{2}H) of the Panamint spring waters and precipitation was conducted and compared with other studies from this region.

Previous studies of springs have used variations in the stable isotopes of water from springs and regional precipitation to determine recharge sources (Gat and Dansgaard, 1972; Clark and Fritz, 1997; Coplen et al., 2000). Fractionation of water isotopes in precipitation is dominated by temp, elevation, precipitation amount, & distance from moisture source (Dansgaard, 1964). This fractionation of water in precipitation leads to distinct isotopic signatures for potential recharge areas (e.g. cool vs warm season; high vs low elevation).

In this chapter, stable isotopes are used to identify the sources of recharge to the Panamint Range groundwater springs and to test the following questions:

1) What is the source(s) of groundwater recharge in the Panamint Range?
2) How much groundwater recharge is occurring in the Panamint Range?

Methods

Spring Sampling

Samples of spring water were collected during a single two-week field campaign in the Panamint Range from May 23, 2017 to June 2, 2017 for oxygen and hydrogen stable isotope analysis. The water samples were collected at each spring using a portable peristaltic pump as designed by Miller and Frisbee (2018) and Masterflex silicon tubing. The tubing was placed in the

spring orifice (where possible) and water was pumped directly into a collection vial after purging the tubing for 10 minutes. Most samples were collected at sites where water could be collected directly from the spring source. Some emergences, however, were diffuse or their true emergences were unreachable due to the extremely rugged terrain of the sampling site. In these cases, the spring runs were sampled downstream of the spring emergence and are indicated with an asterisk in Table 1. In total, 18 springs were sampled for stable isotopes with 7 springs sampled downstream of their emergence point. Samples were stored unrefrigerated in 2 mL glass vials with plastic screw-caps until the time of analysis (within two months).

Three additional springs (Tule Spring, Upper Emigrant Spring, and Poplar Spring A) were sampled as part of the larger project on the southern Great Basin and are included in this study because they emerge in/near the Panamint Range. These springs were sampled May-December 2016. A 50% ethanol (C_2H_5OH) solution was used to disinfect the pump line, the shoes and clothes of the research team, and all equipment between each spring sampling site.

<p style="text-align:center;">Precipitation Sampling</p>

Interpretation of stable isotopic data begins with developing a Local Meteoric Water Line (LMWL) based on the $\delta^{18}O$ and $\delta^{2}H$ values of local precipitation in the study area (Clark and Fritz, 1997). The slope of the LMWL is then compared to the Global Meteoric Water Line (GMWL) originally constructed by Craig (1961). A LMWL is necessary to understand the ways in which environmental conditions impact $\delta^{18}O$ and $\delta^{2}H$ specific to a region of interest (Clark and Fritz, 1997; Coplen et al., 2000). For this reason, it was important to collect precipitation in the Panamint Range for isotopic analysis as this has not been previously collected.

Two precipitation collectors were deployed in the Panamint Range on October 14, 2017. The geographic distribution of precipitation collectors was limited to regions of the range

accessible by dirt roads. Sample collection was also restricted by seasonal closures and poor driving conditions. An oil-type precipitation collector similar to those described by Friedman (1992), Scholl (2006), and Frisbee et al. (2010) was used to minimize the impact of evaporation. This collector type is suitable for arid regions in which the collector must remain unchecked for months at a time because it limits sample evaporation by utilizing a screened opening above a reservoir capped by mineral oil (Friedman 1992; Scholl 2006). The only disadvantage to this design is that the samples must be carefully decanted before they can be analyzed so as not to contaminate the precipitation sample with oil.

The precipitation collectors were emptied, sampled, and reset on March 12, May 18, and September 18, 2018. The waters were decanted and separated from the mineral oil before they were stored in refrigerated 2 mL glass vials with screw-caps. In addition to the precipitation collector samples, one bulk snow sample was collected from the residual snowpack near Thorndike Campground on March 12, 2018. This sample was collected from below the first 8cm of a snowpack at multiple points within that snowpack, melted within a clean 1 L sampling bottle and then decanted into a smaller vial.

To expand upon the precipitation data collected in this study, data were also compiled from a previous precipitation study in the region (Friedman 2002) and integrated into a 'Death Valley' LMWL. Additional LMWLs were constructed for surrounding spring sampling sites from the larger project in the southern Great Basin, east of the Sierra Nevada. These data include a study also conducted by Friedman (1992) in Owens Valley, CA and two studies by Ingraham et al. (1991) and Winograd et al. (1998) in the Spring Mountains, NV. Figure 5 displays the locations and elevations of all precipitation collections considered in this study. All referenced data not original to this study are available in Appendix A.
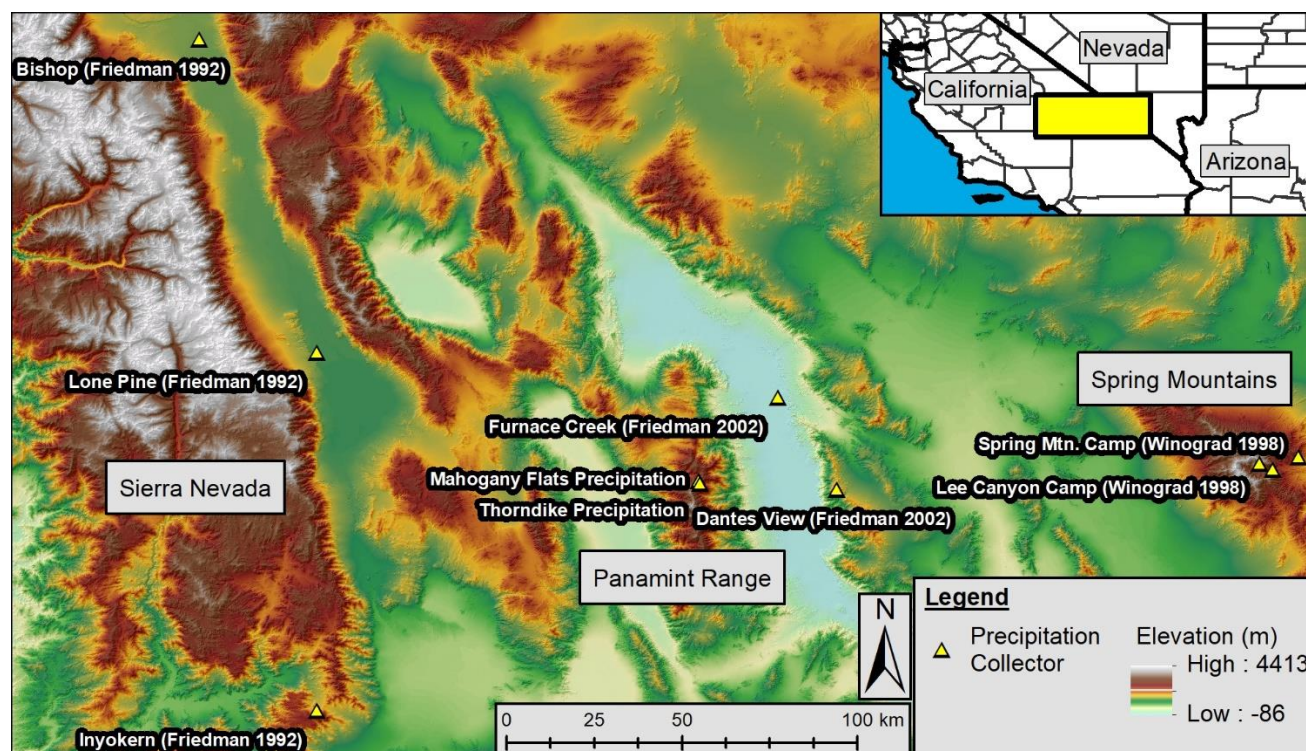
Figure 5. Map view of the GPS locations and credits of all precipitation collector sites considered in the analysis of these data and the larger spring dataset within which the Panamint stable isotope story belongs. Credit: USGS NED (https://lta.cr.usgs.gov/NED).

Stable Isotope Analysis

The measurement of the $\delta^{18}O$ and δ^2H of collected water samples was primarily conducted by the University of California Davis Stable Isotope Facility using a Los Gatos Research Laser Water Isotope Analyzer V2. This instrument uses enhanced absorption spectroscopy to estimate the abundance of these isotopes with a maximum reported precision of 0.3 ‰ for $\delta^{18}O$, and 2.0 ‰ for δ^2H (SIF, 2018). These ratios are then normalized and reported relative to VSMOW.

Results

Stable Isotope Composition of Springs

Results of the stable isotope analysis of the Panamint Range spring waters are reported in Table 2. The $\delta^{18}O$ values in these spring waters range from -14.2 ‰ to -7.7 ‰ with an average value of -12.6 ‰ while δ^2H values range from -104 ‰ to -53 ‰ with an average value of -93 ‰.

One sample, Wheel Spring, was flagged for spectral contamination by the analytical lab. This contamination is likely the result of residual 50% ethanol left in the sampling tube after bacterial decontamination or contamination in the spring prior to sampling.

Table 2. $\delta^{18}O$ and δ^2H Values of Panamint Range Spring Samples

Spring Name	Elevation (m)	Date Sampled	δ^2H (‰)	$\delta^{18}O$ (‰)
Jail Spring	2434	5/24/2017	-101	-14.1
Thorndike Spring	2337	5/25/2017	-103	-14.2
Uppermost Spring	1633	5/31/2017	-95	-12.9
Apron Spring	1606	5/27/2017	-98	-13.2
High Noon Spring	1419	5/27/2017	-98	-13.3
Main Hanaupah Spring #2*	1265	5/28/2017	-100	-13.7
Main Hanaupah Spring #1*	1258	5/28/2017	-93	-12.5
Upper Emigrant Spring	1231	5/19/2016	-100	-13.4
Poplar Spring A	1225	3/13/2017	-104	-14
Limekiln Spring	1223	6/1/2017	-99	-13.3
Unnamed Panamint Spring C*	1206	6/1/2017	-97	-13.4
Wilson Spring	1195	5/29/2017	-53	-7.7
Hanaupah Canyon*	1184	5/28/2017	-100	-13.9
South Hanaupah Spring #3*	1154	5/28/2017	-92	-12.4
Unnamed Panamint Spring E	963	5/26/2017	-94	-12.7
Surprise Canyon*	818	6/1/2017	-96	-13.1
Unnamed Panamint Spring F*	803	5/26/2017	-92	-12.5
Lower Warm Spring B	760	5/30/2017	-93	-12.7
Lower Warm Spring A	755	5/30/2017	-93	-12.4
Wheel Spring**	748	5/26/2017	-61	-8.5
Post Office Spring	321	6/2/2017	-78	-8.8
Warm Sulfur Spring	318	6/1/2017	-95	-13
Tule Spring	-77	3/14/2017	-103	-13.4

Indicates a spring sampled downstream of the spring emergence
**Denotes a sample flagged for spectral contamination*

Panamint precipitation stable isotope values are reported in Table 3. Winter precipitation samples are more depleted than spring waters. The winter precipitation collector samples are also nearly identical to the snowpack sample taken during the field campaign (Snow near Thorndike) in March 2018. The precipitation samples collected in May 2018 likely represent a mixture of late

season snow and spring rainfall and are less depleted than the winter snow samples. Conversely,

the summer precipitation samples collected in September 2018 represent only summer rain and are

enriched in heavy isotopes.

Table 3. δ^{18}O and δ^2H values from precipitation collectors at Mahogany Flats Campground and
Thorndike Campground, Panamint Range, Death Valley National Park, CA and a single snow grab
sample at Thorndike Campground.

Sampling Period	Season	Collection Name	δ^2H (‰)	δ^{18}O (‰)
10/14/2017 – 03/12/2018	Winter 2017-18	Thorndike Precipitation	-123	-16.6
10/14/2017 – 03/12/2018	Winter 2017-18	Mahogany Flats Precipitation	-130	-17.2
10/14/2017 – 03/12/2018	Winter 2017-18	Snow near Thorndike	-124	-16.9
03/12/2018 – 05/18/2018	Spring 2018	Thorndike Precipitation	-107	-14.9
03/12/2018 – 05/18/2018	Spring 2018	Mahogany Flats Precipitation	-104	-14.5
05/18/2018 – 09/18/2018	Summer 2018	Thorndike Precipitation	-47.9	-7.76
05/18/2018 – 09/18/2018	Summer 2018	Mahogany Flats Precipitation	-49.2	-7.71

Comparison of LMWLs

Figure 6 shows the relation between δ^{18}O vs δ^2H of the Panamint spring waters. Also

included are the GMWL and the LMWL derived from the Panamint precipitation data (Table 3).

An additional LMWL from Friedman (2002) is plotted for comparison to Dante's View, and

Furnace Creek, Death Valley, CA. The data used to construct the Friedman line are reported in

Appendix A. The range of stable isotope values from precipitation collected the summer of 2018

(red box) and winter of 2017-2018 (blue box) are also highlighted on this figure. The sample

flagged for spectral contamination, Wheel Spring, is not included.

An evaporation line was also constructed in Figure 6 using the one evaporated stable

isotope sample collected (Post Office Spring) as an end member and the average of the winter

precipitation collector values as the other end member. Post Office Spring emerged along the basin

floor of Panamint Valley as a shallow pool and was therefore prone to evaporation. Evaporative

fractionation is well documented in previous studies and is characterized by a disproportionate

depletion in δ^2H relative to δ^{18}O that results in a sample separation from the LMWL along a

shallower slope that typically ranges between 3 and 6 (Winograd and Friedman, 1972; Coplen et al., 2000; Jaunat et al., 2013). Neither Warm Sulfur Spring nor Tule Spring (the other two basin springs) plotted away from the LMWL and within the 3 to 6 slope range (Coplen et al., 2000). Post Office Spring was the only spring with stable isotope data that showed evaporation despite the fact that it was sampled at the spring source. Wilson Spring is another outlier (near the red summer precipitation box in Figure 6) yet its $\delta^{18}O$ and δ^2H values do not fall within the established range of values in evaporated waters.
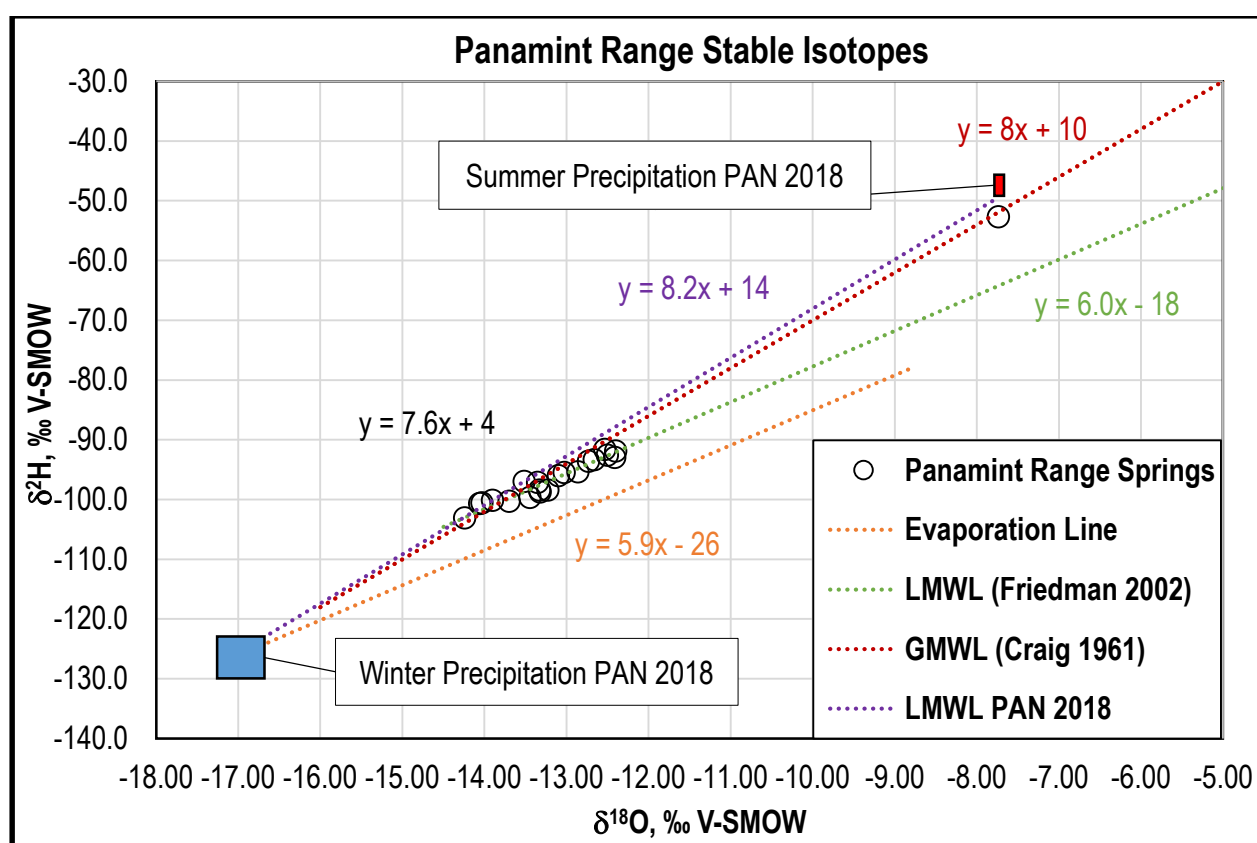
Figure 6. A graphical comparison of Panamint spring water $\delta^{18}O$ and δ^2H values with the Panamint precipitation LMWL (PAN 2018), the Friedman (2002) LMWL, and the GMWL (Craig, 1961). Slopes are shown in colors corresponding to the lines they represent.

Figure 7 compares the stable isotopic composition of the Panamint spring waters (without the outliers Wilson Spring, Wheel Spring, and Post Office Spring) with the stable isotopic composition of other spring waters from across the southern Great Basin along with the GMWL

(Craig, 1967) for reference. These other spring datasets are from Owens Valley, CA (orange) and the Spring Mountains, NV (pink). All spring isotope values are compared to LMWLs that are constructed from published precipitation data (see Appendix A) from the spring mountains & Owens Valley, respectively (Ingraham et al., 1991; Friedman, 1992). Each region is plotted using coordinating colors that contrast them from the black Panamint spring dataset.
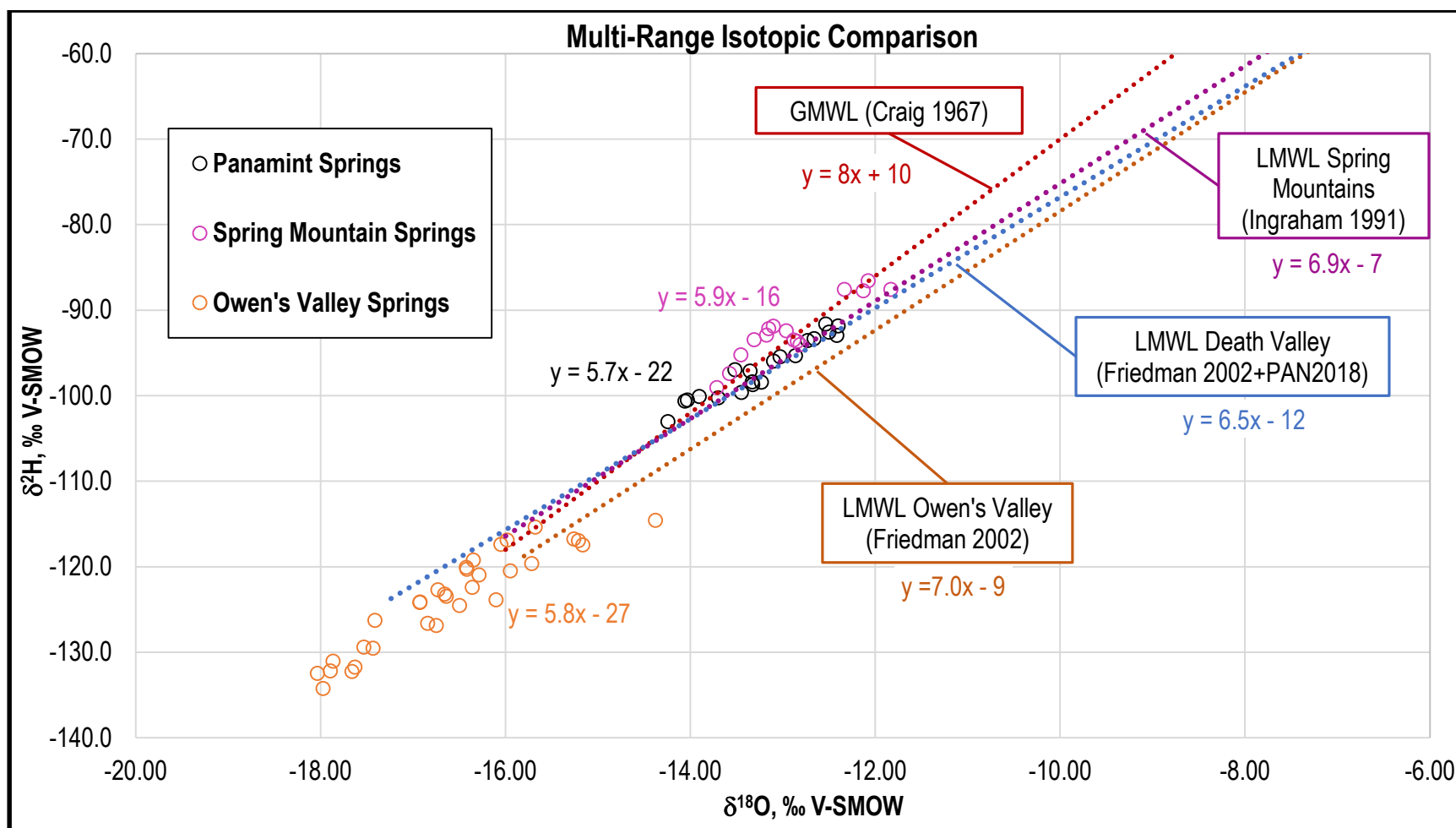
Figure 7. Multi-range isotopic comparison of $\delta^{18}O$ and $\delta^{2}H$ values in regions similar to the Panamint Range compared against the GMWL (Craig, 1967) and several LMWLs constructed from published values and the precipitation campaign dataset (see each colored call out box).

Discussion

<u>Establishing Sources of Recharge</u>

Not all spring waters fall along the GMWL due to localized fractionation factors, however, the isotopic composition of springs should be similar to the slope of the LMWL unless the spring has experienced mixing or fractionation. Factors that influence the agreement of spring waters and a LMWL constructed from precipitation include evaporation, geothermal exchange, and low temperature water-rock exchange (Coplen et al., 2000; Jaunat et al., 2013). Using the relationships between $\delta^{18}O$, $\delta^2 H$, geographic setting, and climatic conditions specific to the study area, the origin of spring recharge can be quantified using stable isotope techniques if the following assumptions are met (Winograd and Friedman, 1972; Mathieu and Bariac, 1996; Coplen et al., 2000; Jaunat et al., 2013):

1) Direct flow paths quickly convey the infiltrating water to the water table such that minimal mixing occurs with surface waters

2) All potential recharge endmembers have been identified and measured.

3) Fractionation processes which can alter the isotopic composition of the recharge before it is discharged can be quantified

If these conditions are met, then the isotopic compositions of spring waters and their precipitation source should be similar.

Two-component mixing models are often used in hydrologic studies to separate sources of waters contributing to a stream or spring based on known end members (Sklash and Farvolden, 1979; Genereux, 1998; Winograd et al., 1998; Liu et al., 2004; Frisbee et al., 2010). This mixing model is commonly applied to stream discharge relationships through hydrograph separation studies but in this case the same model is applied to quantify the sources of recharge using the

$\delta^{18}O$ values of precipitation. The set of equations that defines this model as applied to spring recharge is shown below where f_x is some fraction of either rain or snow:

$$\delta^{18}O_{spring} = f_{snow}\, \delta^{18}O_{snow} + f_{rain}\, \delta^{18}O_{rain} \qquad \text{(Equation 1)}$$

$$f_{rain} + f_{snow} = 1 \qquad \text{(Equation 2)}$$

$$f_{rain} = 1 - f_{snow} \qquad \text{(Equation 3)}$$

$$f_{snow} = (\delta^{18}O_{spring} - \delta^{18}O_{rain}) / (\delta^{18}O_{snow} - \delta^{18}O_{rain}) \qquad \text{(Equation 4)}$$

Equation 1 presents the conceptual model where $\delta^{18}O_{spring}$ is the composition of the spring water and is equal to the fraction of rainwater (f_{rain}) times the $\delta^{18}O_{rain}$ plus the fraction of snowmelt (f_{snow}) times the $\delta^{18}O_{snow}$. The underlying assumption is that these are the only two possible sources of natural recharge for a non-glaciated mountainous watershed. The mixing line between summer and winter precipitation isotope ranges supports two sources of recharge in the Panamint Range (Figure 6; Table 3). If these spring waters were receiving recharge other than snow or rain from the Panamints, the springs would diverge significantly from this mixing line (Figure 6). Post Office Spring (PAN 20) is an exception likely because of increased evaporation and Wilson Spring (PAN 12) is also unique in that it is not sourcing recharge from snow melt as it plots close to the measured range of $\delta^{18}O$ and δ^2H for summer rainwater (Figure 6).

Equation 2 identifies that these fractions will sum to one and this relationship is rearranged mathematically in Equation 3. Equation 4 can be obtained by substituting Equation 3 into Equation 1 thereby providing a method to calculate the fraction of snow-derived recharge for the spring waters. The mixing model presented in Equation 4 yields the results listed in Table 4 for each spring sampled in the Panamints. Samples that were flagged for spectral contamination or evaporation are indicated in Table 4 using asterisks.

Sources of Recharge and Estimated Recharge Fractions

Table 4. Mixing Model Results		
Spring Name	% Snow	% Rain
Thorndike Spring	71	29
Jail Spring	69	31
Main Hanaupah Spring #2	65	35
Hanaupah Canyon	67	33
Limekiln Spring	61	39
Apron Spring	60	40
High Noon Spring	61	39
Unnamed Panamint Spring C	61	39
Surprise Canyon	58	42
Warm Sulfur Spring	58	42
Uppermost Spring	56	44
Unnamed Panamint Spring E	54	46
Lower Warm Spring B	54	46
Lower Warm Spring A	51	49
Main Hanaupah Spring #1	52	48
South Hanaupah Spring #3	51	49
Unnamed Panamint Spring F	52	48
Post Office Spring*	12	88
Wheel Spring**	8	92
Wilson Spring	0	100
Poplar Spring A	69	31
Tule Spring	63	37
Upper Emigrant Spring	62	38

Indicates an evaporated spring sample
**Denotes a sample flagged for spectral contamination*

Figure 8 shows the percent of recharge from snow calculated using this mixing model. Post Office and Wheel Spring were not included in Figure 8. Figure 8 shows, with one major exception (Wilson Spring), that the fraction of recharge sourced from snow across the dataset is relatively similar (if increasing slightly) despite increases in spring emergence elevations. Wilson Spring is an exception because it falls so near the range of δ^{18}O and δ^2H values of rainwater (Figure 6) so it is estimated to be sourced 100% from rain. In all cases, the fraction of recharge sourced from snow is greater than 50 percent in 20 out of the 23 spring waters sampled (Table 4). This indicates that

the springs in the Panamint Range have a strong dependence on seasonal snow pack even though they emerge at a variety of elevations.

% Snow with Elevation
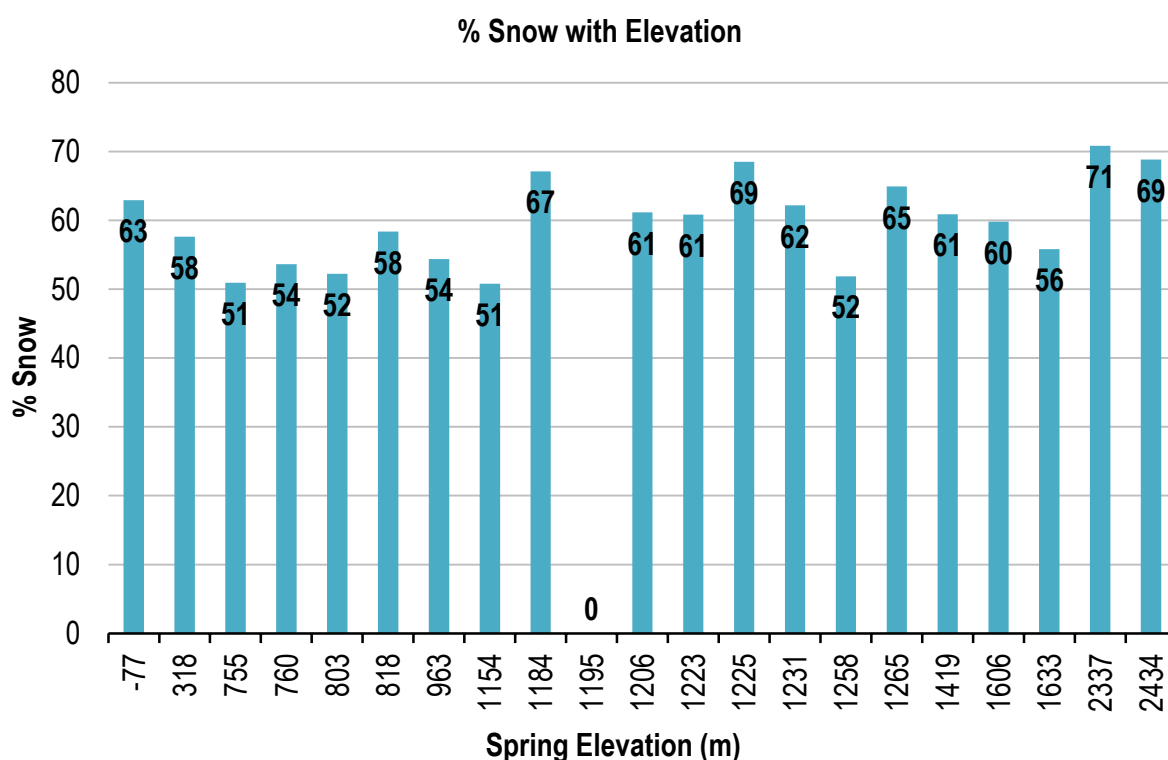
Figure 8. Bar plot of spring elevation versus the modeled percent of snow-derived water at each spring emergence.

The stable isotopes of the springs, separated by spring emergence elevation, are represented in Figure 9 along with the GMWL and LMWLs also used in Figure 6. Based on the isotopic similarity of the springs in Figure 9, it is clear that similar recharge mechanisms must exist across the study area despite differences in their emergence elevations. MBR to the majority of these springs that emerge within the mountain block is a valid assumption in this case because of their dominance in the high to mid-range of elevations away from the mountain front (Bresciani et al., 2018). Figure 9 also supports that the basin springs must be receiving recharge similar to the traditional MBR occurring throughout the rest of the mountain block because the basin springs do not separate significantly from the rest of spring dataset and are not heavily evaporated (with the exception of Post Office Spring).
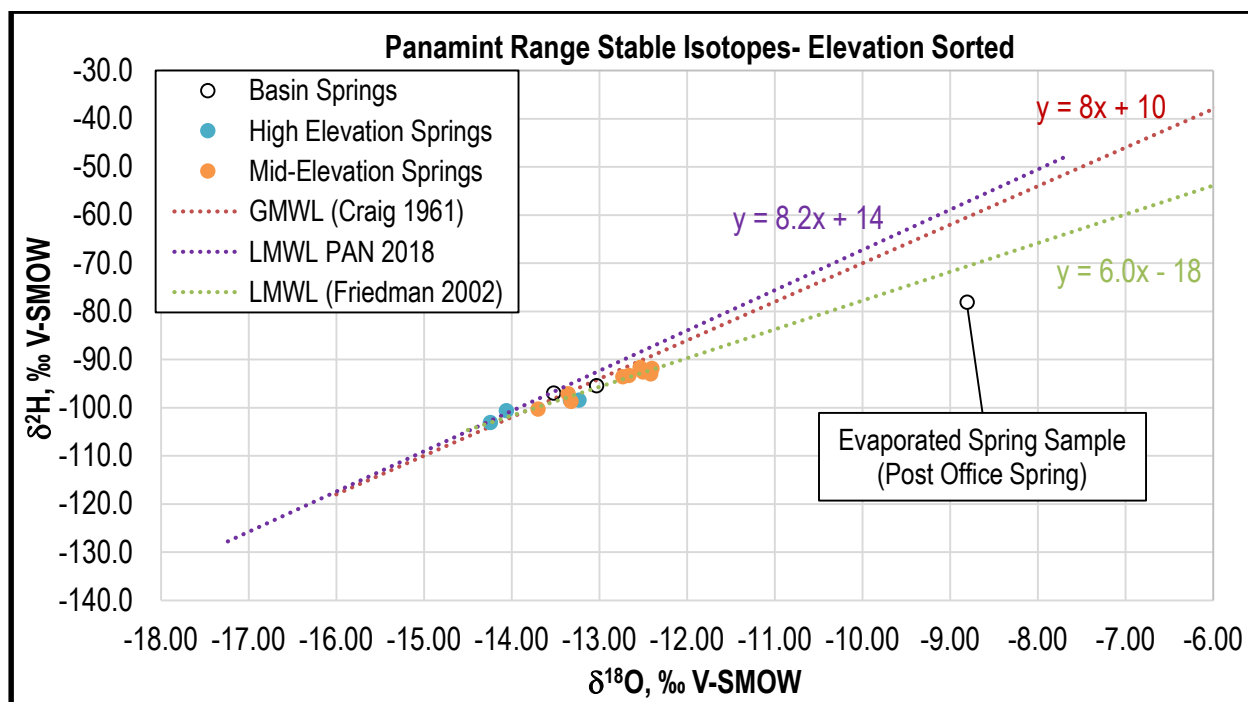
Figure 9. The stable isotopes of the Panamint Range springs separated by the elevation of the spring emergence. High elevation springs emerge between 4654 ft and 7984 ft above sea level, the mid elevation springs emerge between 2453 ft and 4150 ft above sea level and the basin springs emerge along the mountain front in Badwater Basin and Panamint Valley between 254 ft below sea level and 1052 ft above sea level.

Field observations and observations from long-term satellite imagery also support that several mountain block springs are contributing enough water to support perennial streamflow down drainages like Hanaupah Canyon and Surprise Canyon, yet these streams disappear into alluvial aquifers within the drainage and/or the large mountainside bajadas that characterize this landscape (Google Earth, 2015). The springs in the basins also broadly emerge at the toe of these bajadas so it follows that these alluvial aquifers are contributing significant amounts of water to these springs. Basin springs are therefore likely receiving MSR because precipitation in the basins is not frequent enough to support perennial flow and the extreme aridity of the environment of the southern Great Basin does not allow surface runoff all the way down these drainages to the basins, yet they still all emerge along the mountain front with a similar isotopic signature to those emerging within the mountain block (i.e. Warm Sulfur Spring and Tule Spring).

In terms of uncertainty in these data, the stable isotopic composition of recharge is commonly not equal to that of precipitation since the stable isotopic composition of precipitation commonly changes before it recharges the aquifer (Earman et al., 2006; Frisbee et al., 2010; Beria et al., 2018). However, I do not have data on the stable isotopic composition of soil-water or of rain or snowmelt that has infiltrated the soil to address source of uncertainty. Therefore, my estimates are conservative. This discrepancy facilitates the need for more data on spatial variability in precipitation, elevational dependencies, and measurements of the stable isotopic composition of soil-water and infiltration; data which is not available in the Panamint Range.

<div align="center">Quantifying Evapotranspiration and MBR</div>

In addition to discussing the sources of recharge in the Panamint Range, it is useful to also establish a relative water budget. In order to accomplish this task, two models were attempted to estimate recharge. Much like recharge, ET in the Panamint Range has not been quantified within the mountain block. The first model used to estimate MBR is based on a chloride mass-balance approach outlined by Frisbee et al. (2013) and the second model uses the Maxey and Eakin (1949) power law empirical relationship for MFR. Both recharge models are then incorporated into a mountain block water balance equation outlined by Wilson and Guan (2004) in order to calculate ET (as a residual of the water balance) at elevations greater than 1000 meters in the Panamint Range.

Frisbee et al. (2013) used Equation 5 to estimate the average annual recharge calculated for the elevation of the spring emergence where $Cl_{Precip.}$ represents the chloride concentration of the precipitation from the Thorndike Campground precipitation collector in Appendix B (2 mg/L), Cl_{spring} is equal to the measured chloride concentration of the spring water (also shown in mg/L in Appendix B), and P_{spring} is the average annual precipitation (mm/year).

$$MBR = \frac{Cl^-_{Precip.}}{Cl^-_{spring}} \times P_{spring} \qquad \text{(Equation 5)}$$

In the Panamint Range, annual precipitation at higher elevations has been previously reported as approximately 380 mm/year by Webb et al. (1987), but a more modern estimation from PRISM (2004) of 486 mm/year was chosen for these estimates. Equation 5 was solved for all springs and then averaged. The average MBR was estimated to be 112.8 mm/year in the Panamint Range using the chloride mass-balance model.

Maxey and Eakin (1949) present an alternative calculation for MBR based on an experimental dataset from White River Basin, NV where MFR can be equated to MBR (per Wilson and Guan, 2004) and estimated using a power law empirical relationship represented by Equation 6 where P_m is the mean annual precipitation (mm/year).

$$MBR = (9 \times 10^{-9}) \times P_m^{3.72} \qquad \text{(Equation 6)}$$

Equation 6 assumes a P_m value must be less than 600 mm/year and this is validated in the Panamint Range where P_m is estimated to be 486 mm/year (PRISM, 2004). Solving for Equation 6, MBR was estimated as 88.8 mm/year. This model estimated less MBR (24 mm/year) than the chloride mass balance approach (Frisbee et al., 2013). While this difference may seem large, the differences are likely related to regional applicability. While both estimates are still valid, it has been postulated by Wilson and Guan (2004) that the Maxey and Eakin (1946) model may only be most applicable to the area it was developed in (White River Basin, NV). For this reason, the Frisbee et al. (2013) chloride mass balance is likely the best model available to estimate MBR in the Panamint Range.

The typical water balance for a mountain block flow system is identified in Equation 7 following the work of Wilson and Guan (2004):

$$MBR = P - ET_b - RO \qquad \text{(Equation 7)}$$

Here *RO* represents streamflow at the upstream end of the mountain front zone, *P* is the annual precipitation rate (mm/year) and ET_b is the evapotranspiration rate (mm/year). In the case of the Panamint Range (as with other arid regions in the southwestern United States) *RO* is likely negligible because there is little to no surface runoff to the mountain front (Wilson and Guan, 2004). *ET* can therefore be estimated by rearranging Equation 7 to create Equation 8 and solving for ET_b using the MBR estimates outlined in Equations 5 and 6 and 486 mm/year for *P*, the estimated annual precipitation for the region (PRISM, 2004).

$$ET_b = P - MBR \hspace{4cm} \text{(Equation 8)}$$

The chloride mass-balance estimate of MBR therefore results in an estimated ET rate of 373.2 mm/year or 76.8% of annual precipitation. There are large uncertainties associated with estimating ET because it varies with complex terrain and the differences in vegetation cover that characterize mountain ranges (Wilson and Guan, 2008). For this reason, this ET estimate is likely not representative of all nuances in ET in the Panamint mountain range but it is at least the best approximation of this variable available.

Conclusions

This study was conducted to identify the sources of recharge for springs in the Panamint Range, Death Valley, CA. Specifically, the following questions were addressed: 1) What is the source(s) of groundwater recharge in the Panamint Range? 2) How much groundwater recharge is occurring in the Panamint Range?

With respect to question 1, the comparison between $\delta^{18}O$ and δ^2H values of the Panamint Range spring waters with published regional precipitation values suggests that the Panamint spring waters are predominantly derived from high-elevation winter precipitation (snowmelt) rather than summer rain (Figure 6; Figure 8). The fraction of recharge derived from snowmelt ranged from

51% to 71% in all but three of the 23 springs (Post Office, Wheel, and Wilson Spring). The majority of the spring data are also clustered relatively tightly (between -104‰ and -92‰ and between -14‰ and -12.5‰) which suggests that the Panamint Range springs recharge are sourcing from rain and snow but snow is the dominant source of recharge.

The new Panamints precipitation data provide a limited range of values for precipitation because they were sampled only over the course of an 11-month period and only at two high-elevation stations. This may explain why the spring waters relate most closely to the LMWL constructed from previous studies of the greater Death Valley region (Friedman, 2002). Further quantification of the stable isotopes of the precipitation distributed across the Panamint Range is suggested to 1) quantify spatial variability in the stable isotopic composition of precipitation, and 2) to establish a longer time series of isotopic values to compare with the current isotopic record of other regional precipitation. However, it is unlikely that low-elevation recharge is occurring in significant quantities if at all.

The isotopic consistency between most spring waters despite the variety of spring emergence styles and elevations supports that MBR must be the prevailing recharge mechanism for the majority of the springs in the Panamint Range. In comparison, basin springs are likely recharged through MSR as their waters are not isotopically enriched relative to the other spring samples despite their locations down the drainages where evaporation and differential sources of recharge would otherwise alter their stable isotopes. The basin spring waters (apart from the evaporated Post Office Spring sample) are also comparable in their percent snow compositions, according to the two component mixing model presented, to the larger springs dataset. These springs receive between 58% (Warm Sulfur Spring) and 63% (Tule Spring) snow–derived recharge yet they emerge over 7000ft below the snowline. Thus there must be some groundwater

connectivity through the mountain block.

MBR in the Panamint Range was quantified through a series of calculations based on estimated annual precipitation. Based on these models, the Panamint Range likely receive approximately 112.8 mm/year of recharge to the mountain block or approximately 23.5% of annual precipitation. Evapotranspiration was also estimated from these models equaling 373.2 mm/year or approximately 76.8% of the water coming into this system from precipitation. These MBR and ET rates are conservative for the Panamint Range but still characteristic of an arid environment though more data is required to improve the accuracy of these broadly uncertain estimates.

Despite the arid environment of the Panamint Range and its location in the rain shadow of the southern Sierra Nevada, recharge to the mountain aquifer(s) is strongly supported by high-elevation snowpack with smaller contributions of rain. Thus, changes in snow cover and the duration of snow cover associated with climate change in the western United States (e.g. Mote and Sharp, 2016) may have a severe impact on the permanence of these springs.

References

Aishlin, P. & J.P. McNamara (2011). Bedrock infiltration and mountain block recharge accounting using chloride mass balance. *Hydrological Processess*, 25, 1934-1948.

Ajami, H., P.A. Trouch, T. Maddock III, T. Meixner, & C. Eastoe (2011). Quantifying mountain block recharge by means of catchment-scale storage-discharge relationships. *Water Resources Research*, 47, W04504.

Barbour, M.G., N.H. Berg, T.G.F. Kittel, & M.E. Kunz (1991). Snowpack and the Distribution of a Major Vegetation Ecotone in the Sierra Nevada of California. *Journal of Biogeography*, 18(2), 141-149.

Breitenbach, S.F.M., J.F. Adkins, H. Meyer, N. Marwan, K.K. Kumar, & G.H. Haug (2010). Strong influence of water vapor source dynamics on stable isotopes in precipitation observed in Southern Meghalaya, NE India. *Earth and Planetary Science Letters*, 292(1-2), 212-220.

Bresciani, B., R.H. Cranswick, E.W. Banks, J. Batlle-Aguilar, P.G. Cook, & O. Batelaan (2018). Using hydraulic head, chloride and electrical conductivity data to distinguish between mountain front and mountain block recharge to basin aquifers. *Hydrology and Earth System Sciences,* 22, 1629-1648. https://doi.org/10.5194/hess-22-1629-2018

Clark, I., & P. Fritz (1997). *Environmental Isotopes in Hydrogeology*, Lewis Publishers, Boca Raton, Florida.

Coplen T.B. (1993) Uses of environmental isotopes. In *Regional Ground-water Quality,* cd. W.M. Alley, pp.227-254. Van Nostrand Reinhold, New York.

Coplen, T.B., A.L. Herczeg, & C. Barnes (2000). Isotope engineering: using stable isotopes of the water molecule to solve practical problems. In: Cook, P.G., & A.L. Herczeg (eds) *Environmental Tracers in Subsurface Hydrology*, Springer, Boston, MA.

Craig, H. (1961). Isotopic Variations in Meteoric Waters. *Science*, 133, 3465, 1702-1703.

Dansgaard, W. (1964). Stable isotopes in precipitation. *Tellus*, 16(4), 436-468.

Earman S, Campbell AR, Phillips FM, Newman BD. (2006). Isotopic exchange between snow and atmospheric water vapor: estimation of the snowmelt component of groundwater recharge in the southwestern United States. Journal of Geophysical Research 111: D09302. DOI:10.1029/2005JD006470.

Freeze, R.A., and J.A. Cherry (1979). *Groundwater*, Prentice-Hall, Englewood Cliffs, NJ.

Friedman, I., G.I. Smith, J.D. Gleason, A. Wardern, & J.M. Harris (1992). Stable Isotope Composition of Waters in Southeastern California 1. Modern Precipitation. *Journal of Geophysical Research*, 97(D5), 5795-5812.

Friedman, I., G.I. Smith, C.A. Johnson, & R.J. Moscati (2002). Stable isotope compositions of waters in the Great Basin, United States 2. Modern precipitation. *Journal of Geophysical Research*, 107(D19), 4401. https://doi.org/10.1029/2001JD000566

Frisbee, M.D., F.M. Phillips, A.R. Campbell, J.M.H. Hendrickx, & E.M. Engle (2010). Modified passive capillary samplers for collecting samples of snowmelt infiltration for stable isotope analysis in remote, seasonally inaccessible watersheds 2: field evaluation. *Hydrological Processes*, 24, 834-849.

Frisbee, M.D., F.M. Phillips, A.F. White, A.R. Campbell, & F. Liu (2013). Effect of source integration on the geochemical fluxes from springs. *Applied Geochemistry*, 28, 32-54. http://dx.doi.org/10.1016/j.apgeochem.2012.08.028

Gat, J.R. (1971). Comments on stable isotope method in regional groundwater investigations. *Water Resources Research*, 7(4), 980-993.

Gat, J.R., & W. Dansgaard (1972). Stable isotope survey of the fresh water occurrences in Israel and the northern Jordan Rift Valley. *Journal of Hydrology*, 16, 177-212.

Gat, J.R. (1980). Chapter 1- The isotopes of hydrogen and oxygen in precipitation. In: P. Fritz, & J.C. Fontes (eds) *Handbook of Environmental Isotope Geochemistry, The Terrestrial Environment, A*, Elsevier, 21-47.

Genereux, D. (1998). Quantifying uncertainty in tracer-based hydrograph separations. *Water Resources Research*, 34(4), 915-919.

Google Earth V 7.3.2591 (September 5th, 2015). Panamint Range, CA. 36°11'15.40"N 117° 1'22.18"W, Eye alt 15469 feet. Landsat/Copernicus. http://www.earth.google.com [November 2, 2018]

Ingraham, N.L., B.F. Lyles, R.L. Jacobson, & J.W. Hess (1991). Stable isotopic study of precipitation and spring discharge in southern Nevada. *Journal of Hydrology*, 125, 243-258.

Ingraham, N.L., & B.E. Taylor (1991). Light stable isotope systematics of large-scale hydrologic regimes in California and Nevada. *Water Resources Research*, 27(1), 77-90.

Jaunat, J., H.C. Celle-Jeanton, F. Huneau, A. Dupuy, P.L. Coustumer (2013). Characterization of the input signal to aquifers in the French Basque Country: Emphasis on parameters influencing the chemical and isotopic composition of recharge waters. *Journal of Hydrology*, 496, 57-70.

Liu, F., M.W. Williams and Nel Caine (2004). Source waters and flow paths in an alpine catchment, Colorado Front Range, United States. *Water Resources Research*, 40, W09401.

Manning, A.H., & D.K. Solomon (2003). Using noble gases to investigate mountain front recharge. *Journal of Hydrology*, 275, 194-207.

Mathieu, R. & T. Bariac (1996). An isotopic study (2H and 18O) of water movements in clayey soils under a semiarid climate. *Water Resources Research*, 32(4), 779-789.

Maxey, G.B. & T.E. Eakin (1949). Ground water in White River Valley, White Pine, Nye, and Lincoln counties. *Nevada Department of Conservation and Natural Resources Water Resources Bulletin,* 8.

Miller, J.B. & M.D. Frisbee (2018). Using 3D printing to create a robust and compact peristaltic field pump: an update to the Montana Drill Pump. *Groundwater Monitoring & Remediation*, 38(3), 75-78.

Mote, P.W., & D. Sharp (2016). 2016 update to data originally published in: Mote, P.W., A.F. Hamlet, L.P. Clark, & D.P. Lettenmaier (2005). Declining mountain snowpack in Western North America. *Bulletin of the American Meteorological Society*, 86(1), 39-49.

(SAHRA) Arizona Board of Regents (2005). Oxygen. *Sustainability of semi-Arid Hydrology and Riparian Areas (SAHRA)*, University of Arizona. Web. http://web.sahra.arizona.edu/programs/isotopes/oxygen.html#7

(SIF) UC Davis Stable Isotope Facility (2018). Oxygen (^{18}O) and Hydrogen (D/H) Analysis of Water. Web. https://stableisotopefacility.ucdavis.edu/18owater.html

Scholl, M. (2006). Precipitation isotope collector designs. *U.S. Geological Survey, Water Resources Division*. https://water.usgs.gov/nrp/proj.bib/hawaii/precip_methods.htm

Sklash, M.G. & R.N. Farvolden (1979). The role of groundwater in storm runoff. *Journal of Hydrology*, 43, 45-65.

Wallace, W.J. (1980). Death Valley Indian Farming. *Journal of California and Great Basin Anthropology*, 2(2), 269-272.

Webb, R.H., J.W. Steiger, & R.M. Turner (1987). Dynamics of Mojave Desert Shrub Assemblages in the Panamint Mountains, California. *Ecology*, 68(3), 478-490.

White, P.J. (2006). Troubled Waters: Timbisha Shoshone, Miners, and Dispossession at Warm Spring, *The Journal of the Society for Industrial Archeology*, 32(1), 5-24.

Wilson, J. L. & H. Guan (2004). Mountain-Block Hydrology and Mountain-Front Recharge. *Groundwater Recharge in a Desert Environment: The Southwestern United States*. American Geophysical Union. https://doi.org/10.1029/009WSA08

Winograd, I.J., & I. Friedman (1972). Deuterium as a tracer of regional ground-water flow southern Great Basin, Nevada and California. *GSA Bulletin*, 83(12), 3691-3708.

Winograd, I.J., A.C. Riggs, T.B. Coplen (1998). The relative contributions of summer and cool-season precipitation to groundwater recharge, Spring Mountains, Nevada, USA. *Hydrogeology Journal*, 6, 77-93.

GROUNDWATER FLOW IN THE PANAMINT RANGE: ESTABLISHING SPRING RESIDENCE TIMES AND FLOWPATHS USING MULTIPLE ENVIRONMENTAL TRACERS

Introduction

Current understanding of groundwater flow processes, groundwater residence times, and geochemical processes in the remote, broadly inaccessible mountainous terrain in the Panamint Range, Death Valley, CA is extremely limited. Previous studies have postulated connections between the more heavily studied basin springs in Death Valley and the springs emerging within the Panamint mountain block, however the spring processes have not been thoroughly quantified in the Panamint Range to support these claims (Li et al., 1997). In fact, to date a thorough analysis of groundwater flowpaths, residence times or geochemical processes has not been completed on springs within the Panamint mountain block. Establishing trends in spring water residence times as they relate to a conceptual model of groundwater flow in the Panamint Range is therefore valuable because it adds insight into the broader groundwater flow system of the southern Great Basin and the spring ecosystems that rely on it.

Due to the complex nature of natural groundwater flow systems and the fact that these processes are hidden from direct observation in the subsurface, indirect methods of observation including geochemical evolution, groundwater residence times, and the identification of groundwater flowpaths using geochemical and isotopic tracers must be used to understand the groundwater flow system. In this case, that means sampling multiple springs across the Panamint Range and analyzing them using a multi-tracer and geochemical approach. Estimations of groundwater residence time, especially, have been used in this manner in many previous works using various radiometric dating ranges of the isotopes found commonly in groundwater flow systems around the world (Plummer et al., 2001; Rademacher et al., 2001; Cook et al., 2005;

Manning and Solomon, 2005; Samborska et al., 2013; Frisbee et al., 2017). Due to variability in the half-lives of each isotope, a single isotope may have a range that is too limited to accurately date a single spring sample. For this reason, a multiple isotope approach is often required to accurately estimate a distribution of groundwater residence times when its distribution not known a priori. Figure 10 displays the broad radiometric dating range of multiple isotopes commonly used in hydrogeologic studies.
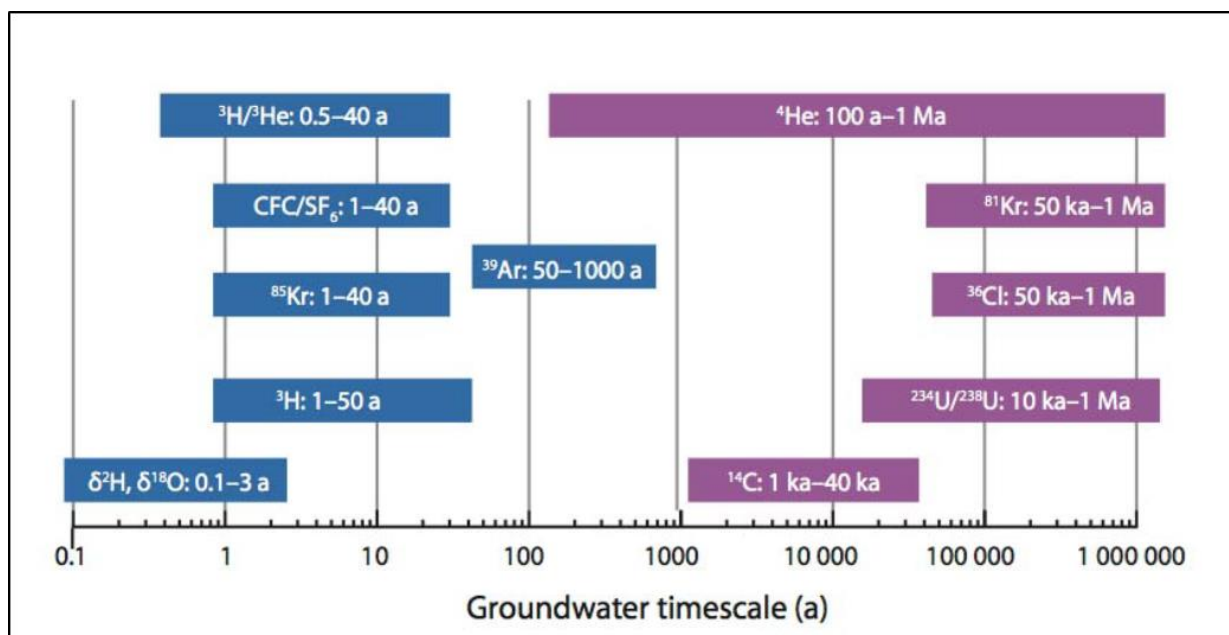
Figure 10. Diagram of the applicable dating ranges for the major radiometric dating methods in hydrogeology from the IAEA (2013).

General chemistry is likewise useful to discuss the general geochemical evolution occurring between the springs. Water is a universal solvent so differences in the chemistry of groundwaters are kinetically- derived based on the interaction of these waters with its container, in this case the regional geology of the Panamint Range (Franks, 1973; Rademacher et al., 2001; White, 2010). Patterns in spring water geochemistry can therefore indicate differences in how groundwater is interacting with geologic materials, describing general groundwater flowpaths that correspond to groundwater residence times (Kloppmann et al., 1998).

Geochemical mixing models and end member mixing analyses are commonly used to

identify groundwater flowpaths utilizing these same geochemical parameters from spring waters (Frisbee et al., 2017). Strontium isotopes ($^{87}Sr/^{86}Sr$) are also useful as they are often used in hydrogeology to identify groundwater flowpaths (Clow et al., 1997; Hogan, 2003; Wang et al., 2005; Shand et al., 2007; Raiber et al., 2009). Kinetic mineral weathering in groundwater extends to $^{87}Sr/^{86}Sr$ values as well as it also is enriched in waters as they interact with regional geology and can be used to correlate rock units with the waters leaching it (Frisbee et al., 2017).

Previous work on groundwater flow processes in mountainous settings have identified the importance of groundwater recharge in mountain blocks to basin aquifers in arid regions in the southwestern United States (Wilson and Guan, 2004). In these areas where precipitation is limited (typically desert basins) orographic effects on these mountain ranges create the greatest capacity for groundwater recharge as they are often the only regions where temperatures are low enough to support seasonal snow packs that are resistant to evapotranspiration and can generate substantial recharge (Roe, 2005). Despite the connection between mountain block hydrology and recharge to basin aquifers, few previous works have studied groundwater flow processes within arid region mountain blocks (Flint et al., 2001; Wilson and Guan, 2004). For this reason, an analysis of groundwater flow in the Panamint Mountains through the study of its broadly uncharacterized mountain block springs serves to illuminate broader understanding of groundwater flow in mountain block flow systems throughout the southern Great Basin.

In this chapter geochemical tracers and a multiple isotope approach are utilized to estimate spring residence times, identify groundwater flowpaths and address the geochemical evolution of springs in the Panamint Range. The following research questions are addressed:

1) Is groundwater flow in the Panamint Range is primarily conducted through dolomite aquifers?

2) How and over what time scale is the water held in storage and subsequently circulated through the mountain block (i.e. what are the groundwater residence times of springs)?

3) What flowpaths and/or geologic units support flow to local- and regional-scale springs? How do these flowpaths and geologic units impact the geochemistry and residence times of these springs?

Methods

Field Methods

Chlorine-36 (^{36}Cl), tritium (^{3}H), Chlorofluorocarbons (CFCs), and radiocarbon (^{14}C) were chosen for analysis in this study out of the options in an attempt to capture the widest range of possible groundwater residence times (Figure 10). All geochemistry and environmental isotope samples were collected at the same time as the ^{2}H and ^{18}O samples described in the previous chapter and in a similar fashion, during a single two-week field campaign in the remote backcountry of the Panamint Range from May 23, 2017 to June 2, 2017. Samples of spring water were collected at each spring using a portable peristaltic pump and Masterflex Viton tubing (Miller and Frisbee, 2018). Field geochemical measurements were measured with a YSI (YSI Incorporated) Professional Plus (Quarto) multi-parameter probe. Parameters measured in the field include temperature (^{o}C), pressure (mmHg), pH, conductivity (µs/cm), oxidation-reduction potential (ORP; mV), and dissolved oxygen (DO; mgL-1 and %). Specific conductance (SpC; µS/cm at 25 ^{o}C) and total dissolved solids (TDS; mgL-1) were calculated as a function of conductivity by the YSI Pro Plus such that SpC is equal to the measured conductivity multiplied by 1.91 (default temperature coefficient for waters at 25 ^{o}C) and TDS is equal to the measured conductivity multiplied by 0.65 (default TDS constant based on present ionic species). Calibration

on the YSI Pro Plus was conducted once a day and between springs of chemical extremes (elevated TDS or pH values) using pH and alkalinity standards in a three-point calibration. The tubing was placed in the spring orifice (where possible) after field geochemical measurements were made and water was pumped directly into a series of plastic screw-top Nalgene collection bottles after purging the tubing for 10 minutes. The volume and filtration of the water samples varied based on the individual tracer: Two – 500 mL bottles for radiocarbon (unfiltered), one 1L bottle for ^{36}Cl (filtered), one 1L bottle for tritium (filtered), one 250 mL bottle for general chemistry (filtered), one 125 mL bottle for ^{87}Sr/^{86}Sr (filtered) and three additional 500 mL glass bottles with a metal lids for CFCs. A 0.22 um polyethersulfone membrane Sterivex-GP pressure filter was used during filling. These filters were replaced at each spring and saved for microbial analysis according to a separate methodology specific to those samples. Sample bottles were tightly capped and taped closed. Sample bottles were stored unrefrigerated in light-proof storage bins while in the field.

Most samples were collected at high quality sampling sites where water could be collected directly from the spring emergence. Some emergences, however, were diffuse or it was physically impossible to reach their true emergences due to the extremely rugged terrain of the sampling site. In these cases, springs were sampled downstream of the emergence in the spring run and are indicated with an asterisk in Table 1. In total, 18 unique springs were sampled with 7 total springs sampled downstream of their point of emergence. Samples were then stored unrefrigerated in their bottles until the time of analysis.

Three additional springs (Tule Spring, Upper Emigrant Spring, and Poplar Spring A) were sampled as part of the larger project in the southern Great Basin and are included in this study since they emerge in the Panamint Range. These springs were sampled in May-December 2016. Similar sample collection methodologies were used for these samples. A 50% ethanol (C_2H_5OH)

solution was used to disinfect the pump line, the shoes and clothes of the research team, and all equipment between each spring sampling site to prevent cross-contamination between springs.

<div align="center">General Geochemistry Analysis</div>

Water samples were analyzed by the New Mexico Bureau of Geology & Mineral Resources - Analytical Chemistry Laboratory using a PerkinElmer Optima 5300 DV ICP-OES (Inductively Coupled Plasma Mass Spectrometer) for the following cations: Na^+, K^+, Mg^{2+}, Sr^{2+} and Ca^{2+}. Anions Br^-, Cl^-, F^-, NO_2^-, NO_3^-, PO_4^{3-}, and SO_4^{2-} were analyzed in this lab using a Dionex ICS-5000 ion chromatograph with conductivity detector and electrochemical detector. Alkalinity, and hardness were also calculated by the lab during their analyses.

Two unit-less multivariate analyses, Principal Component Analysis (PCA) and Hierarchical Clustering Analysis (HCA), were used to interpret the general geochemistry data and identify patterns in the dataset (Christophersen and Hooper, 1992; Cloutier et al., 2008). PCA was used first to generate eigenvectors and scores that describe analyte similarity between multiple samples. HCA was then conducted using the eigenvectors generated by PCA in order to create relevant geochemical groupings among the springs based on the overall variance between the samples (Cloutier et al., 2008). An important note about HCA is that the number of clusters that it generates is non-unique so an appropriate cluster number must be dictated during the analysis based on this sample similarity (Cloutier et al., 2008). In this case, four clusters were chosen based on these factors.

Inverse geochemical modeling using PHREEQC geochemical modeling software was performed to determine the minerals (and geologic units) being weathered (Parkhurst, 1995). The chemistry of the regional precipitation is used as a starting chemistry in the model since we do not know the chemistry of water as it percolates and subsequently recharges the mountain aquifer and

results in the measured sample chemistry (Sharif et al., 2008). Therefore, these geochemical models (exchanges) are likely too high. Precipitation samples collected near Mahogany Flats Campground and Thorndike Campground at high elevations in the Panamint Range were analyzed (also by the New Mexico Bureau of Geology & Mineral Resources - Analytical Chemistry Laboratory) and used as the initial chemistry in the models. Evaporation effects are not accounted for in these models either prior to recharge, along the flowpath, or in the discharge zone leading to an estimate of initial chemistry that is less concentrated than what may be true to the landscape. These disparities further create modeled exchanges that are likely too high.

Stable Isotopes of Strontium

Water samples and rock samples were collected for strontium isotopic analyses. Rock leaching samples were prepared for $^{87}Sr/^{86}Sr$ analysis from whole-rock hand samples collected near the spring emerge during the field campaign from the following geologic units: the Noonday Dolomite, the Carrara Formation, the Kingston Peak Formation, the Johnnie Formation, and the Bird Spring Formation. Rock-leaching of strontium in a laboratory setting is used to get approximate values of more easily weathered strontium-bearing minerals (Bailey et al., 2000; Frisbee et al. 2017). In this case, hand samples from these units were crushed to a fine gravel (5-10 mm pieces), placed in one liter of deionized water that had a pH of 7, and left to weather (leach) for two months in ambient room temperatures (21ºC). The water was decanted and their strontium concentrations were measured. $^{87}Sr/^{86}Sr$ ratios of the springs and rock-leaching samples were analyzed with a Nu Plasma HR multicollector inductively-coupled-plasma mass-spectrometer (MC-ICPMS) at the University of Illinois Urbana-Champaign isotope geochemistry laboratory. Bulk Sr^{2+} concentrations were reported in the general chemistry analysis obtained from the New Mexico Bureau of Geology and Mineral Resources- Analytical Chemistry Laboratory. Strontium

isotopes were used to identify flowpaths in the Panamint Range.

<div align="center">Environmental Isotopes and Spring Residence Times</div>

Multiple environmental tracers were used in the estimation of spring residence times to capture the widest range of possibilities. These groundwater tracers included both radioactive isotopes (Tritium, ^{36}Cl, and ^{14}C) and nonreactive organic compounds (Chlorofluorocarbons). Tritium (^{3}H) is the first of these isotopes is commonly found within the water molecule as ^{3}H^{1}HO and is often used in hydrogeology to establish groundwater residence times in the range of years to decades due to its 12.32-year half-life (Solomon and Cook, 2000; Stewart and Morgenstern, 2016). Tritium occurs naturally in the atmosphere through spallation but has also had a spike in its atmospheric deposition due to nuclear weapons testing during the 1950's and 1960's (Solomon and Cook, 2000). For this reason, elevated tritium in groundwater can indicate waters that were recharged during these anthropogenic periods of elevated atmospheric tritium. Tritium in the Panamint Range spring samples was analyzed at the University of Miami Tritium Laboratory using their low level gas proportional counter with a reported uncertainty of +/- 0.09 TU. Tritium units (TU) represent one molecule of ^{3}H^{1}HO in 10^{18} molecules of H$_2$0 and are commonly used to express the tritium content of waters relative to a common standard (NBS-4926C; Solomon and Cook, 2000).

Chlorine-36 (^{36}Cl) in this application was measured by the Purdue Rare Isotope Measurement (PRIME) lab using an accelerator mass spectrometer (AMS) with a relative measurement uncertainty between 2.3 and 4.5%. ^{36}Cl is commonly used in hydrogeology to date old groundwaters because of its relatively long half-life of approximately 301,000 years (Bentley et al., 1986; Phillips, 1986). However, just as tritium has a period of elevated atmospheric deposition due to nuclear weapons testing, ^{36}Cl is likewise subject to a period of accelerated

anthropogenic ^{36}Cl deposition during the 1950's and 1960's that was outside of its natural rate of deposition from atmospheric spallation reactions (Phillips, 2000).

Chlorofluorocarbons (CFCs) are non-reactive anthropogenically-derived organic compounds that were released into the atmosphere from the 1940's to the early 1990's, with the exception of SF_6, due to a moratorium on these substances (Jackson et al., 1992). CFC-12, CFC-11, CFC-13, and SF_6 were also analyzed by the University of Miami Tritium Laboratory in this application with a reported error that ranged between +/- 0.05 to +/- 0.013 for each sample. CFCs and SF_6 are commonly used to date young groundwaters because of their known atmospheric time series (Busenberg and Plummer, 1992; Volk et al., 1997). The atmospheric lifetimes of these compounds are approximately as follows: CFC-11 as 45 years, CFC-12 as 87 years, and CFC-13 as 100 years (Volk et al., 19997).

While these properties of CFCs make for a good groundwater tracer, CFCs residence time estimate are also highly sensitive to expose to the atmosphere as it would alter the CFC content of the water sample. CFCs re-equilibrate quickly when discharged to surface-water bodies so samples from streams or spring runs with turbulent or shallow flows will yield especially unreliable samples. For this reason, bedrock spring sources are most appropriate for groundwater age dating with this method and then only if they are sampled at the spring emergence (Clark and Fritz, 1997; USGS, 2017). CFCs were only collected at two springs, Lower Warm Spring A and B. The diffuse nature of many of the other Panamint Spring emergences prohibited their collection. If the spring waters did not emerge directly from bedrock or if they emerged diffusely they were not sampled for CFCs. CFCs residence times were then calculated using a USGS spreadsheet (USGS, 2014). The primary variables which can affect CFC residence time are recharge elevation and recharge temperature. In this case, these variables were approximated to 2438 m and 5 ⁰C respectively.

Radiocarbon (^{14}C) has been used in many studies to establish spring water residence times (e.g. Back et al., 1983; Campana and Simpson, 1984; Rose et al., 1995; Frisbee et al., 2013). ^{14}C in this case was analyzed by the University of Arizona AMS Laboratory; δ^{13}C had a reported measurement uncertainty of +/- 0.1 and the percent modern carbon (pmC) values (^{14}C) had a measured range of uncertainty between +/- 0.12 and +/- 0.26. Radiocarbon is generated naturally through spallation in the upper atmosphere and is then sequestered into the natural carbon sinks in the environment such that atmospheric CO^2 and dissolved inorganic carbon (DIC) in carbonate rock can affect the measured ^{14}C values through carbon exchange processes (Clark and Fritz, 1997). These additional sources of carbon can mix and exchange differentially through mineral dissolution with the true groundwater pmC (Fontes and Garnier, 1979). For this reason, measured ^{14}C values must be corrected to account for carbon exchange processes in carbonate aquifers.

The Panamint Range spring water dataset was corrected using Netpath XL (Parkhurst and Charlton, 2008). Table 5 includes the information used to correct these samples for carbon exchange in the subsurface. Citations are given for the range of ^{13}C values estimated from the geology present near each spring emergence in the final column and ^{13}C from soil CO_2 was modeled within a published range for the Great Basin between -12 and -20 δ ^{13}C developed by Quade et al., (1989). Many radiocarbon models can be used: Vogel (1967), Pearson (1964), Fontes and Garnier (1975), Han and Plummer (2013), but only three model approaches were most appropriate for this setting based on the model criteria outlined in Han and Plummer (2016). These models were the Fontes and Garnier (1975), Han and Plummer (2013) and Ingerson and Pearson (1964) radiocarbon correction because they take into account carbon isotope mixing, exchange between soil CO2 and DIC and exchange between solid carbonate and DIC (Han and Plummer, 2016). Only the springs sampled at the spring emergence were corrected. The remainder of the

springs require more extensive corrections and will not be discussed in this chapter. Springs requiring additional correction are marked with an asterisk in Table 5.

TracerLPM is an excel-based lumped parameter model used to calculate groundwater age from environmental tracers assuming simple aquifer geometries and well-constrained flow configurations that agree with established flow models (Jurgens et al., 2012). In this case, ^{3}H was chosen for modeling because it has an established time series of atmospheric deposition near the study area in Modesto, CA (Michel, 1989). This time series extends from 1850 to 2018 and records atmospheric tritium at half-year intervals which can be used to calculate the spring water residence times (Michel, 1989; Jurgens et al., 2012). Modeling with TracerLPM involved specifying the sample data, choosing a dispersion model and a tritium time series (Michel, 1989) and using its built-in convolution integral to solve the model and minimize error in the calculated age based on the agreement between the measured data and the tritium time series.

A dispersion flow model was chosen to simulate groundwater flow in the Panamint Mountain block because this model incorporates the advection dispersion equation in a semi-infinite medium making it closer to natural flow processes likely occurring within the range than either the piston or exponential flow models (Kreft and Zuber, 1978; Zuber and Maloszewski, 1982). The dispersion flow model is also most applicable in situations where mixing occurs within the aquifer due to differences in groundwater velocity across the study area as would likely be seen in a mountain block with variable relief (Jurgens et al., 2012). The dispersion model (see Equation 13 of Jurgens et al, 2012), is preloaded into TracerLPM, where τ_s is the mean age, v is the velocity, x is the outlet position, t-t' are the model boundaries, and DP represents the inverse Peclet number (Jurgens et al., 2012). The model boundaries in this application were set to minimize error on a spring-by-spring basis within TracerLPM. The dispersion parameter *(DP)* is equal to the inverse

of the Peclet number (*i.e.,* the ratio of advection to dispersion). *DP* was allowed to vary within each model between 0.01 and 0.99 (where a low *DP* represents the influence of mostly advective processes and high values represent mostly dispersive forces). Unsaturated zone travel times were assumed negligible because no data was taken to constrain either of these parameters in the field. The model was then optimized to the tritium tracer and a mean residence time was estimated for each spring.

Table 5. Netpath Model Inputs and General Chemistry concentrations

Sample ID	pH	Ca++ mg/L	Mg++ mg/L	Na+ mg/L	K+ mg/L	HCO3 -mg/L	SO4- mg/L	Cl- mg/L	Temp (ºC)	pmC	13C Soil CO2	13C Calcite	13C Calcite Range
PAN 1-Jail Spring	7.9	146	5.7	9.2	2.4	158	67.0	3.3	9.0	76.5	-17.7	-1.0	negative 4 to 2 [Petterson et al. 2011; Prave 1999]
PAN 3- Unnamed Panamint Spring E*	7.9	27.2	41.1	35.1	5.6	258	347.0	30.9	18.8	77.2	-18.8	-3.0	negative 3 to negative 1 [Prave 1999]
PAN 5- Wheel Spring*	7.2	352	58.9	36.3	3.7	167	168	53.9	22.6	64.9	-12.0	-0.1	broad range -0.09 high in Emigrant pass [Faggetter et al. 2017]
PAN 6- High Noon	7.9	359	136	39.7	8.6	263	1180	21.5	17.3	41.7	-19.9	-2.0	negative 4 to 2 [Petterson et al. 2011; Prave 1999]
PAN 7- Apron Spring	8.0	35.4	232	33.9	9.0	349	1510	18.3	17.7	48.1	-17.4	-5.5	negative 4 to 2 [Petterson et al. 2011; Prave 1999]
PAN 8- Main Hanaupah Spring #2*	7.2	95.6	11.1	4.4	1.4	134	28.8	1.6	15.1	75.9	-17.3	-4.0	negative 4 to 2 [Petterson et al. 2011; Prave 1999]
PAN 11- South Hanaupah Spring #3*	8.1	91.1	28.9	15.4	3.2	302	137	6.7	16.1	84.3	-20	-6.5	negative 6 to negative 3 [Bergman et al. 2011; Petterson et al. 2011]
PAN 12- Wilson Spring*	7.8	64.0	67.9	16.1	2.6	271	282	11.7	20.4	81.1	-19.8	-7.6	negative 4 to 2 [Petterson et al. 2011; Prave 1999]
PAN 13- Lower Warm Spring A	7.3	64.2	21.4	33.5	3.2	130	179	25.9	34.4	34.1	-12.3	3.0	negative 2 to 3 [Brand et al. 2007]
PAN 14- Lower Warm Spring B	7.7	40.2	21.6	33.9	3.3	128	177	25.8	34.3	30.3	-13.5	2.0	negative 2 to 3 [Brand et al. 2007]
PAN 15- Uppermost Spring	7.5	89.4	72.6	23.0	2.9	485	41	12.9	16.5	45.1	-19.5	-3.0	negative 6 to negative 2 [Corsetti and Kaufman 2003]
PAN 16- Limekiln Spring	7.6	92.9	40.5	11.6	3.9	224	214	8.4	19.4	53.7	-18.6	-1.0	1 to 6 [Prave 1999]
PAN 17- Unnamed Panamint Spring C	8.3	85.0	39.9	11.3	3.8	257	204	7.6	16.5	60.2	-12.6	-5.0	negative 5 to 5 [Corsetti and Kaufman 2003]
PAN 19- Warm Sulfur Spring	7.8	107.0	45.8	575	28.4	179	354	873	32.0	46.3	-18.9	-1.0	1 to 6 [Prave 1999]
IES-019- Tule Spring*	7.5	0.3	74.80	490	9.7	115	141	994	26.8	77.6	-12.0	-2.7	1 to 6 [Prave 1999]
Panamint Precipitation	6.2	8.2	0.65	2.6	1.1		2.1	2.0		1.0			

Results

General Geochemistry

All geochemistry data for the springs studied can be found in Appendix B. The major cations and anions of the Panamint Range spring waters were fit into four distinct geochemical groups through the combination of principal component analysis and hierarchical clustering. Figure 11 displays the dendrogram of the major groupings of the Panamint Range spring dataset based on the HCA. This dendrogram was then used to determine the appropriate number of clusters based on the geochemical similarity of the spring waters. Four major hierarchical clustering groups were identified and are separated by color in Figure 11. Group 1 is blue, Group 2 is red, Group 3 is green and Group 4 is purple. Figure 12 illustrates these same geochemical groups in map view across the Panamint Range using the same color scheme along with the spring sample names rather than the numerical sample code shown on the x-axis of Figure 11.
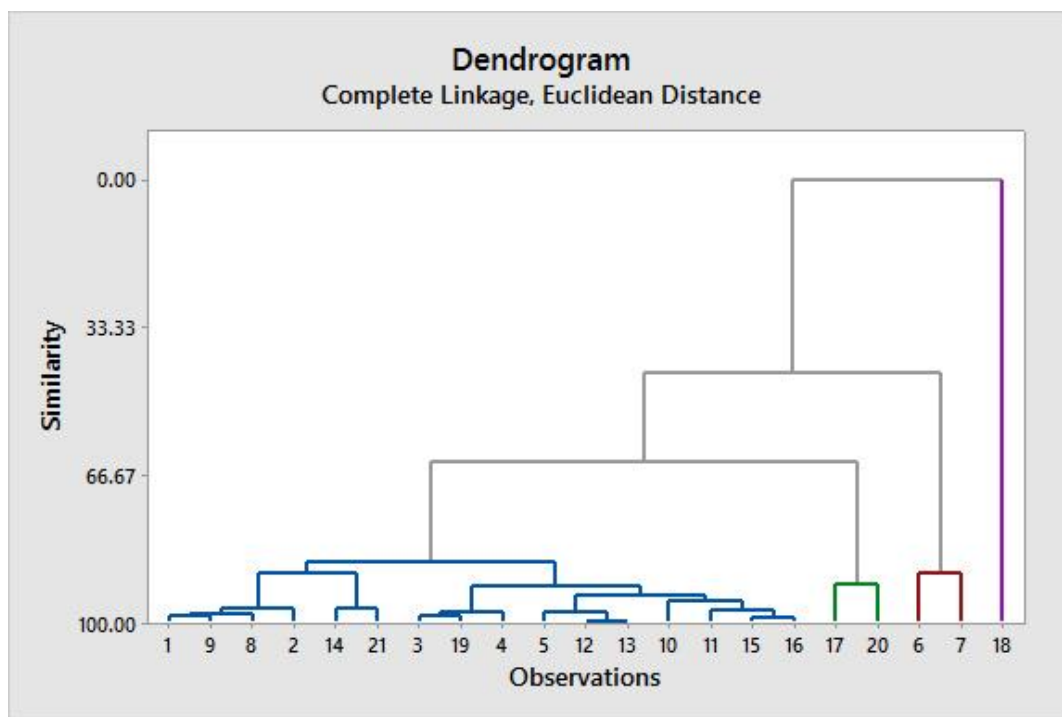
Figure 11. Dendrogram of the Panamint Range springs dataset based on the statistical similarity (%) of the concentrations of major cations and anions between the springs. Group 1 is blue, Group 2 is red, Group 3 is green and Group 4 is purple.
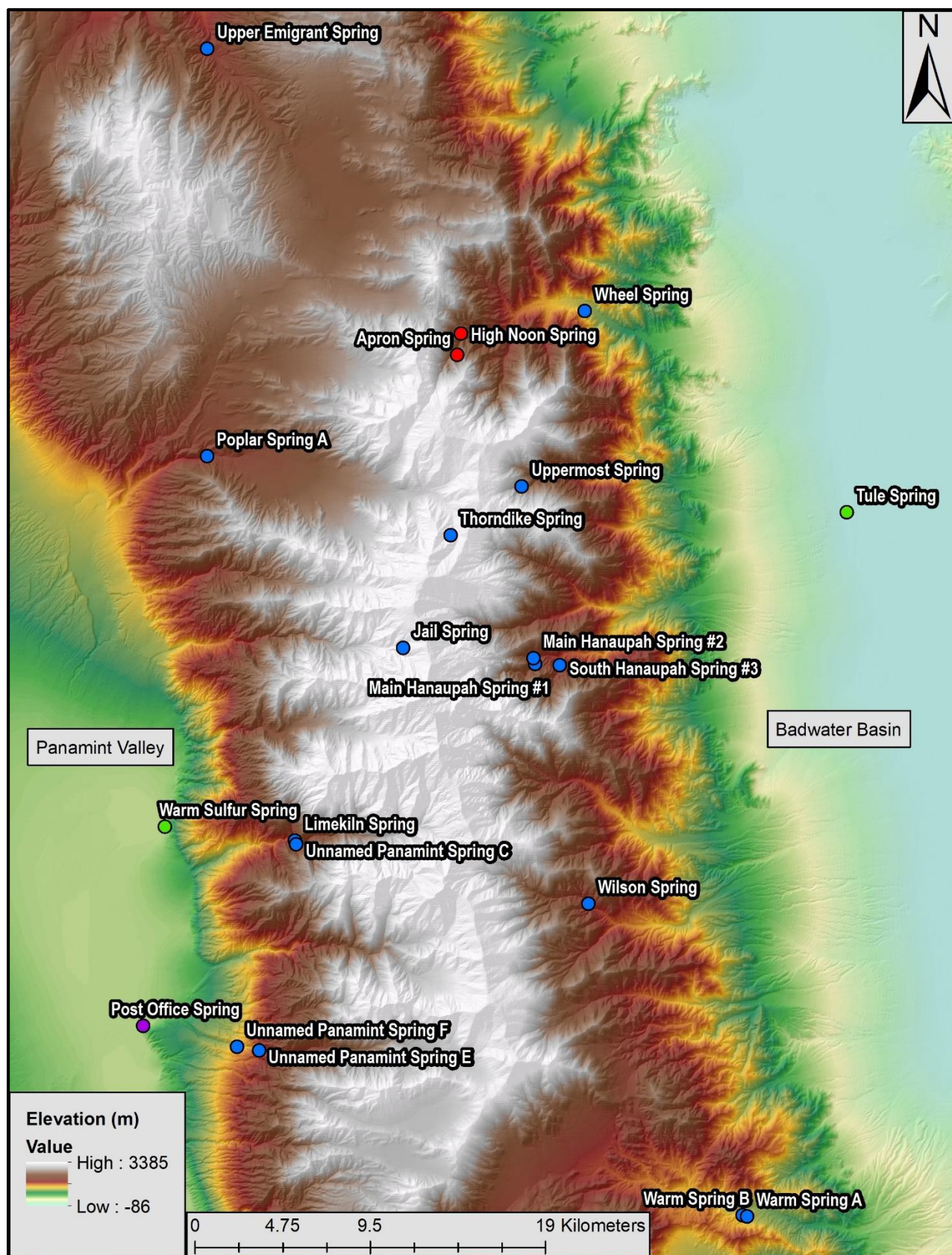
Figure 12. Color coordinated map of the major geochemical groups identified in Figure 11.

Table 6. Eigenanalysis and Eignvectors of the Principal Component Analysis of the Panamint
Range Springs

Principal Component Analysis

Eigenanalysis of the Correlation Matrix

Eigenvalue	6.2897	1.9671	1.3991	0.9437	0.6488	0.3879	0.1874	0.1201	0.0412	0.0141
Proportion	0.524	0.164	0.117	0.079	0.054	0.032	0.016	0.010	0.003	0.001
Cumulative	0.524	0.688	0.805	0.883	0.937	0.970	0.985	0.995	0.999	1.000
Eigenvalue	0.0009	0.0000								
Proportion	0.000	0.000								
Cumulative	1.000	1.000								

Eigenvectors

Variable	PC1	PC2	PC3	PC4	PC5	PC6	PC7	PC8	PC9	PC10
Temp	0.024	-0.414	-0.573	-0.352	-0.085	-0.233	0.547	0.062	-0.037	-0.089
H+	-0.099	-0.507	0.013	0.255	0.748	0.003	-0.121	0.173	-0.253	0.007
Ca	0.378	0.120	0.031	0.070	0.044	0.354	0.151	0.195	-0.118	-0.625
Mg	0.331	0.208	-0.185	0.180	0.355	0.012	0.251	-0.649	0.125	0.300
Na	0.336	-0.343	0.123	0.017	-0.190	-0.117	-0.175	-0.116	-0.035	-0.110
K	0.365	-0.182	0.093	0.035	-0.318	-0.048	-0.095	0.134	-0.495	0.530
Sr	0.376	-0.083	0.147	-0.036	0.132	0.065	0.138	0.501	0.665	0.307
Cl	0.307	-0.416	0.103	0.029	-0.122	-0.101	-0.270	-0.392	0.267	-0.297
SO4	0.374	0.147	-0.075	0.125	0.029	0.309	0.234	0.063	-0.326	-0.003
HCO3	0.248	0.327	0.274	-0.169	0.243	-0.766	0.074	0.110	-0.163	-0.174
SI	0.211	0.170	-0.395	-0.597	0.239	0.153	-0.573	0.035	-0.036	0.048
F	0.091	0.159	-0.587	0.608	-0.139	-0.291	-0.282	0.230	0.103	-0.068

Variable	PC11	PC12
Temp	0.039	-0.002
H+	0.019	0.002
Ca	0.334	-0.364
Mg	0.077	-0.241
Na	-0.673	-0.440
K	0.398	-0.101
Sr	-0.012	0.020
Cl	0.306	0.465
SO4	-0.419	0.617
HCO3	0.008	0.090
SI	-0.022	-0.004
F	-0.000	0.002

The PCA of the general chemistry of these spring samples gives geochemical meaning to
the groups established in the hierarchical clustering shown in Figure 11 and Figure 12. Each

component of the PCA has an associated Eigenvalue that represents the amount of total variance in the data set that corresponds to that component (see the proportion value associated with the eigenanalysis in Table 6). Likewise, the Eigenvectors in Table 6 can be used to establish which of the geochemical inputs constitute that component. Component 1 (PC1 in Figure 13) of this analysis represented 52% of the total variance among the spring waters. PC1 represents the total dissolved solids (TDS) in the spring samples because its eigenvectors (Table 6) were almost all positive and greater than 0.3, indicating that this component is dependent on the sum of all the major cations and anions combined. Component 2 (PC2) captured 16% of the total spring variance and is controlled by the carbonate dissolution occurring along flowpaths as the eigenvectors show a strong positive correlation with bicarbonate, calcium, magnesium rather than a positive correlation with chloride or sodium, which would be related more closely to evaporate dissolution (Table 6). Component 3 (PC3; Figure 14) controls 12% of the total variance in the spring general geochemistry and represents inversely the temperature and fluorine concentrations (i.e. the higher the temperature and fluorine concentration, the more negative the PC3 value). All other generated components in this PCA accounted individually for 8% or less of the total variance and are therefore not significant enough to describe the factors controlling spring water chemistry in the Panamint Range.

Figure 13 shows a scatterplot of PC1 vs PC2 colored by major geochemical group. Figure 14 shows a scatterplot of PC1 vs PC3 colored by major geochemical group. These two plots display the varying degrees that TDS (PC1), carbonate dissolution (PC2) and temperature (PC3) impact the individual spring samples. The majority of the spring waters (16/21) cluster together as Group 1 in PC1 vs PC2. PC1 vs PC3 (Figure 14) displays more spread with respect to Group 1, but only in springs with warmer temperatures (i.e. spring pools and thermal springs).
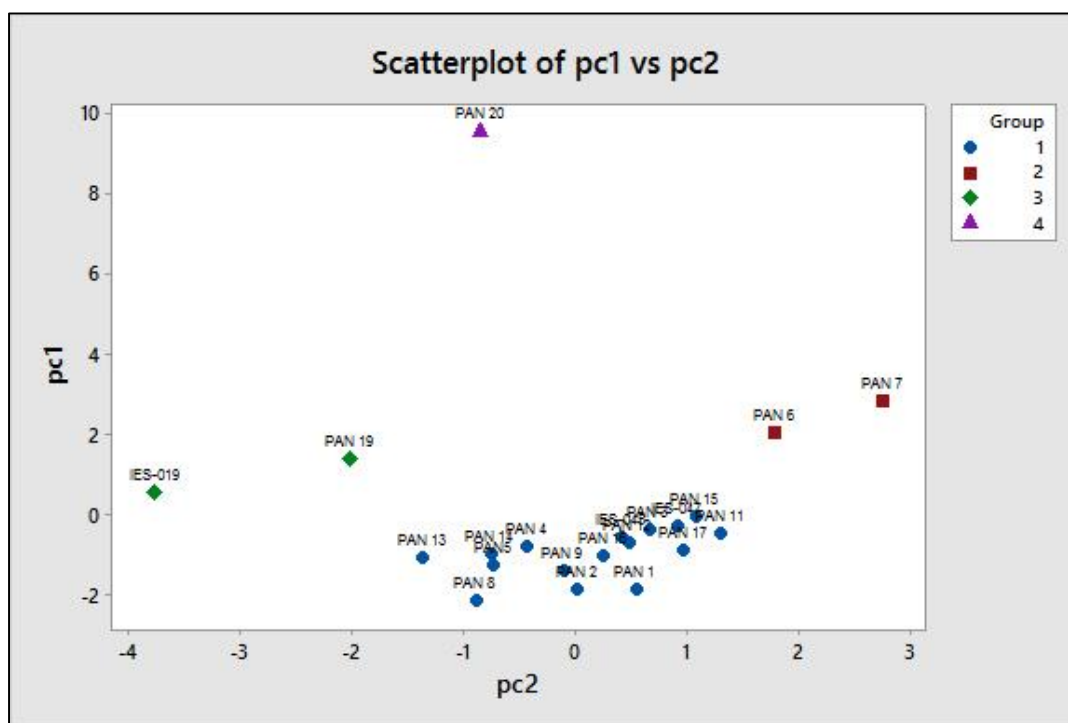
Figure 13. Scatterplot of PC1 vs PC2 with spring ID labels separated by color according to major geochemical group. PC1 represents 52% and PC2 represents 16% of the total variance in the sample geochemistry.
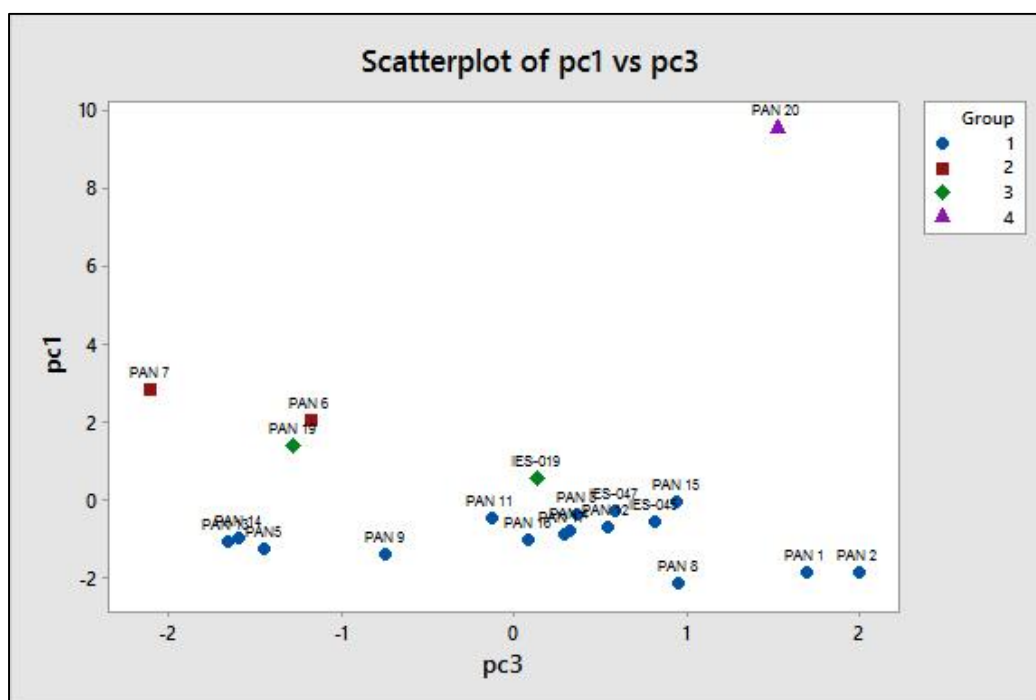
Figure 14. Scatterplot of PCA1 vs PCA3 with spring ID labels separated by color according to major geochemical group. PCA1 represents 52% and PCA 3 represents 11% of the total variance in the sample geochemistry.

Spring waters with higher solute concentrations are separated into Groups, 2, 3, and 4 in

Figure 11, Figure 12, Figure 13, and Figure 14 and can also be identified as unique in a simple ternary diagram (Piper, 1941) of the general chemistry (Figure 15). While the hierarchical group color coordination has been applied to this figure, the separations are based solely on concentrations rather than the PCA. The PHREEQC inverse geochemical modeling results likewise showed a significantly higher phase mole transfer for samples in Groups 2, 3, and 4. The results of this modeling are shown in Figure 16.

These inverse geochemical models show that the dissolution of dolomite, halite, and gypsum is common at each spring as well as a precipitation of calcite and formation of illite and kaolinite. The inverse modeling of IES-019 (Tule Spring) is not shown since its chemistry is likely the result of mixing with basin brines (Li et al., 1997). Further support for dolomitic weathering (dedolomitization) in the Panamint Range is shown in Figure 17. There is a one-to-one relationship between the concentrations of calcium + magnesium and sulfate + 1/2*bicarbonate within the Panamint Range spring dataset indicative of dedolomitization (Back et al., 1983; Bischoff et al., 1994; Fisher and Mullican, 1997).
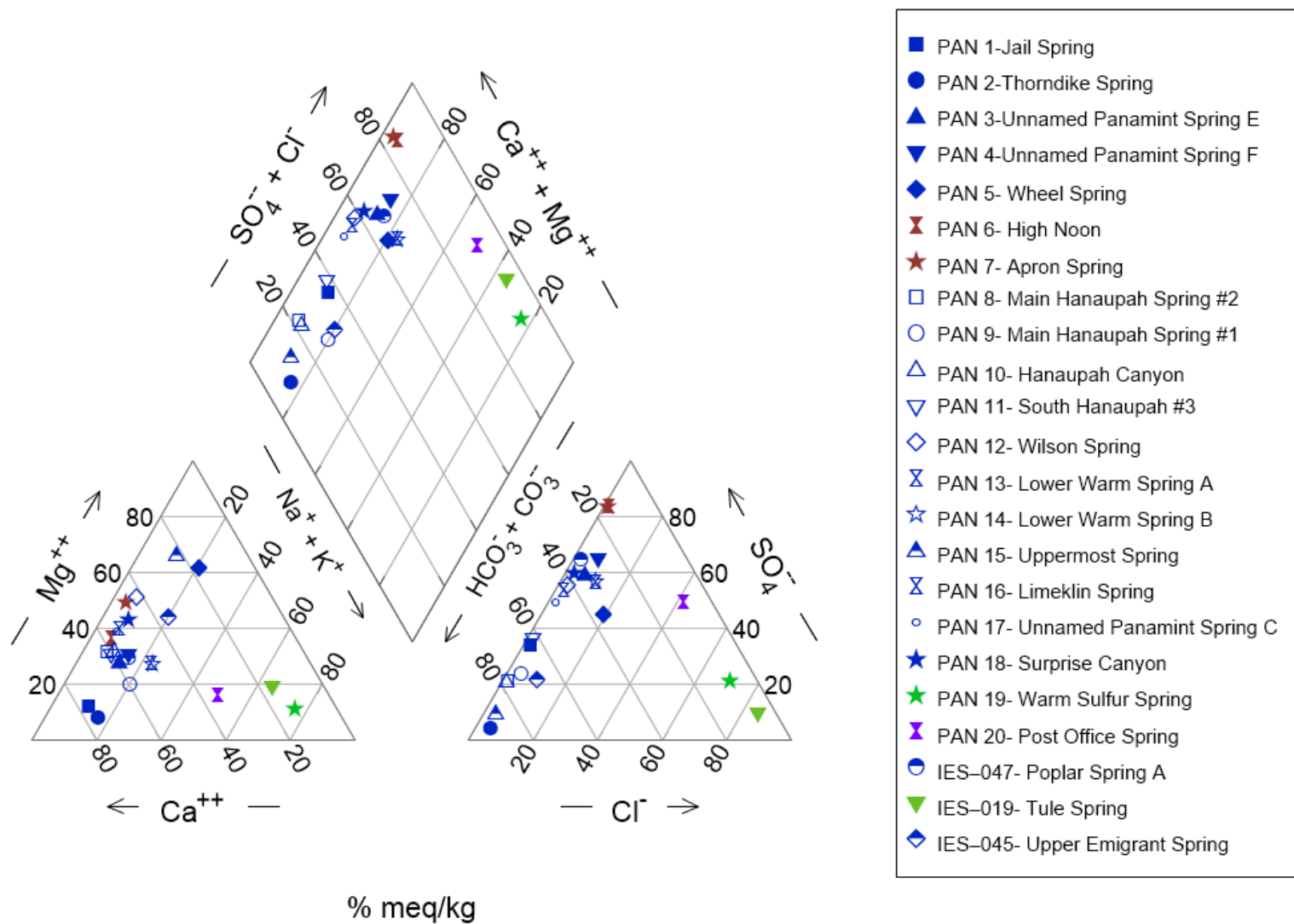
Figure 15. Trilinear diagram (Piper, 1944) of the Panamint Range spring waters colored according to their primary geochemical group determined by PCA.
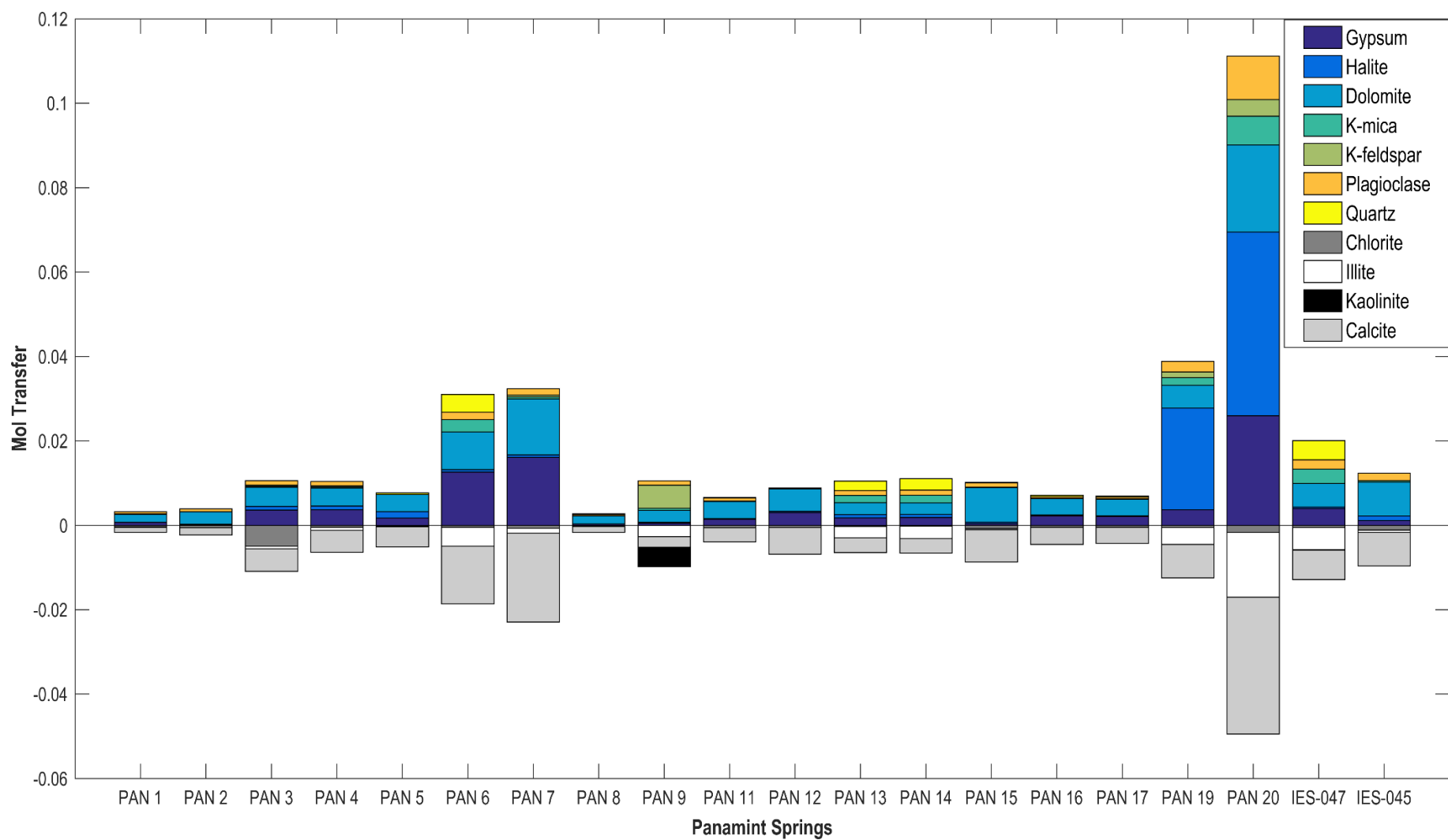
Figure 16. PHREEQC model results reported as the mole transfer of minerals in solution beginning with precipitation as the input to the point of spring discharge. Uncertainty in all of these models was specified to 2.5%.
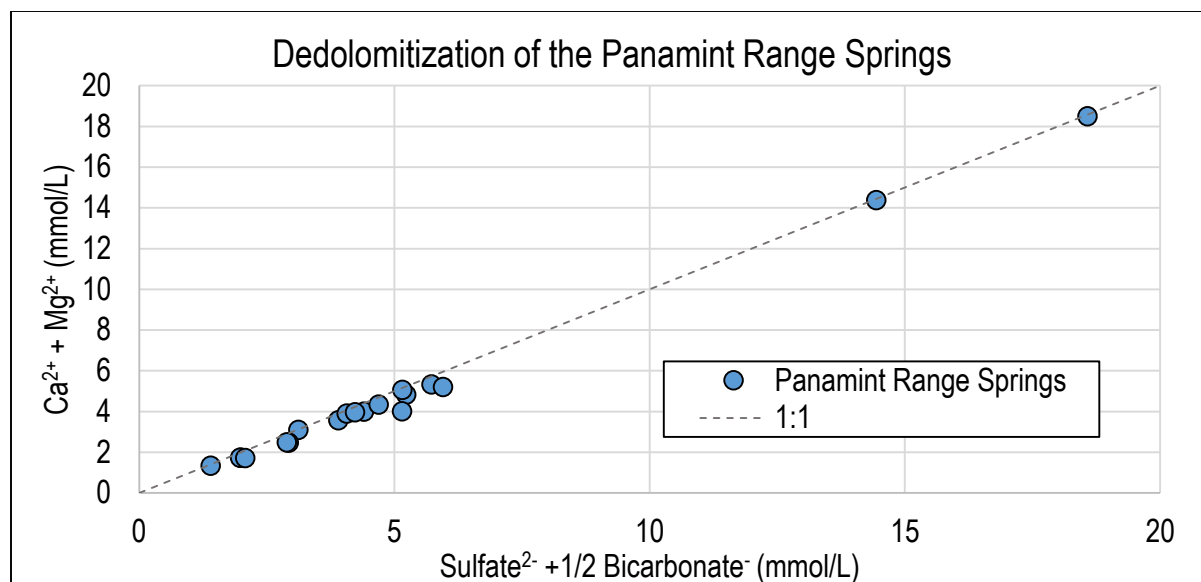
Figure 17. Plot of calcium + magnesium vs sulfate + 1/2*bicarbonate concentrations of the Panamint Range spring dataset with a line indicating a 1:1 linear relationship representing spring dedolomitization (Back et al. 1983; Fisher and Mullican, 1997).

Tritium and Chlorine-36

Chlorine-36 ratios (^{36}Cl/Cl) and tritium are compared to spring emergence elevation in Figure 18 and Figure 19. Tritium concentrations were highest at high elevations and were lowest at low elevations approaching tritium dead (Figure 18). Chlorine-36 concentrations exhibited the same trend with elevation (Figure 19). Spring ^{36}Cl/Cl ratios were highest at high elevations and lowest at low elevations. Figure 20 shows the relationship between tritium and chlorine-36 ratios with springs colored according to elevation groups presented in Figure 18 and Figure 19. The spring waters with elevated tritium and chlorine-36 were at both high and middle elevation ranges (1200 – 2500 m above sea level). Elevated ratios of chlorine-36 and tritium are identified in Figure 18, Figure 19, and Figure 20 indicate bomb-pulse derived recharge at these locations and must be discharging groundwater that recharged around the bomb-pulse (approximately 60 years ago) when atmospheric concentrations were at their highest.
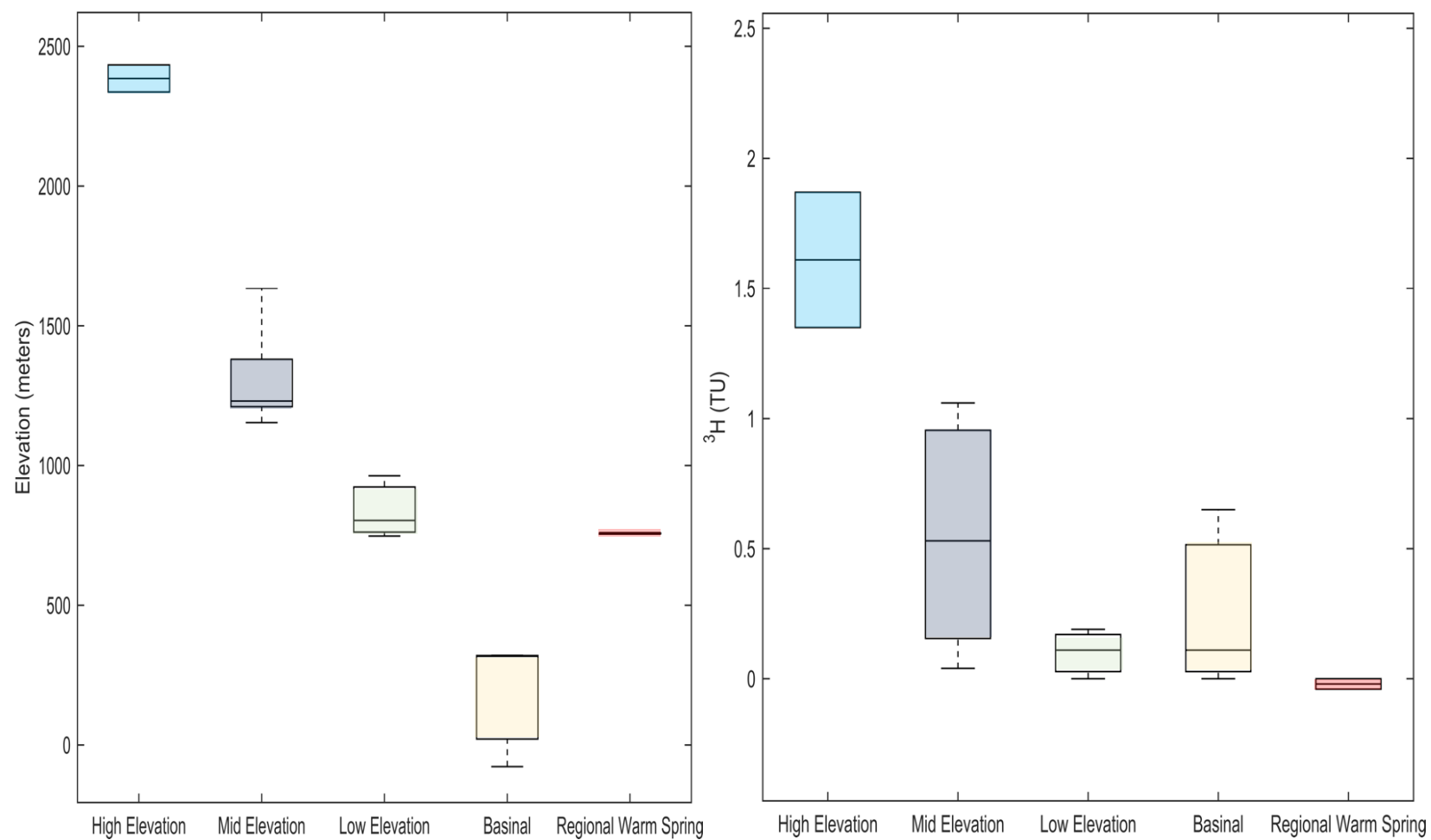
Figure 18. Box plots of spring tritium concentrations color-coordinated with a distribution of spring emergence elevations.
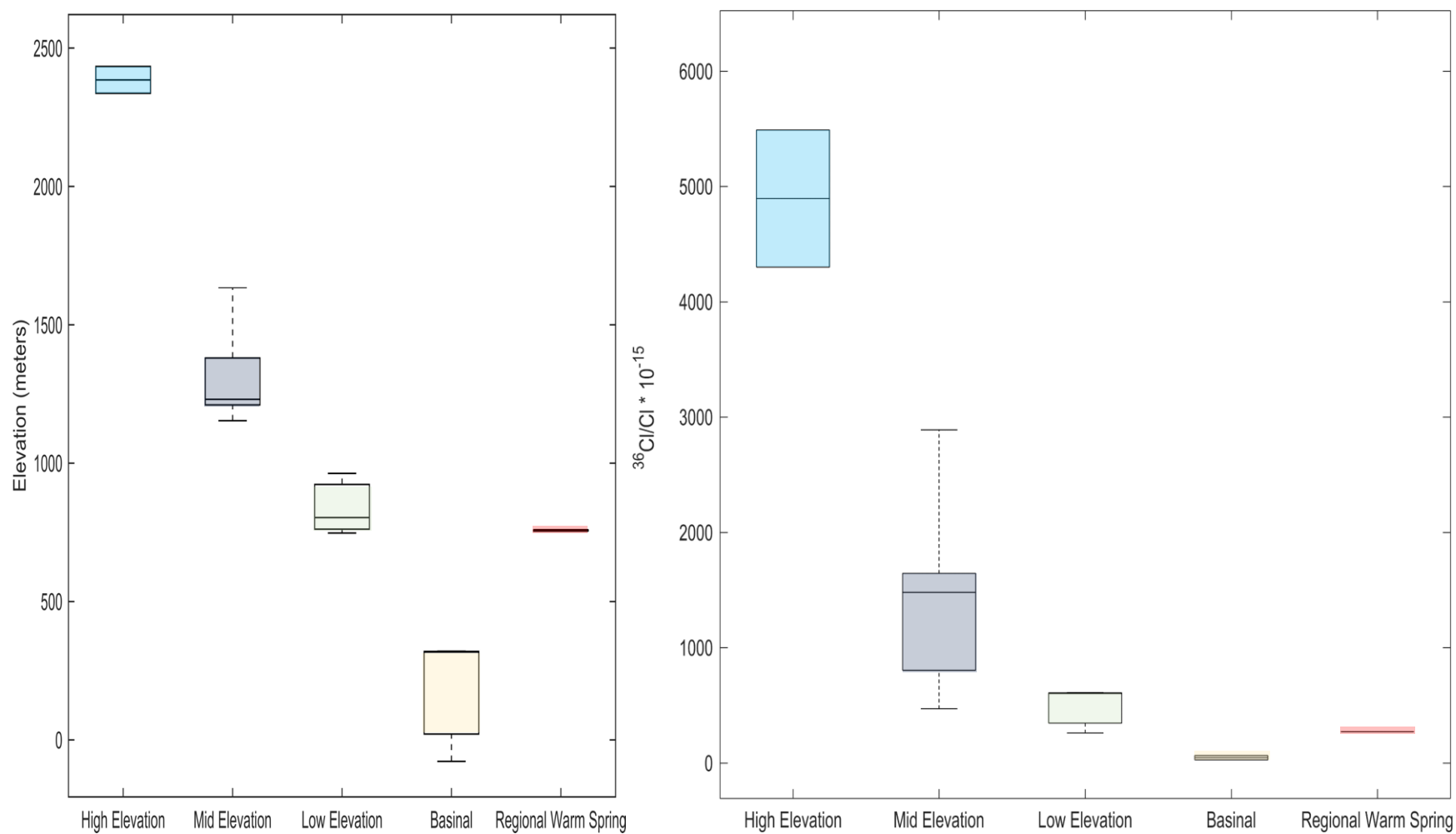
Figure 19. Box plots of spring Chlorine-36 concentrations color-coordinated with a distribution of spring emergence elevations.
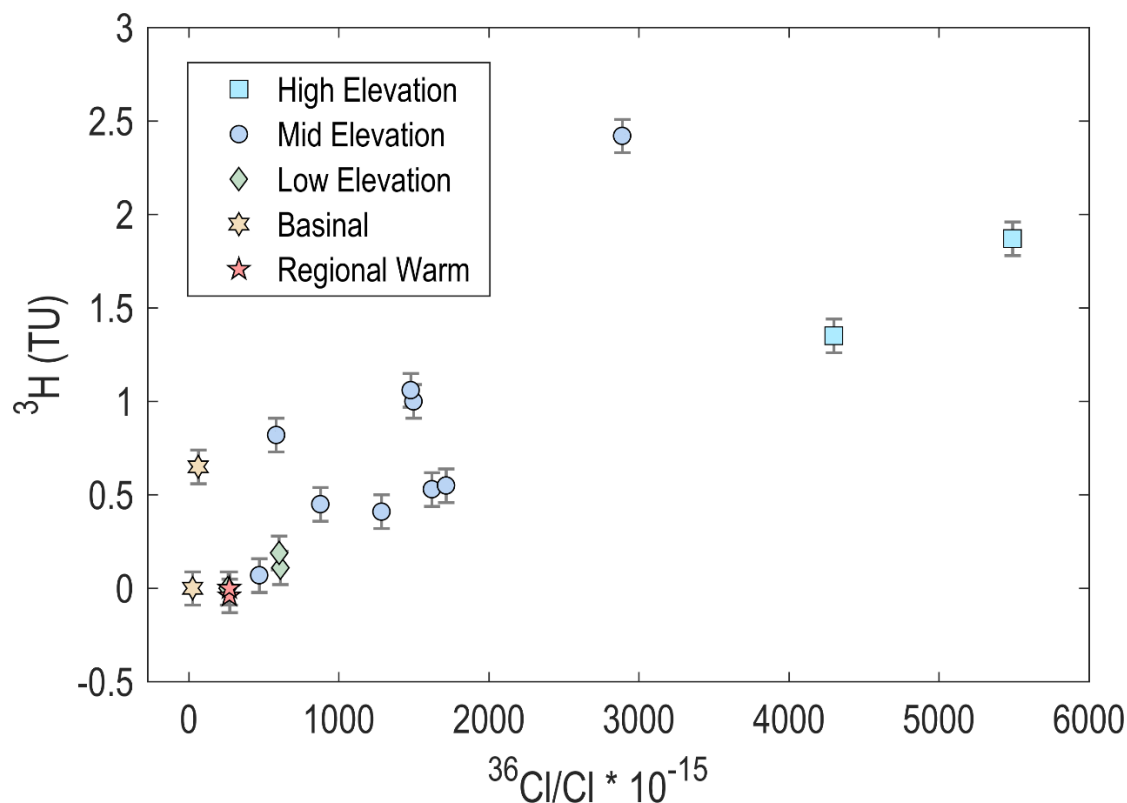
Figure 20. Spring tritium concentration vs Chlorine-36 ratios shown with color coordination related to spring emergence elevation group.

Figure 21 displays the relationships explored in Figure 20 but is expanded to show two possible groundwater flowpath families. The Hanaupah Canyon spring complex (bold text) and orange line defines one flowpath family while the remaining springs define a second groundwater pathway flowpath family in the Panamint Range. Springs which have ^{36}Cl/Cl ratios influenced by mixing with evaporites are separate from these trends and are highlighted in yellow. Mixing with evaporites or basin brines will dilute the ^{36}Cl/Cl of a spring and therefore mask its background ^{36}Cl/Cl ratio.
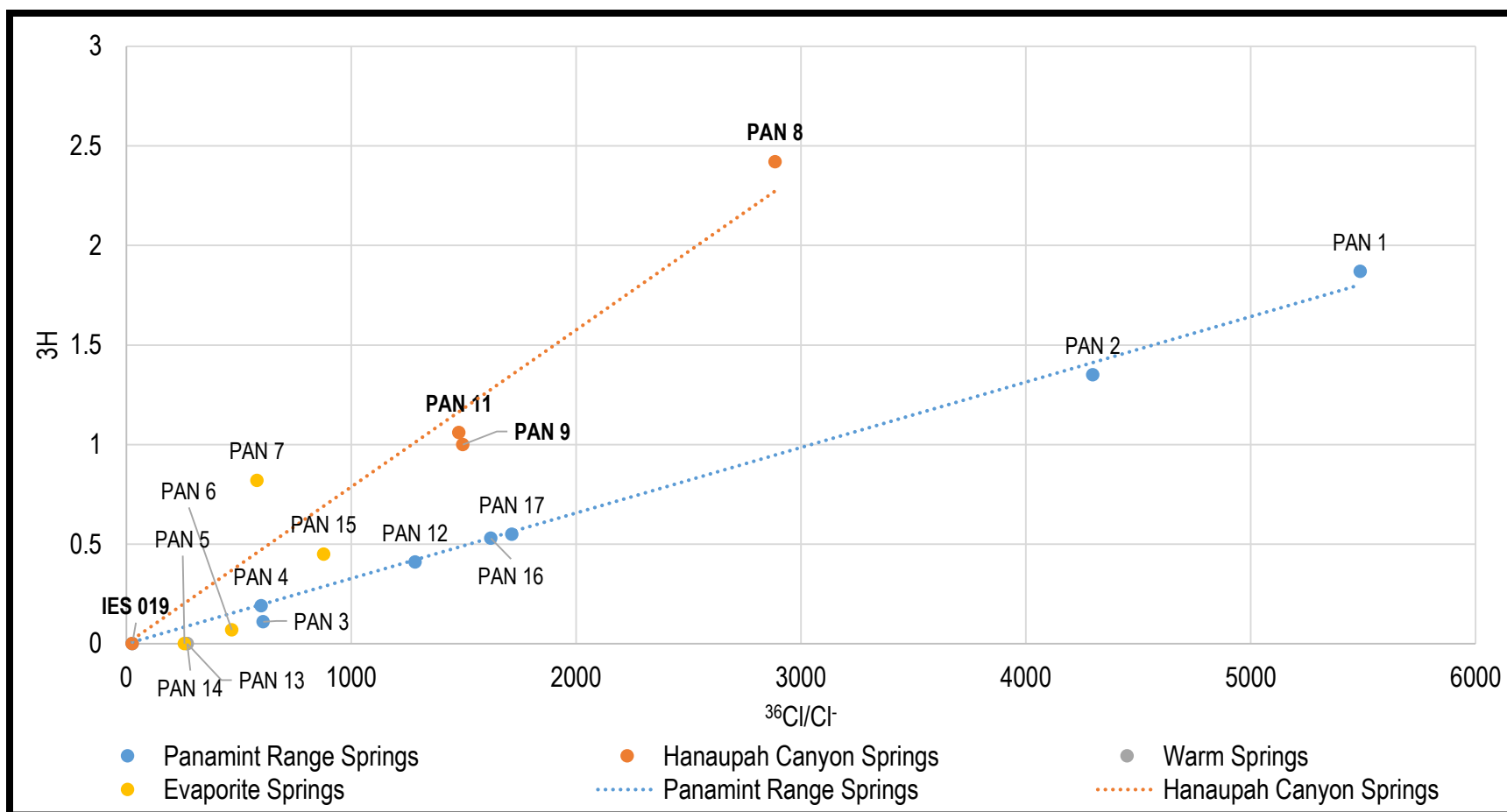
Figure 21. Proposed groundwater flowpath families developed from trends in Chlorine-36 ratios and tritium concentrations of select springs. Drainage samples i.e. non-spring water samples were (PAN 10 and PAN 18) omitted in this plot because they capture potential surface water rather than groundwater flowpaths.

Tritium Residence Times

The TracerLPM tritium time-series-based dispersion model was successful for all 17 springs. The dispersion parameter and mean residence time calculated for each of these springs is given in Table 7 along with the spring name, elevation, tritium (TU), and ^{36}Cl/Cl for reference. Residence time estimates of the tritium dispersion model ranged between 67 years and 1160 years with the shortest residence times in the Hanaupah Canyon spring complex and high elevation springs (Jail Spring and Thorndike Spring). The longest modeled spring residence times were in Pleasant Canyon (Unnamed Panamint Spring E and F) and at Upper Emigrant Spring. These residence times have a zero modeled error because the solution converged exactly on these parameters, however an error of zero is not likely the true error as both the tritium time series and spring tritium values have measurement errors associated with them that would propagate throughout the model. The mixing model also assumes a well-mixed aquifer that receives fully integrated random recharge with tritium values that range between 0.1 and 0.25 TU. The limits of the mixing model are also dictated by the length of the time series (currently 1850-2020) and suggest that residence times of spring waters below 2 TU should have residence times around 200 years. Future research will investigate the input function and its impact on tritium residence times.

Table 7. Spring residence time estimations from a tritium time-series-based dispersion model.

Spring Name	Sampling Date	Elevation (m)	TU	^{36}Cl/Cl	Mean Residence Time (years)	Dispersion Parameter
Jail Spring	5/24/2017	2434	1.87	5487	109	0.31
Thorndike Spring	5/25/2017	2337	1.35	4298	208	0.85
Uppermost Spring	5/31/2017	1633	0.45	877	426	0.78
Apron Spring	5/27/2017	1606	0.82	581	172	0.27
High Noon Spring	5/27/2017	1419	0.07	468	622	0.6
Main Hanaupah Spring #2	5/28/2017	1265	2.42	2885	67	0.41
Main Hanaupah Spring #1	5/28/2017	1258	1	1496	307	0.99
Upper Emigrant Spring	5/19/2016	1231	0.02	NO DATA	1160	0.92
Poplar Spring	3/13/2017	1225	0.15	NO DATA	695	0.87
Limekiln Spring	6/1/2017	1223	0.53	1620	361	0.69
Unnamed Panamint Spring C	6/1/2017	1206	0.55	1715	415	0.86
Wilson Spring	5/29/2017	1195	0.41	1285	388	0.65
South Hanaupah Spring #3	5/28/2017	1154	1.06	1479	244	0.73
Unnamed Panamint Spring E	5/26/2017	963	0.11	609	625	0.69
Unnamed Panamint Spring F	5/26/2017	803	0.19	600	658	0.89
Post Office Spring	6/2/2017	321	0.65	64	388	0.89
Warm Sulfur Spring	6/1/2017	318	0.11	NO DATA	625	0.69

Figure 22 displays the relationship between the modeled tritium residence time estimation and the ^{36}Cl ratios of the spring water dataset. Basin spring Post Office Spring was not included in this comparison because of the influence of brines on this spring that is likely manipulating it ^{36}Cl ratio. Spring waters without ^{36}Cl/Cl measurements were also not included in Figure 22 (Table 7). Figure 22 shows a linear negative relationship between the tritium and ^{36}Cl/Cl values of these springs such that residence times decrease with increasing ^{36}Cl ratios. Hanaupah Canyon springs and the Pleasant Canyon springs (Unnamed Panamint Spring E and F) are identified as outliers to this trend in Figure 22. Tracer/tracer dispersion modeling approaches were also attempted between the tritium and ^{36}Cl measurements for the spring waters however these models only converged for springs with ^{36}Cl ratios greater than 4000 (Jail Spring and Thorndike Spring).
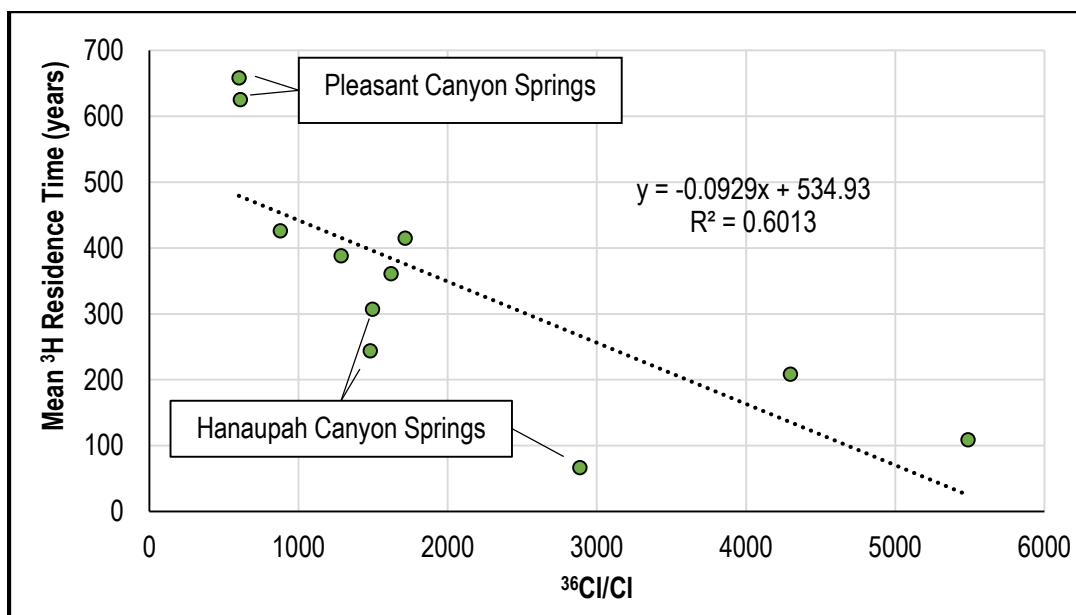
Figure 22. Plot of the modeled mean tritium residence times versus ^{36}Cl ratios of the Panamint Range springs.

^{87}Sr/^{86}Sr and Groundwater Flowpaths

^{87}Sr/^{86}Sr ratios for the Panamint Range spring waters grouped by the drainage or canyon in which they emerge is presented in Figure 23 and Table 8. Alternative flowpath families A, B, and C are also identified on this figure using colored boxes based on horizontal trends in the data that represent ^{87}Sr/^{86}Sr ratios. This figure also contains multiple rock leaching (RL) samples and the whole rock strontium ratios for the following formations from Paces et al. (2007); the Stirling Quartzite, the Johnnie Formation, the Noonday Dolomite, the Kingston Peak Formation, the Beck Spring Dolomite, and the Crystal Spring Formation (Pahrump Group). These formations are the predominant geologies in the Panamint Range and they all had the same ^{87}Sr/^{86}Sr ratio of 0.7055 so they are all represented as a single 'whole rock' value in Figure 23 (Paces et al. 2007). The springs, their ^{87}Sr/^{86}Sr, their Sr^{2+} concentrations (mg/L), their $1/Sr^{2+}$ values and their drainage groups are reported in Table 8. PAN 1, PAN 12, PAN 15 & IES-047 were not grouped because they were the only springs sampled in their drainages. The results of the rock leaching done on

select rock samples collected in the field is given in Table 8 along with an indication of which drainage group each RL sample is most similar to in the last column.

Table 8. Measured $^{87}Sr/^{86}Sr$ and Sr^{2+}(mg/L) of the spring dataset divided by emergence drainage.

Sample Name	$^{87}Sr/^{86}Sr$	Sr^{2+}	$1/Sr^{2+}$	Drainage Group
PAN1- Jail Spring	0.72875	0.17	5.78	Jail Spring
PAN2-Thorndike Spring	0.72168	0.28	3.58	Wildrose Canyon
PAN3- Unnamed Panamint Spring E	0.73236	0.81	1.23	Pleasant Canyon
PAN4- Unnamed Panamint Spring F	0.73164	0.80	1.25	Pleasant Canyon
PAN5- Wheel Spring	0.72323	0.56	1.78	Trail Canyon
PAN6- High Noon Spring	0.72146	3.00	0.33	Trail Canyon
PAN7- Apron Spring	0.72479	1.44	0.69	Trail Canyon
PAN8- Main Hanaupah Spring #2	0.71889	0.11	9.26	Hanaupah Canyon
PAN9-Main Hanaupah Spring #1	0.71579	0.22	4.57	Hanaupah Canyon
PAN10- Hanaupah Canyon	0.71579	0.15	6.90	Hanaupah Canyon
PAN11- South Hanaupah Spring #3	0.71674	0.52	1.93	Hanaupah Canyon
PAN12- Wilson Spring	0.71418	1.06	0.94	Wilson Spring
PAN13- Lower Warm Spring A	0.71245	0.81	1.23	Warm Spring Canyon
PAN14- Lower Warm Spring B	0.71249	0.81	1.24	Warm Spring Canyon
PAN15- Uppermost Spring	0.73342	1.85	0.54	Uppermost Spring
PAN16- Limekiln Spring	0.73373	0.46	2.17	Surprise Canyon
PAN17- Unnamed Panamint Spring C	0.73311	0.45	2.22	Surprise Canyon
PAN18- Surprise Canyon	0.73329	0.51	1.97	Surprise Canyon
PAN19- Warm Sulfur Spring	0.72393	0.86	1.16	Surprise Canyon
PAN20- Post Office Spring	0.72373	8.78	0.11	Pleasant Canyon
IES-047 Poplar Spring	0.71645	1.19	0.84	Wildrose Canyon
IES-045 Upper Emigrant Spring	0.72198	0.89	1.12	Emigrant Spring
IES-019 Tule Spring	0.71701	2.41	0.41	Hanaupah Canyon
Noonday Dolomite RL 1	0.72292	n/a	n/a	Trail Canyon
Johnnie Formation RL	0.72223	n/a	n/a	Trail Canyon
Carrara Formation RL	0.72132	n/a	n/a	Trail Canyon
Noonday Dolomite RL 2	0.71659	n/a	n/a	Hanaupah Canyon
Kingston Peak Formation RL	0.71370	n/a	n/a	Wilson Spring
Bird Spring Formation RL	0.71031	n/a	n/a	Warm Spring Canyon
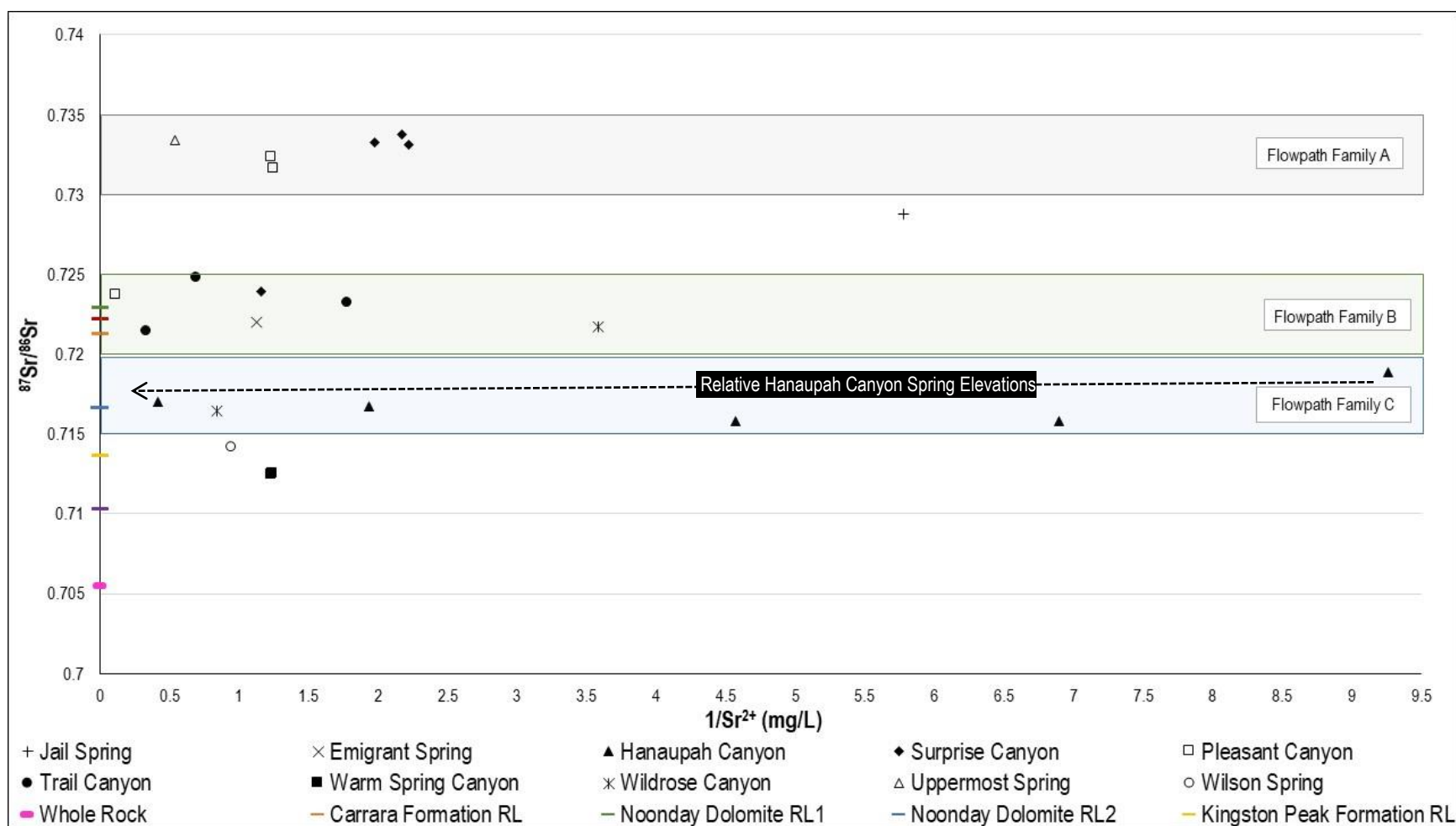
Figure 23. Plot of the $^{87}Sr/^{86}Sr$ vs $1/[Sr^{2+}]$ of the spring dataset grouped by canyon/drainage with proposed flowpaths. Flowpath Family A is shown in grey, Flowpath Family B in green and Flowpath Family C in blue. All whole rock and RL $^{87}Sr/^{86}Sr$ are shown along the y-axis as these estimate do not have a corresponding $1/[Sr^{2+}]$ value. The trend in spring emergence elevation is highlighted using a dashed arrow within Flowpath C.

Radiocarbon and Spring Residence Times

The majority of spring samples showed evidence of equilibration with the atmosphere at the time of collection. This was likely due to the diffuse emergence style that was common in the field and the fact that some springs were sampled far from the spring emergence in the spring run. Figure 24 illustrates this point through the comparison of pmC values and chlorine-normalized ^{36}Cl values. A line was generated between the two field areas at the lower and upper limit of ^{36}Cl concentrations (Lower Warm Spring A and B and Jail Spring) that had the least amount of atmospheric equilibration due to their landscape placements and direct discharge styles. If the springs had all not been un-equilibrated with the atmosphere, then the data should have, in principle, fallen closer to the line. Equilibration with the atmosphere, on the other hand, artificially raises sample pmC (Rose and Davisson 1996). Figure 24 shows that many of the spring pmC values (the orange dots) were well above the zone of un-equilibrated samples (the green line) indicating mixing with atmospheric (totally modern) carbon. Some springs fall in a more ambiguous zone (yellow box) where their pmC values may or may not be the true value for that spring based on the sampling conditions. The samples that fall within the yellow box and along the green line are the only samples appropriate for residence time calculation because they can be assumed to be free of atmospheric equilibration.
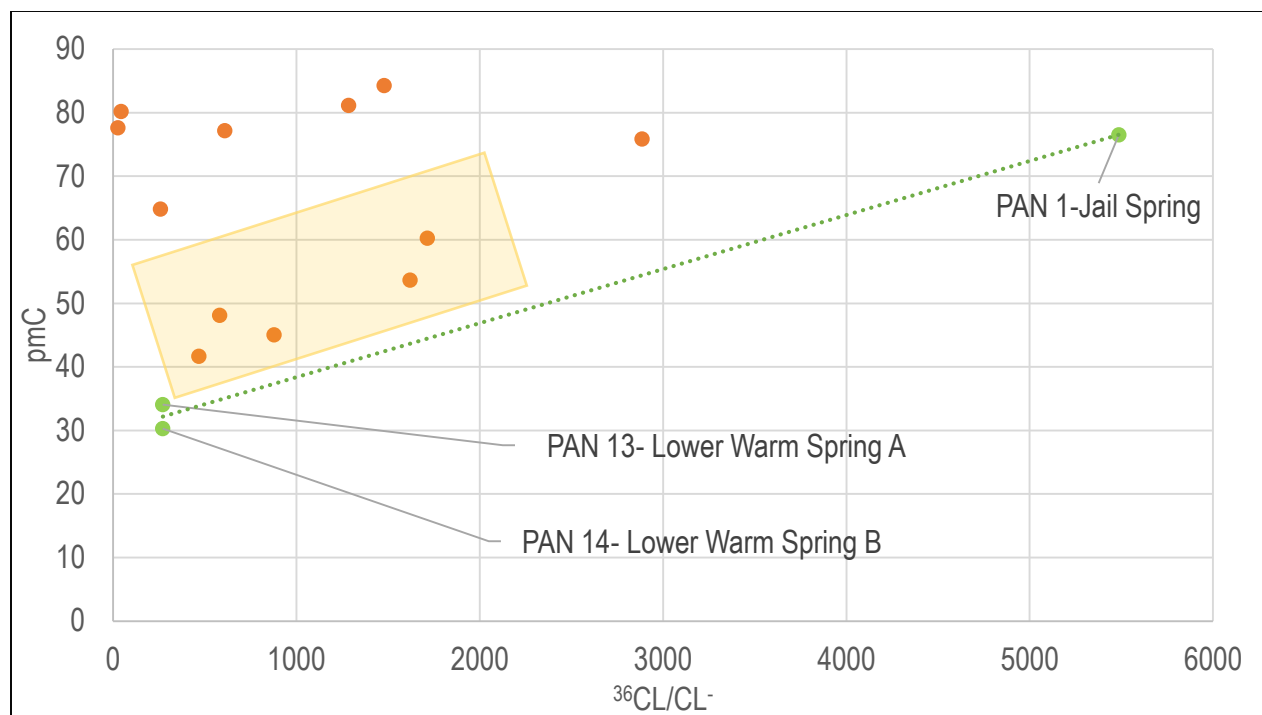
Figure 24. pmC vs normalized ^{36}Cl for the Panamint Range spring dataset. Samples with elevated pmC values are indicated in orange and samples that are not equilibrated with the atmosphere are indicated in green. The samples falling within the orange box simply have elevated pmC values but may have experienced some limited atmospheric equilibration.

Table 9 shows the results of the Netpath modeling using $\delta^{13}C$ values from the model and the measured values to estimate the agreement between the model and the real world. The differences between these values is less than 0.03 for all models, indicating a minimization of modeling errors based on the inputs outlined in Table 5. Table 9 also shows the residence times of the springs according to multiple radiocarbon modeling approaches calculated within NetpathXL. The Fontes and Garnier (1975), Han and Plummer (2013) and Ingerson and Pearson (1964) radiocarbon correction models were determined to be most appropriate for the geologic setting of the Panamint Range. Lower Warm Spring A and B have residences times that ranged from 1414 to 1834 years respectively.

Table 9. Netpath Model Results for Spring Samples Not Equilibrated with the Atmosphere

Sample Name	Computed ^{13}C	Observed ^{13}C	Difference (^{13}C Values)	Ingerson and Pearson Residence Time	Fontes and Garnier Residence Time	Han and Plummer Residence Time
PAN 1-Jail Spring	-9.0931	-9.1	0.0069	-3991	-3968	-3986
PAN 6- High Noon	-5.8075	-5.8	0.0075	-6838	-6838	-6838
PAN 7- Apron Spring	-7.6972	-7.7	0.0028	-10343	-10343	-10343
PAN 13- Lower Warm Spring A	-4.3022	-4.3	0.0022	1409	1421	1412
PAN 14- Lower Warm Spring B	-4.7963	-4.8	0.0037	1829	1842	1832
PAN 15- Uppermost Spring	-10.1911	-10.2	0.0089	-562	-559	-561
PAN 16- Limekiln Spring	-7.5033	-7.5	0.0033	-3604	-3596	-3602
PAN 17- Unnamed Panamint Spring C	-7.8048	-7.8	0.0048	-4521	-4512	-4519
PAN 19- Warm Sulfur Spring	-8.0776	-8.1	0.0224	-2342	-2340	-2342

CFC residence times were also estimated for Lower Warm Spring A (PAN 13) and Lower Warm Spring B but these samples yielded very small CFC concentrations indicating that little, if any, CFCs are present in the spring discharge. Table 10 displays the concentrations of CFC-12, CFC-13, and CFC-113 corrected using the USGS (2014) spreadsheet for analyzing CFC data. These springs contain a substantial proportion of recharge older than approximately 70 years (Figure 10; Clark and Fritz, 1997).

Table 10. Corrected CFC concentrations for Lower Warm Spring A and B.

Sample Name	Sample Date	Sampling Time	Corrected concentrations			Percent error in concentrations		
			CFC-12	CFC-11	CFC-113	CFC-12	CFC-11	CFC-113
			pmol/kg	pmol/kg	pmol/kg	%	%	%
Pan13-A	05/30/17	8:00 AM	0.478	0.665	0.08	0.01	0.013	0.005
Pan13-B	05/30/17	8:00 AM	0.474	0.66	0.073	0.009	0.013	0.005
Pan13-C	05/30/17	8:00 AM	0.468	0.668	0.072	0.009	0.013	0.005
Pan14-A	05/30/17	10:00 AM	0.436	0.629	0.063	0.009	0.013	0.005
Pan14-B	05/30/17	10:00 AM	0.457	0.657	0	0.009	0.013	0.005
Pan14-C	05/30/17	10:00 AM	0.35	0.053	0.011	0.007	0.005	0.005

Discussion

Additional geologic maps are necessary in order to closely examine the influences of regional geology on groundwater flow in the Panamint Range. Figure 25 is an enlargement of the Workman et al. (2018) geologic map that shows the regional geology present near Hanaupah Canyon on the eastern side of the Panamint Range. Figure 26 shows a similar enlargement of the Workman et al. (2018) geologic map for the western side of the Panamint Range near Surprise Canyon. All geologic units referenced in Figure 25 and Figure 26 are the same as those in the legend presented in Figure 3 for the Workman et al. (2018) geologic map.
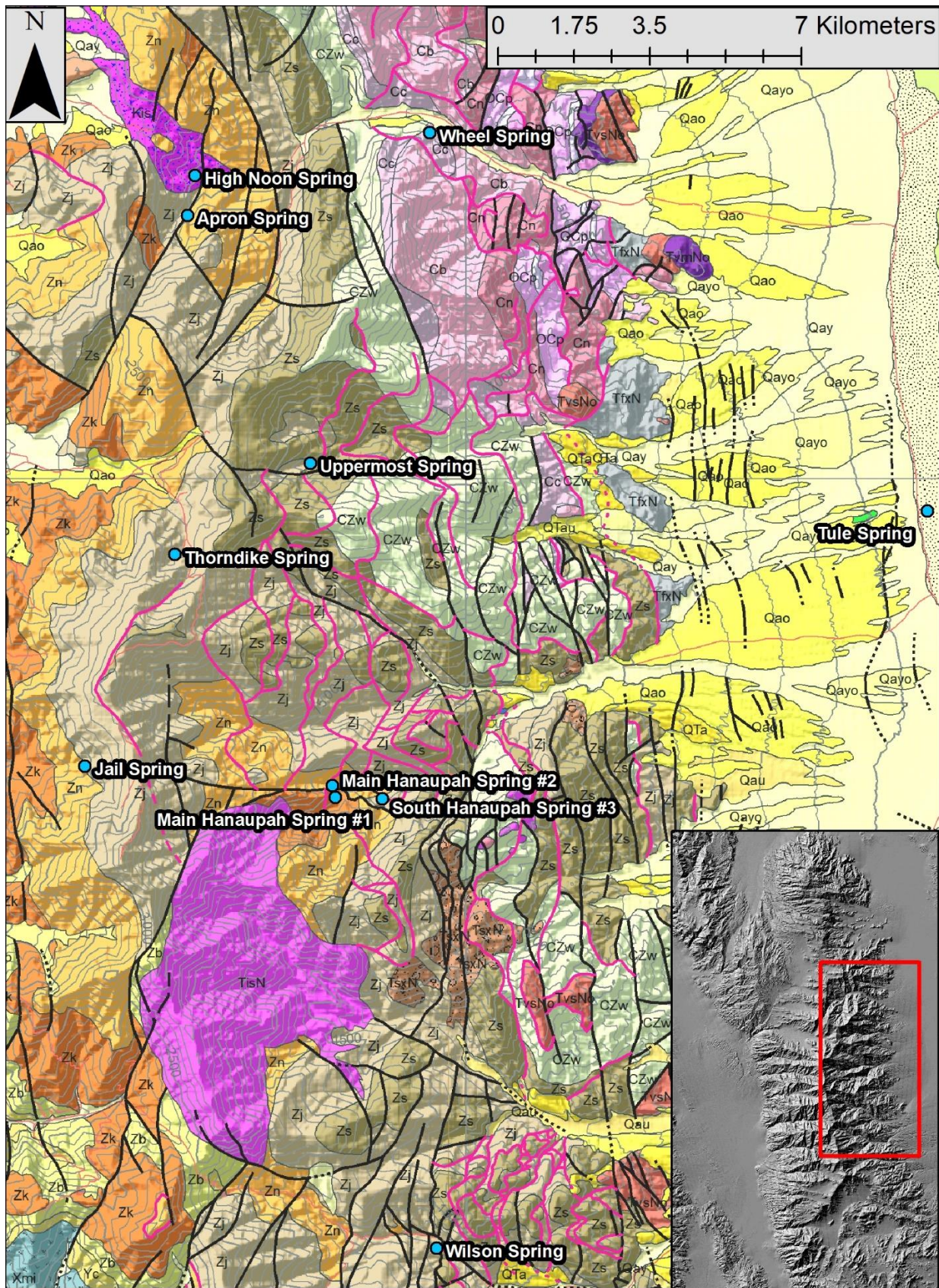
Figure 25. Expansion of the Workman et al. (2018) geologic map near Hanaupah Canyon.

Figure 26. Expansion of the Workman et al. (2018) geologic map near Surprise Canyon.

General Geochemistry

The Principal Component Analysis of the Panamint Range Springs identified three factors as the primary sources for geochemical variance within the spring waters: TDS (PC1), carbonate dissolution (PC2), and temperature/fluoride (PC3). These factors identified in the PCA suggest that carbonate rock must be the primary aquifer supporting the sampled springs. Strong ties to carbonate dissolution separate these springs away from a system with multiple water-bearing units and instead narrows discussion to the carbonates of the Panamint Range as the only aquifer in the mountain block.

The grouping of these springs by their general chemistry can be used to develop a conceptual model for groundwater flow in the Panamint Range. The geochemistry of most spring waters is related only to the length of the flowpath from recharge to discharge. As the flowpaths in this conceptual model increase in length, geochemical evolution also increases. The geochemical groups of the Panamint spring waters are likewise dictated by elevation. For example, Group 1 captures the majority of the sampled springs and represents mountain block springs with local or intermediate flowpaths, Group 2 represents springs with elevated mineral weathering due to evaporite deposits at the spring emergence, Group 3 strictly includes basin springs on both sides of the range with regional flowpaths. Group 4 has only one spring (Post Office Spring) and is influenced by a regional flowpath and the evaporation within the spring pool and/or interactions with solute-rich basin brines established in the previous chapter.

Some exceptions to this simple pathway model were identified by Figure 13 and Figure 14. Lower Warm Springs A and B (PAN 13 and PAN 14), as the only two warm springs, stand out in Figure 14 because of their significantly higher temperatures relative to the other springs in Group 1. The remaining spread in Figure 14 is likely due to a difference in spring discharge in Group 1 that increases temperature in springs with lower discharge within the spring run. The remaining

geochemical groups are simply more chemically evolved relative to Group 1 because of their placement in the landscape (i.e. the springs with regional groundwater flowpaths and interactions with evaporites or brines). This dolomite dissolution identified in Figure 16, in combination with the dolomite dissolution indicated by PC2, support a distinctive carbonate aquifer type conducting flow throughout the range with only slight variation in the dissolving minerals.

Support for a dolomitic aquifer in the Panamint Range comes from the dedolomitization relationship established in Figure 17. The 1:1 relationship in Figure 17 results from the dissolution of dolomite according to the established chemical reaction outlined below as Equation 9 (Raines and Dewers, 1997; Fisher and Mullican, 1997).

$$CaMg(CO3)_2 + CaSO4 \times 2H_2O = 2CaCO_3 + Mg^{2+}(aq) + SO_4{}^{2-}(aq) + 2H_2O \quad \text{(Equation 9)}$$
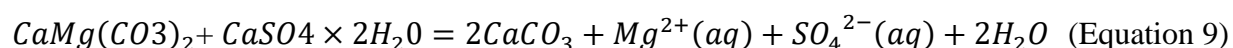
This relationship has been well documented such that the dissolution of gypsum drives continual dissolution of dolomite; as the calcium ion is released into the aquifer, it is subsequently precipitated as calcite (Plummer and Back, 1980; Back et al., 1983; Bischoff et al., 1994). The precipitation of calcite in each PREEQC geochemical model shown in Figure 16 agrees well with this concept of an aquifer undergoing gypsum-driven dedolomitization, as does the placement of the majority on the springs on the trilinear diagram in Figure 15 (Back et al., 1983; Bischoff et al., 1994).

<h3 style="text-align:center">[36]Cl, Tritium, and the Hanaupah Canyon Separation</h3>

The elevation dependence of [36]Cl and tritium in the Panamint Range implies an increase in residence time and flowpath length as elevation decreases, as expected for groundwater flow in the mountain block fueled by MBR (Wilson and Guan, 2004; Manning and Solomon, 2005). However, the presence of very high [36]Cl/Cl at elevation in the Panamint Range suggests that there is substantial storage at high elevations that is allowing for spring residence times high in the

mountain block to fall within the approximate 40-60-year window for above-background 36Cl deposition (Clark and Fritz, 1997). The tritium residence time estimates further support this idea as even the shortest residence time was 66 years and from within the mountain block at an elevation of approximately 1200m (Table 7). Therefore, the high elevation springs of the Panamint Range must have enough mountain block storage to retain waters for several decades before they are discharged.

Tritium and ^{36}Cl have two different fallout curves after they were introduced into the atmosphere during nuclear testing (Clark and Fritz, 1997). Peak ^{36}Cl fallout in the Panamint mountains was likely around 1957 (Clark and Fritz, 1997) and the time of peak tritium fallout was around 1964 according to the dataset from Modesto, CA published by Michel, (1989). Tritium enrichment in Hanaupah Canyon relative to the other springs (Figure 21; Figure 22) is therefore likely the result of slightly shorter residence times for the springs along the Hanaupah Canyon Fault (more recent recharge).

Indeed, previous studies indicate that faults may act as conduits rather than barriers to flow (Bense and Person, 2006; Celico et al., 2006) thus, the Hanaupah Canyon Fault may fit well within this vein of hydrologic study but further, more specific study on the fault is recommended before such claims can be confirmed. However, the development of a detailed geologic map by Workman et al. (2018) on the field area helps to illustrate such observations by overlaying spring emergence locations over detailed depictions of faults and geologic contacts. Figure 25 shows the Hanauaph Canyon spring complex emerging along a fault and near an intrusive body. One or both of these geologic features are likely directing flow into Hanaupah Canyon and changing mountain block storage near the drainage, accounting for the elevated tritium of these spring waters relative to its ^{36}Cl/Cl (Figure 21; Figure 22).

<u>^{87}Sr/^{86}Sr and Groundwater Flowpaths</u>

Strontium ratios in the Panamint Range spring waters exhibit a variety of distributions related to the location of the spring emergence. Strontium in spring waters is sourced from minerals that the waters are actively weathering (Clark and Fritz, 1997). In this way, strontium concentration (or $1/Sr^{2+}$ value) also indicates a relative residence time since strontium release is kinetically controlled (Frisbee et al., 2017). High values of $1/Sr^{2+}$ are indicative of short residence time waters and low values of $1/Sr^{2+}$ are likely showing longer residence times. Based on this relationship, lower $1/Sr^{2+}$ values in Figure 23 show longer relative residence times and higher $1/Sr^{2+}$ values indicate shorter residence times.

The kinetic nature of strontium dissolution and the conservative ^{87}Sr/^{86}Sr ratios that it generates are often used to identify groundwater flowpaths (Clow et al., 1997; Hogan, 2003; Wang et al., 2005; Shand et al., 2007; Raiber et al., 2009). Flowpath Families A, B, and C in Figure 23 are based on the ^{87}Sr/^{86}Sr ratios. These ^{87}Sr/^{86}Sr values were then compared with ^{87}Sr/^{86}Sr results from lab rock leaching (RL) experiments to identify the primary rock/water interactions occurring along the flowpaths of the Panamint Range springs. Whole rock strontium estimates from Paces et al., (2007) were all significantly lower than the observed spring waters values so the RL samples were used heavily to draw comparisons. The disparity between the range of whole rock and RL strontium ratios were the result of differential weathering between the whole rock samples and the physically/chemically weathered RL samples. Flowpath Family A is the major exception to this approach because it does not have a known RL endmember (Figure 23).

The oldest geologic unit mapped in the Panamint Range is the Proterozoic World Beater Complex (Albee et al., 1981). This unit is also represented as undifferentiated Paleoproterozoic basement rock in the Workman et al. (2018) geologic map (Figure 26). Figure 26 shows this unit emerging up Surprise Canyon and Pleasant Canyon but not necessarily near Uppermost Spring

(see Figure 25). The World Beater Complex may therefore be the missing RL samples needed to create a $^{87}Sr/^{86}Sr$ end member that matches up with the springs in Flowpath Family A. Jail Spring also does not have a RL value associated with it but appears somewhat related in terms of $^{87}Sr/^{86}Sr$ to these older geologic units (Figure 23). The fact that Uppermost Spring still groups with Surprise Canyon and Pleasant Canyon in terms of $^{87}Sr/^{86}Sr$ despite emerging in a Johnnie Formation/Stirling Quartzite contact (Figure 25) suggests that either the World Beater Complex may also be interfering with Uppermost Spring at depth or that there are additional sources of radiogenic strontium near this emergence. Additional sources or radiogenic strontium may also be the justification for the elevated $^{87}Sr/^{86}Sr$ in the all springs in Flowpath Family A rather than just a missing RL endmember from the World Beater Complex.

Flowpath Family B is somewhat ambiguous because there are three RL samples in this flowpath; the Noonday Dolomite, the Carrara Formation, and the Johnnie Formation. Geochemical data from these springs indicate a strong dedolomitization trend (Figure 17; Back et al., 1983), which suggests that Flowpath Family B is likely dominated either by flow through the Noonday Dolomite or through the dolomite layers/cements of the Johnnie Formation as the younger Carrara Formation is comprised entirely of limestone and terrigenous clastic rock instead of dolomite (Palmer and Halley, 1979). Flow through the Noonday Dolomite/Johnnie Formation contact area is likely present along flowpaths of springs emerging in Pleasant Canyon, Trail Canyon, Surprise Canyon, Emigrant Spring and Wildrose Canyon (Figure 23).

Flowpath Family C presents a clear correlation between the $^{87}Sr/^{86}Sr$ values of the Noonday Dolomite RL sample, Hanaupah Canyon springs, and Poplar Spring (Wildrose Canyon). Due to the heterogeneity of the Noonday Dolomite and its members as outlined by Petterson et al., (2011), it is not unexpected that the two RL samples from this unit returned different $^{87}Sr/^{86}Sr$ values. A

continuum of groundwater flow that extends from the mid-elevation emergences of the Hanaupah spring complex, past the mountain front, all the way to Tule Spring in Badwater Basin is observed with relative $1/Sr^{2+}$ spring residence times that increase as spring elevations decrease similar to trends shown in Frisbee et al. (2017). This flowpath family confirms a connection previously suggested by Li et al. (1997) and Lowenstein and Risacher (2009) between groundwater flow in Hanaupah Canyon and groundwater flow to Tule Spring.

The final three $^{87}Sr/^{86}Sr$ samples, Wilson Spring and the two Lower Warm Springs fall in between the Kingston Peak and Bird Spring Formation RL samples in Figure 23. Lower Warm Spring A and B emerge in an allochthon of Bird Spring Formation (Lower Permian) surrounded by significantly older units (i.e. the Proterozoic Pahrump Group) that are much further down section (Workman et al., 2018). Therefore, the strontium ratios from these spring waters may be elevated away from the Bird Spring Formation RL values due to interactions of additional units of contrasting age. The Wilson Spring sample can likewise be better understood in the context of its geology. While Wilson Spring emerges near the Johnnie Formation and Noonday Dolomite, it is also emerging near younger alluvium (Workman et al., 2018) that can skew the strontium concentrations younger at this location.

<u>Tule Spring End Member Mixing Analysis</u>

Based on the $^{87}Sr/^{86}Sr$ data connecting Tule Spring and Hanaupah Canyon, a two end member mixing model was prepared in order to attempt to quantify the proportion of water contributing to Tule Spring directly from the Hanaupah Canyon spring complex. This kind of mixing analysis is commonly used in hydrogeochemistry to estimate the amount of mixing contributing to a spring water between two known chemical end members (Frisbee et al., 2017). In this case, ^{36}Cl was the conservative tracer picked to evaluate the degree of mixing between Main

Hanaupah Spring #2 (^{36}Cl ratio of 2885) and the basin brines that characterize this region (assumed to have a ^{36}Cl ratio of 1) within Tule Spring (^{36}Cl ratio of 27). The brine water 36Cl ratio of 1 is a reasonable assumption because these waters would be so saline that the Cl concentration would minimize the 36Cl greatly until it reaches ratios similar to that of seawater (^{36}Cl/Cl= 0.5 as reported by Argento et al., 2010). Equation 10 represents the mixing model used to evaluate these proportions where f_1 and f_2 are some fraction of the whole ^{36}Cl/Cl value:

$$^{36}Cl/Cl_{Tule\ Spring} = \ ^{36}Cl/Cl_{Brine} \times f_1 + \ ^{36}Cl/Cl_{Hanaupah\ Canyon} \times f_2 \qquad \text{(Equation 10)}$$

While the brine ^{36}Cl/Cl was allowed to vary between 0.1 and 27 (the ^{36}Cl/Cl of Tule Spring), the model itself only converged on the measured ratio from Tule Spring when the ^{36}Cl/Cl$_{Brine}$ value was set to 1. This model supported that approximately 99% of water in Tule Spring is sourced from basin brines with the remaining 1.0% of water sourced from Hanaupah Canyon.

Spring Residence Times

TracerLPM dispersion models based on spring tritium and a time series of atmospheric deposition were used to estimate spring residence times in the Panamint Range. Only 17 of the springs in this study were modeled as some samples were tritium dead (particularly in basin springs). Out of these models, several patterns emerged in the distribution of residence times between the springs in this study. High elevation springs and springs in Hanaupah Canyon returned the shortest groundwater residence times, with the longest residence times in Upper Emigrant Spring, Unnamed Panamint Spring E, and Unnamed Panamint Spring F (Table 7). As shown in Figure 22, these springs deviate from the larger pattern of spring residence times which generally decreases with increasing ^{36}Cl at higher elevations. Residence times in Hanaupah Canyon ranged from 67 to 307 years and residence times in Pleasant Canyon (Unnamed Panamint Springs E and F) ranged between 625 and 658 years (Table 7).

Radiocarbon was also used to estimate groundwater residence time in the Panamint Range yet many samples were too equilibrated with atmospheric sources of carbon to calculate spring residence times (Figure 24). Some samples also fell outside of the 1,000- to 40,000-years-old window in which radiometric dating with ^{14}C is possible, particularly those with elevated tritium concentrations (Figure 10; Clark and Fritz, 1997). For these reasons, only the Lower Warm Spring A and B samples returned a positive age after they were modeled in NetpathXL. Lower Warm Spring A returned a residence time of approximately 1414 years and Lower Warm Spring B returned a residence time of approximately 1834 years. The higher temperatures of these spring waters relative to the others indicate a deeper circulation depth for these waters before they emerge as springs, increasing their residence times relative to the other Panamint Range springs sampled (Appendix B; Allen et al., 2005). The proximity of these springs to a major fault system likewise supports pathways toward deeper circulation that is unique only to this area of the Panamint Range (Blair, 1999; Workman et al. 2002).

While a residence time was not established for every spring in this investigation, the consistency in the spring geochemistry for the majority of the springs combined with the heterogeneity in the residence times that were found support a heterogeneous topography-driven groundwater flow model (Toth, 1963). A heterogeneous topography-driven groundwater flow model in this context represents a flow system where waters are generally getting older and more chemically evolved as spring emergence elevation decreases yet there are differences in mountain block storage and flow velocity between canyons and along variable flowpaths. For example, the Hanaupah Canyon spring complex appears to be discharging younger groundwater than surrounding drainages, yet Tule Spring (the basin spring at the end of the Hanaupah Canyon flowpath family) still follows a topography-driven groundwater flow model in that it is composed

of highly chemically evolved groundwater likely associated with a longer residence time than those in the mountain block. Surprise Canyon also shows some degree of geochemical evolution from high to low elevations yet its mountain block spring residence times (625-658 years) are much higher than the flow system in Hanaupah Canyon. In this way, localized geology within each drainage in the Panamint Range is greatly impacting groundwater flow processes within that drainage even though the overall mechanism driving flow is likely the same: topography-driven flow. An important exception to this kind of pattern is in Lower Warm Spring A and B as it is likely receiving more deeply-circulating groundwater flow driven by faulting rather than topography. Due to the heterogeneous nature of this groundwater flow model, further study into the differences in mountain block storage across the Panamint Range is recommended.

There is an assumption of piston flow to the spring for many of these residence time estimations. In these cases, the times reported are representative of all parts of the groundwater flow system despite the heterogeneities in groundwater flow that may be present in a natural flow system (Campana and Simpson, 1984; Plummer et al., 2001). The tritium dispersion models attempt to add greater complexity into the modeling of this flow system by incorporating the advection and dispersion equation but neither model is likely completely representative of flow as there was heterogeneity found in all residence time estimations (i.e. atmospheric equilibration in ^{14}C samples collected at the spring source). These sources of uncertainty can include anything from carbonate aquifer bifurcation to the mixing of groundwater of different ages and are considerations in the study of any natural groundwater flow system (Campana and Simpson, 1984).

Conclusions

The Principal Component Analysis of the Panamint Range Springs identified three factors as the primary sources of geochemical variance in these waters: TDS, carbonate dissolution, and

temperature. The carbonate dissolution in these springs was of particular importance, as the spring general geochemistry supported the classification of this aquifer as dolomite through gypsum-driven dedolomitization in most of the springs sampled (Back et al., 1983; Bischoff et al., 1994; Li et al., 1997). This classification implies that the dolomite units of the Panamint Range are conducting flow to the majority of its springs and are actively precipitating calcite, as indicated in the inverse geochemical modeling shown in Figure 16.

Flow path information from $^{87}Sr/^{86}Sr$ further supports the importance of dolomites in the region by identifying the Noonday Dolomite as the primary aquifer for several groups of springs with similarly weathered minerals. The Hanaupah Canyon spring group in Figure 23 shows the most distinctive groundwater flowpath highlighted by the strontium data and demonstrates a connection between the mid elevation springs of the Hanaupah Canyon spring complex and Tule Spring in Badwater basin. Groundwater flow in the Panamint Range is therefore dictated primarily by topography despite faulting along the mountain front.

Spring water residence times in the Panamint Range, however, indicate flow through a relatively heterogeneous groundwater flow system. Tritium-based spring residence time models estimate residence times as young as 67 years in Hanaupah Canyon and as old as 658 years in Pleasant Canyon. Lower Warm Springs A and B (Warm Spring Canyon) exhibit signs of deeper circulation depths based on their elevated temperatures and bedrock emergence styles near a mapped fault. Radiocarbon residence time estimates were inconclusive for the majority of the springs sampled but they were effective for Lower Warm Spring A and B, likely because of these longer groundwater flowpaths present at these sites based on these elevated circulation depths. Groundwater residence times from ^{14}C of 1414 and 1834 years were calculated at Lower Warm Spring A and B (respectively).

The 60 to 1800 year turnover rate of groundwaters for springs in the Panamint Range springs highlights a key landscape vulnerability for the spring ecosystems supported by these local-to intermediate-scale groundwater flowpaths. The vast majority of springs in the mountain block have mean residence times less than 700 years. With relatively short groundwater residence times the majority of the Panamint Range spring ecosystems are more vulnerable to perturbations in climate than springs supported by longer flowpaths. Changes in recharge are especially important to consider as significant droughts in southern California have already reduced the source of MBR in this system over the last decade (Borsa et al., 2014). While groundwater flow from the Panamint Range may only affect a few rural communities, results presented here support a simple topography-driven groundwater flow model that could be applied to similar ranges in the southern Great Basin near larger communities. This conceptual model will better inform the broader understanding of groundwater flow throughout the Great Basin in times of changing climate.

References

Albee, A.L., T.C. Labotka, M.A. Lanphere, & S.D. McDowell (1981). Geologic Map of Telescope Peak Quadrangle, California. *U.S. Geological Survey*. Map of GQ-1532.

Allen, D.M., S.E. Grasby, & D.A. Voormeij (2005). Determining the circulation depth of thermal springs in the southern Rocky Mountain Trench, south-eastern British Columbia, Canada using geothermometry and borehole temperature logs. *Hydrogeology Journal*, 14, 159-172.

Argento, D.C., J.O. Stone, L.K. Fifield, & S.G. Tims (2010). Chlorine-36 in seawater. *Nuclear Instruments and Methods in Physics Research B*, 268, 1226-1228.

Back, W., B. Hanshaw, N. Plummer, P. Rahn, C. Rightmire, & M. Rubin (1983), Process and rate of dedolomitization: Mass transfer and 14C dating in a regional carbonate aquifer. *Geological Society of America Bulletin*, 94, 1415-1429.

Bailey, T.R., J.M. McArthur, H. Prince, & M.F. Thirlwall (2000). Dissolution methods for strontium isotope stratigraphy: whole rock analysis. *Chemical Geology*, 167, 313-319.

Blair, T.C. (1999). Sedimentology of the debris-flow-dominated Warm Spring Canyon alluvial fan, Death Valley, California. *Sedimentology*, 46, 941-965.

Bense, V. F., & M. A. Person (2006). Faults as conduit-barrier systems to fluid flow in siliciclastic sedimentary aquifers. *Water Resour. Res.,* 42, W05421, doi:10.1029/2005WR004480.

Bentley, H.W., F.M. Phillips, S.N. Davis, S. Gifford, D. Elmore, L.E. Tubbs, & H.E. Gove (1982). Thermonuclear ^{36}Cl pulse in natural water. *Nature*, 300, 737-740.

Bergmann, K.D., R.A. Zentmyer, & W.W. Fischer (2011). The stratigraphic expression of a large negative carbon isotope excursion from the Ediacaran Johnnie Formation, Death Valley. *Precambrian Research*, 188, 45-56.

Bischoff, J.L., R. Juliá, W.C. Shanks, & R.J. Rosenbauer (1994). Karstification without carbonic acid: Bedrock dissolution by gypsum-driven dedolomitization. *Geology*, 22(11), 995–998. doi: https://doi.org/10.1130/0091-7613(1994)022<0995:KWCABD>2.3.CO;2

Borsa, A.A., D.C. Agnew, D.R. Cayan (2014). Ongoing drought-induced uplift in the western United States. *Science*, 345 (6204), 1587-1589.

Brand, U., G.D. Webster, K. Azmy, & A. Logan (2007). Bathymetry and productivity of the southern Great Basin seaway, Nevada, USA: An evaluation of isotope and trace element chemistry in mid-Carboniferous and modern brachiopods. *Palaeogeography, Palaeoclimatology, Palaeoecology,* 256, 273-297.

Busenberg, E. and L.N. Plummer (1992). Use of Chlorofluorocarbons (CCl3F and CCl2F2) as hydrologic tracers and age-dating tools: the alluvium and terrace system of central Oklahoma. *Water Resources Research*, 28(9), 2257-2283.

Campana, M.E. & E.S. Simpson, (1984). Groundwater residence times and recharge rates using a discrete-state compartment model and 14C data. *Journal of Hydrology*, 72, 171-185.

Celico, F., E. Petrella, & P. Celico (2006). Hydrogeological behavior of some fault zones in a carbonate aquifer of Southern Italy: an experimentally based model. *Terra Nova*, 18, 308-313. doi:10.1111/j.1365-3121.2006.00694.x

Christophersen, N., & R.P. Hooper (1992). Multivariate analysis of stream water chemical data: the use of principal components analysis for the end-member mixing problem. *Water Resources Research*, 28(1), 99-107.

Clark, I., & P. Fritz (1997). *Environmental Isotopes in Hydrogeology*, Lewis Publishers: Boca Raton, Florida.

Cloutier, V., R. Lefebvre, R. Therrien, M.M. Savard (2008). Multivariate statistical analysis of geochemical data as indicative of the hydrogeochemical evolution of groundwater in a sedimentary rock aquifer system. *Journal of Hydrology*, 353, 294-313.

Clow, D.W., M.A. Mast, T.D. Bullen, & J.T. Turk (1997). Strontium-87/strontium-86 as a tracer of mineral weathering reactions and calcium sources in an alpine/subalpine watershed, Loch Vale, Colorado. *Water Resources Research*, 33(6), 1335-1351.

Cook, P.G. & N.I. Robinson (2002). Estimating groundwater recharge in fractured rock from environmental ^{3}H and ^{36}Cl, Clare Valley, South Australia. Water Resources Research, 38(4), 1136.

Cook, P.G., A.J. Love, N.I. Robinson, & C.T. Simmons (2005). Groundwater ages in fractured rock aquifers. *Journal of Hydrology*, 308, 284-301.

Corsetti, F.A., & A.J. Kaufman (2003). Stratigraphic investigations of carbon isotope anomalies and Neoproterozoic ice ages in Death Valley, California. *GSA Bulletin*, 115(8), 916-932.

Davis, S.N., S. Moysey, L. DeWayne Cecil, & M. Zreda (2003). Chlorine-36 in groundwater of the United States: empirical data. *Hydrogeology Journal*, 11, 217-227.

Fabryka-Martin, J. T., A.L. Flint, D.S. Sweetkind, A.V. Wolfsberg, S.S. Levy, G.J. C. Roemer, ... & M.C. Duff (1997). Evaluation of flow and transport models of Yucca Mountain, based on chlorine-36 studies for FY97. *YMP Milestone Rep SP2224M3*, Los Alamos National Laboratory, Los Alamos, New Mexico.

Faggetter, L.E., P.B. Wignall, S.B. Pruss, R.J. Newton, Y. Sun, & S.F. Crowley. Trilobite extinctions, facies changes and the ROECE carbon isotope excursion at the Cambrian Series 2-3 boundary, Great Basin, western USA. *Palaeogeography, Palaeoclimatology, Palaeoecology*, 478, 53-66.

Fisher, R.S. & W.F. Mullican III (1997). Hydrochemical evolution of sodium-sulfate and sodium-chloride groundwater beneath the northern Chihuahuan Desert, Trans-Pecos, Texas, USA. *Hydrogeology Journal*, 5(2), 4-16.

Flint, A.L., L.E. Flint, E.M. Kwicklis, G.S. Bodvarsson, & J.M. Fabryka-Martin (2001). Hydrology of Yucca Mountain, Nevada. *Reviews of Geophysics*, 39(4), 447-470.

Fontes, J.C., & J.M. Garnier (1979). Determination of the initial 14C activity of the total dissolved carbon: A review of the existing models and a new approach. *Water Resources Research*, 15(2), 399-413.

Franks, F. (1973). The Solvent Properties of Water. In: Franks F. (eds) Water in Crystalline Hydrates Aqueous Solutions of Simple Nonelectrolytes. *Water (A Comprehensive Treatise):* Springer, Boston, MA, 2, 1-54.

Frisbee, M.D., Z.P. Meyers, N.S. Stewart-Maddox, M.W. Caffee, P. Bogeholz, & M.N. Hughes (2017). What is the source of baseflow in agriculturally fragmented catchments? Complex groundwater/surface-water interactions in three tributary catchments of the Wabash River, Indiana, USA. *Hydrological Processes*, 31, 4019-4038.

Frisbee, M.D., J.L. Wilson, J.D. Gomez-Velez, F.M. Phillips, & A.R. Campbell (2013). Are we missing the tail (and the tale) of residence time distributions in watersheds? *Geophysical Research Letters*, 40(17), 4633-4637.

Han, L.F., & L.N. Plummer (2013). Revision of Fontes & Garnier's model for the initial 14C content of dissolved inorganic carbon used in groundwater dating. *Chemical Geology*, 351, 105–114.

Han, L.F., & L.N. Plummer (2016). A review of single-sample-based models and other approaches for radiocarbon dating of dissolved inorganic carbon in groundwater. *Earth-Science Reviews*, 152, 119-142.

Hogan, J.F. (2003). Tracing hydrologic flow paths in a small forested watershed using variations in $^{87}Sr/^{86}Sr$, Ca/Sr, Ba/Sr and $\delta\ ^{18}O$. *Water Resources Research*, 39(10), 1282.

Hubbert, M.K. (1940). The theory of groundwater motion. *Journal of Geology*, 48. 785-944.

International Atomic Energy Agency (IAEA) (2013). *Isotopes Methods for Dating Old Groundwater*, International Atomic Energy Agency, 2-3.

Ingerson, E., & F.J. Pearson Jr. (1964). Estimation of age and rate of motion of groundwater by the ^{14}C method. *Recent Researches in the Fields of Hydrosphere, Atmosphere and Nuclear Chemistry*, 263-283.

Integrated Earth Systems (IES) (2016). Collaborative Research: Tectonic and climatic forcing of hydrological systems in the southern Great Basin: Implications for ancient and future aquatic ecosystem resilience. *Grant EAR 1516680* (Unpublished NSF Grant).

Jurgens, B.C., J.K. Bohlke, & S.M. Eberts (2012). TracerLPM (Version 1): An Excel Workbook for Interpreting Groundwater Age Distributions from Environmental Tracer Data. *U.S. Geological Survey,* National Water-Quality Assessment Program Techniques and Methods 4-F3.

Kloppmann, W., L. Dever, & W.M. Edmunds (1998). Residence time of chalk groundwaters in the Paris Basin and the North German Basin: A geochemical approach. *Applied Geochemistry*, 13(5), 593-606.

Kreft, A. & A. Zuber (1978). On the physical meaning of the dispersion equation and its solution for different initial and boundary conditions. *Chemical Engineering Science*, 33(11), 1471-1480.

Li, J., T.K. Lowenstein, & I.R. Blackburn (1997). Responses of evaporite mineralogy to inflow water sources and climate during the past 100k.y. in Death Valley, California. *Geologic Society of America* Bulletin, 109, 1361–1371, doi: 10.1130/0016-7606(1997)109\1361:ROEMTI[2.3.CO;2

Lowenstein, T.K. & F. Risacher (2009). Closed basin brine evolution and the influence of Ca-Cl inflow waters: Death Valley and Bristol Dry Lake California, Qaidam Basin, China, and Salar de Atacama, Chile. *Aquatic Geochemistry*, 15, 71-94.

Maloszewski, P., & A. Zuber (1982). Determining the turnover time of groundwater systems with the aid of environmental tracers: 1. Models and their applicability. *Journal of Hydrology*, 57(3-4), 207-231.

Manning, A. H., & D. K. Solomon (2005). An integrated environmental tracer approach to characterizing groundwater circulation in a mountain block. *Water Resour. Res*., 41, W12412, doi:10.1029/2005WR004178

Mayo, A.L., T.H. Morris, S. Peltier, E.C. Peterson, K. Payne, L.S. Holman, D. Tingey, T. Fogel, B.J. Black, & T.D. Gibbs (2003). Active and inactive groundwater flow systems: Evidence from a stratified, mountainous terrain. *GSA Bulletin*, 115(12), 1456-1472.

Michel, R.M. (1989). Tritium deposition in the Continental United States, 1953-1983. *U.S. Geological Survey*, Water Resources Investigations Report 89-4072.

Miller, J.B. & M.D. Frisbee (2018). Using 3D printing to create a robust and compact peristaltic field pump: an update to the Montana Drill Pump. *Groundwater Monitoring & Remediation*, 38(3), 75-78.

Moysey, S., S.N. Davis, M. Zreda, & L. DeWayne Cecil (2003). The distribution of meteoric [36]Cl/Cl in the United States: a comparison of models. *Hydrogeology Journal*, 11, 615-627.

Paces, J. B., Z.E. Peterman, K. Futa, T.A. Oliver and B.D. Marshall, (2007). Strontium isotopic composition of Paleozoic carbonate rocks in the Nevada Test Site vicinity, Clark, Lincoln, and Nye Counties, Nevada, and Inyo County, California. *U.S. Department of Interior, U.S. Geological Survey*, Data Series 280.

Palmer, A.R., & R.B. Halley (1979). Physical Stratigraphy and Trilobite Biostratigraphry of the Carrara Formation (Lower and Middle Cambrian) in the Southern Great Basin. *U.S. Geological Survey*, Professional Paper 1047.

Parkhurst, D.L. (1995). Users guide to PHREEQC- a computer program for speciation, reaction-path, advective-transport, and inverse geochemical calculations. *U.S. Geological Survey,* Water-Resources Investigations Report 95-4227.

Parkhurst, D.L., & S.R. Charlton (2008). NetpathXL—An Excel® interface to the program NETPATH. *U.S. Geological Survey Techniques and Methods*, 6-A-26, 11.

Petterson, R., A.R. Prave, B.P. Wernicke, & A.E. Fallick (2011). The Neoproterozoic Noonday Formation, Death Valley region, California. *GSA Bulletin*, 123(7/8), 1317-1336.

Phillips, F. M., H. W. Bentley, S. N. Davis, D. Elmore, and G. B. Swanick (1986). Chlorine 36 dating of very old groundwater: 2. Milk River Aquifer, Alberta, Canada, *Water Resour. Res.,* 22(13), 2003–2016, doi: 10.1029/WR022i013p02003.

Phillips, F.M. (2000). Chlorine-36. In: *Environmental Tracers in Subsurface Hydrology*, Kluwer Academic Publishers, Boston, MA.

Piper, A. M., (1944). A graphic procedure in the geochemical interpretation of water-analyses, *American Geophysical Union Transactions*, 25, 914-923.

Plummer, N., & W. Back (1980) The mass balance approach: Application to interpreting the chemical evolution of hydrologic systems. *American Journal of Science*, 80, 130-142.

Plummer, L.N., E. Busenberg, J.K. Bohlke, D.L. Nelms, R.L. Michel, & P. Schlosser (2001). Groundwater residence times in Shenandoah National Park, Blue Ridge Mountains, Virginia, USA: a multi-tracer approach. *Chemical Geology*, 179(1-4), 93-111.

Prave, A.R. (1999). Two diamictities, two cap carbonates, two δ^{13}C excursions, two rifts: The Neoproterozoic Kingston Peak Formation, Death Valley, California. *Geology*, 27, 339-342.

PRISM Climate Group (PRISM) (2004). [Recent years annual precipitation dataset] *Oregon State University*, http://prism.oregonstate.edu

Quade, J., T.E. Cerling, & J.R. Bowman (1989). Systematic variations in the carbon and oxygen isotopic composition of pedogenic carbonate along elevation transects in the southern Great Basin, United States. *Geological Society of America Bulletin*, 101, 464-475.

Rademacher, L.K., J.F. Clark, G. Bryant Hudson, D.C. Erman, & N.A. Erman (2001). Chemical evolution of shallow groundwater as recorded by springs, Sagehen basin; Nevada County, California. *Chemical Geology*, 179, 37-51.

Raiber, M., J.A. Webb, & D.A. Bennetts (2009). Strontium isotopes as tracers to delineate aquifer interactions and the influence of rainfall in the basalt plains of southeastern Australia. *Journal of Hydrology*, 367(3/4), 188-199.

Raines, M.A., & T.A. Dewers (1997). Dedolomitization as a driving mechanism for karst generation in Permian Blaine Formation, Southwestern Oklahoma, USA. *Carbonates and Evaporites*, 12(1), 24-31.

Roe, G.H. (2005). Orographic Precipitation. *Annual Review of Earth and Planetary Sciences*, 33, 645-671. doi: 10.1146/annurev.earth.33.092203.122541

Rose, T.P., M.L. Davisson, & R.E. Criss (1995). Isotope hydrology of voluminous cold springs in fractured rock from an active volcanic region, northeastern California. *Journal of Hydrology*, 179, 207-236.

Rose, T.P. & M.L. Davisson (1996). Radiocarbon in hydrologic systems containing dissolved magmatic carbon dioxide. *Science*, 273, 1367-1369.

Samborska, K., A. Różkowski, & P. Małoszewski (2013). Estimation of groundwater residence time using environmental radioisotopes (^{14}C, T) in carbonate aquifers, southern Poland. *Isotopes in Environmental and Health Studies*, 49(1), 73-97, doi: 10.1080/10256016.2012.677041

Shand, P., D.P. Darbyshire, D. Gooddy, & A.H. Haria (2007). ^{87}Sr/^{86}Sr as an indicator of flowpaths and weathering rates in the Plynlimon experimental catchments, Wales. *UK Chemical Geology*, 236, 247-265.

Sharif, M.U., R.K. Davis, K.F. Steele, B. Kim, T.M. Kresse, & J.A. Fazio (2007). Inverse geochemical modeling of groundwater evolution with emphasis on arsenic in the Mississippi River Valley alluvial aquifer, Arkansas (USA). *Journal of Hydrology*, 350, 41-55.

Solomon, D.K., and P.G. Cook (2000). ^{3}H and ^{3}He. In: *Environmental Tracers in Subsurface Hydrology*, Kuwer Academic Publishers.

Stewart, M.K., & U. Morgenstern (2016). Importance of tritium-based transit times in hydrological systems. *WIREs Water*, 3, 145-154.

Toth, J. (1963). A theoretical analysis of groundwater flow in small drainage basins: *Journal of Geophysical Research*, 68. 4795-4812.

US Geological Survey (USGS) (2014). USGS spreadsheet program for preliminary evaluation of CFC data. *USGS*: The Reston Groundwater Dating Laboratory. Web: https://water.usgs.gov/lab/software/USGS_CFC/

US Geological Survey (USGS) (2017). CFC bottle sampling method. *USGS*: The Reston Groundwater Dating Laboratory. Web: https://water.usgs.gov/lab/chlorofluorocarbons/sampling/bottles/

Veizer, J. (1989). Strontium isotopes in seawater through time. *Annual Review of Earth and Planetary Science*, 17, 141-167.

Volk, C.M., J.W. Elkins, D.W. Fahey, G.S. Dutton, J.M. Gilligan, M. Loewenstein, … & M.R. Gunson (1997). Evaluatoin of source gas lifetimes from stratospheric observations. *Journal of Geophysics Research- Atmospheric*, 102(D21), 25543-25564.

Vogel, J.C. (1967). Investigation of groundwater flow with radiocarbon. *Isotopes in Hydrology, 1967*. IAEA, Vienna, 355–368.

Wang, Y., Q. Guo, C. Su, T. Ma (2005). Strontium isotope characterization and major ion geochemistry of karst water flow, Shentou, northern China. *Journal of Hydrology*, 328, 592-603.

White, W.B. (2010). Chapter 6- Springwater geochemistry. In: *Groundwater Hydrology of Springs, Engineering, Theory, Management and Sustainability*, Elsevier, Inc.

Wilson, J. L. & H. Guan (2004). Mountain-block Hydrology and Mountain-front Recharge. *Groundwater Recharge in a Desert Environment: The Southwestern United States*. American Geophysical Union. https://doi.org/10.1029/009WSA08

Workman, J.B., C.M. Menges, C.J. Frindrich, & R.A. Thompson (2018). Geologic map of Death Valley National Park, Nevada and California (Unpublished geologic map). *U.S. Geological Survey*, Denver, CO.

A PRELIMINARY ASSESSMENT OF THE RELATIONSHIP BETWEEN GROUNDWATER FLOW PROCESSES AND MICROBIOLOGICAL AND BENTHIC MACROINVERTEBRATE COMMUNITIES IN THE SPRING ECOSYSTEMS OF THE PANAMINT RANGE, DEATH VALLEY, CA

The following chapter was co-written by

Carolyn L. Gleason[1], Khaled Pordel[2], Ariel Friel[3], and Santiago Gudiño-Rosales[3]

1)Department of Earth, Atmospheric, and Planetary Sciences, Purdue University, 550 Stadium Mall Drive, West Lafayette, IN 47907, 2) Natural Resource and Environmental Science, University of Nevada Reno, 1664 N. Virginia Street, Fleischmann Agriculture, Room 217, Reno, NV 89557, & 3) School of Life Sciences and Nevada Institute of Personalized Medicine, University of Nevada, Las Vegas, 4505 S. Maryland Parkway, Las Vegas, NV 89154-4004

Introduction

Groundwater dependent ecosystems are defined as ecosystems whose composition, structure, and function rely on a regular/reliable supply of groundwater (Kløve et al., 2008). This definition clearly applies to the ecosystem supported by spring discharge, but it also applies to the ecosystem within the aquifer itself on the microbial scale (Probst et al., 2014). A study of spring community structures at these contrasting scales is valuable as both macroinvertebrates and microbes are important functional contributors to their environments contributing both as sources of food and as biochemical processors (Sherr and Sherr, 1988; Mallory et al., 1994; Mermillon-Blondin et al., 2003; Probst et al., 2014).

Hydrological processes impact the community supported by springs as geology, residence time, and geochemical evolution of these waters determines biodiversity (Kamp, 1995; Kløve et al., 2008). Spring ecosystem macroinvertebrates and microbial communities are dependent on geochemistry, while simultaneously being sensitive to changes in the groundwater flow in terms of the biodiversity in these communities. Groundwater supported systems like springs are currently facing multiple impacts including from climate change, water consumption, and irrigation which shifted groundwater levels and their temporal patterns (Kløve et al.,2014). To better track changes in groundwater and understand how regional groundwater flow systems are responding, combined

studies of ecology and geochemistry of springs are becoming a necessary standard in the field of hydrogeology (Springer et al., 2008).

Many of the Panamint Range springs in this study were not previously sampled for geochemistry or spring ecology. However, adding this component to this study was important because of the potential these communities have for tracking future climatic changes in the southern Great Basin, as well as their relation to current ecological health. In this section, collaboration between three researchers has measured metrics across disciplines for ecological diversity and the factors influencing the community structure of both benthic macroinvertebrates (BMI) and microbes and combined these data with the geochemical analysis presented in the previous chapter. The following research questions about the Panamint Range springs are addressed:

1) Is the distribution of organisms in microbial and BMI communities in springs in the Panamint Range dictated by topographic controls influencing spring geochemistry?

2) Do community structures from mountain block springs in the Panamint Range suggest a single aquifer type that conducts flow throughout the range?

Methods

The majority of the sampling in this study occurred during a two-week field campaign in the backcountry of the Panamint Range from May 23, 2017 to June 2, 2017. The geochemical data described in the previous chapter and its analysis was provided to microbiologist Ariel Friel and aquatic ecologic Khaled Pordel for use in the ecological analysis outlined in this chapter. The raw geochemical data were used in ecologic analyses and serve as the commonality between the BMI, microbe, and hydrogeological datasets. The differences in the representation of the geochemical data observed between results arise from analytical approaches of each collaborator

and practice within their discipline.

BMI Collection & Analysis

BMI samples were collected according to methodologies common to the field of spring ecology (e.g. Vinson et al., 1996). A 500μm net was oriented perpendicular to the spring run thalweg and used to scoop BMI in a single motion. Collections were made at 5 m intervals along a longitudinal transect from the spring emergence by roiling the spring substrate to release BMIs and allow them to drift downstream into the net. Samples were placed into plastic screw-top sampling jars and preserved in 90% ethyl alcohol. Samples were then processed by the Rhithron Aquatic Laboratory, Missoula, MT for species identification and quantification. Only fourteen of the twenty Panamint springs were sampled for BMIs due to limitations in spring discharge. It is impossible to collect BMI samples using this methodology for springs with limited, shallow diffuse discharge as there was not enough water flow to separate the BMIs from the sediments disturbed during sampling.

Relationships between spring emergence environment and the structure and functional characteristics of BMI communities were examined using multivariate analysis (Canonical Correspondence Analysis [CCA], Non-Metric Multidimensional Scaling [NMDS], Detrended Correspondence Analysis (DCA) and Analysis of Similarity [ANOSIM]). CCA is a multivariate analysis approach that can be used to examine relationships between the physicochemical environment and biological communities using a direct gradient analysis (ter Braak and Verdonschot, 1995). NMDS is another multivariate analysis that constructs a configuration of statistical similarities/dissimilarities based on a specified number of dimensions (Minchin, 1987). Detrended correspondence analysis (DCA) is another statistical tool often used to represent primary data gradients and understand its distribution (Hill and Gauch, 1980). ANOSIM is an

assessment of the relationship between BMI community characteristics and predetermined groups (i.e. disturbance levels) of springs (i.e. communities) determined using the other statistical analyses and field observations. It tests the null hypothesis that there are no differences between groups and calculates global and pair-wise (between groups) R values that are a test statistic centered around zero. Values near zero indicate similarity within and among groups (hence no difference between groups), and higher values indicate dissimilarity between groups (Clarke and Gorley 2006).

CCA was used in this study to complement DCA, NMDS and ANOSIM and thoroughly identify physicochemical characteristics of the environment that were most influential in structuring the BMI community. CANOCO v. 4.5 was used to calculate CCA (ter Braak and Verdonschot, 1995).

Microbial Analysis

Planktonic and benthic community samples were collected for each spring at the same time as hydrogeochemical sampling from the spring emergence. Planktonic microbial biomass was collected by passing no more than 2 L of groundwater through a 0.22 um polyethersulfone membrane Sterivex-GP pressure filters (Millipore, MA, USA). Benthic microbial biomass was gathered using a shovel (disinfected with 50% ethanol prior to use) by collecting the top 1 cm of spring sediment or benthic microbial mat at 2m intervals from the spring emergence to approximately 8m down the spring run. One filter and four benthic samples were collected for each spring; benthic samples were chosen to represent the substrate diversity of the spring run. Filter and benthic samples were stabilized and stored in the field and in lab (until DNA extraction) using RNA*later*™ (Thermo Fisher Scientific, Waltham, MA) without refrigeration.

For each spring, the filter outflow channel was sealed with Parafilm M (Bemis NA, Neenah, WI) after 2 L of pumping followed by the addition of 2.5 mL of RNA*later*™ to the filter.

Filters were further secured by placing a sterilized metal plug piece into the inflow channel and using electrical tape to reinforce the outflow/inflow channels and protect against pressure changes. 0.5 mL of benthic microbial biomass was collected with a sterilized spatula and added to a 2 mL UV-sterilized Eppendorf tube (Eppendorf, Hamburg, Germany). After collection, 0.5 mL of RNA*later*™ was added to the sample and tubes were sealed using electrical tape. Sealed filters were stored in sterile 50 mL Falcon tubes and were added to spring-specific Ziploc bags containing the matching benthic samples until DNA extraction. In-field and in-lab storage for additional spring samples (IES 019, IES 045, IES 047) differed from PAN1-PAN20 in that they were stored on dry ice (field) or in the -80 freezer (lab) until DNA extraction and without the addition of RNA*later*™.

16S rRNA gene amplicon sequencing

DNA was extracted from the Sterivex filters and benthic samples using the FastDNA™ SPIN Kit for Soil (MP Biomedicals, Santa Ana, CA) according to manufacturer's instructions. The V4 region of the 16S rRNA was amplified and sequenced using the updated bacterial- and archaeal-specific 515F/806R primer set. Amplification and sequencing were performed at Argonne National Laboratory (Lemont, IL) on an Illumina MiSeq platform (2x151 bp).

Sequence processing and statistical analyses

Paired-end Illumina MiSeq reads were loaded into the 2018.4.0 version of Qiime2 (Caporaso et al., 2010) and quality filtered, aligned, and analyzed. Quality filtering of reads and removal of chimera sequences was performed using the q2 -dada2 plugin in Qiime2 (Callahan et al., 2016). Reads were truncated at the first base with a PHRED score lower than 30; filtered reads were then clustered into sequence variants. Variants were aligned using mafft (Katoh and Standley, 2013) through the q2 -alignment plugin at default settings. Sequence variants were then

taxonomically classified using the Silva nr. 99 reference database with the classify -sklearn function of the q2 -feature -classifier plugin (Caporaso et al., 2010).

After sequence processing, taxonomy, abundance, and metadata tables were imported into R and turned into a single operable object using the package phyloseq version 1.22.3 (McMurdie and Holmes, 2013). Alpha-diversity metrics (Observed, Shannon, and InvSimpson) were generated using Phyloseq to represent sample species diversity (McMurdie and Holmes, 2013). Phyloseq was also used to generate proportions of phyla across the samples (McMurdie and Holmes, 2013); ggplot2 version 2.2.1 was used to visualize this data (Wickham, 2009). Bray-Curtis dissimilarity matrices for filter, liquid, and benthic samples were generated using vegan version 2.4.4 (Okanen et al., 2009). The dissimilarity between samples was then visualized via non-metric multidimensional scaling using vegan and base R graphics (Okanen et al., 2009). Environmental arrows demonstrating correlations between the ordinational coordinates of the samples and the direction of most change in the metadata based on geochemistry were plotted using vegan (Okanen et al, 2009). Metadata was first log transformed for normalization. Consequently, a value of 100 was added to elevation and a value of 110 was added to ORP to result in positive values needed for the log transformation of the metadata.

Results

BMI Analysis

Table 11 is a catalogue of all BMI data collected and denotes relevant field notes and the overall sample quality. Red indicates samples that were not used in these analyses and green indicates the samples that were used in the statistical analysis. Samples were omitted due to poor sample quality (e.g. two or less taxa found in the sample) or due to low spring discharge. In total, twelve BMI samples were utilized in this analysis.

DCA showed that the BMI data are strongly unimodal. Consequently, CCA is an applicable technique to examine the relationship between the structure of BMI communities and environmental factors in Panamint Range springs. In this study, temperature, pH, calcium concentration and elevation were statistically significant ($p < 0.05$) variables influencing the structure of the BMI communities based on the CCA.

Eigenvalues from CCA (Table 12) showed that axis 1 and 2 are the most important axes to explain the variance in BMI data. CCA triplot of samples, species, and environmental variables based on the first two axes explain 35.9 percent of the variance in species data Figure 27; Figure 28). Additionally, the first two axes of CCA analysis explained 56.9 percent of the species-environment correlation (Table 12).

Table 11. Springs survey list for hydrological and ecological samples.

	Spring Condition- Field notes	BMI sample Condition
Pan 1	Lowest temp; highest elevation; Low flow (Marked as a suspect sample)	Two taxa >> sample was removed
Pan 2	Too Disturbed (Pipe); Near Camp Ground; low flow	No BMI sample was collected
Pan 3	Watercress and willow indicate stable spring; High discharge	Acceptable BMI sample
Pan 4	Too disturbed	No BMI sample was collected
Pan 5	Anthropogenic spring emergence; hardly any surface water)	No BMI sample was collected
Pan 6	Highest Calcium; high TDS, very diffuse flow	Acceptable BMI sample
Pan 7	Highest Calcium; high TDS, very diffuse flow	Acceptable BMI sample
Pan 8	Largest discharge; Highest pH; Low temp	Acceptable BMI sample
Pan 9	Most biologically active spring ;frog-tadpoles-predatory invertebrates;	Acceptable BMI sample
Pan 10	Mixing Hanaupah Springs	No BMI sample was collected
Pan 11	Thick tuffs mat along spring run.	Acceptable BMI sample
Pan 12	Very diffuse spring	No BMI sample was collected
Pan 13	Highest temperature; Close to abandoned mining structures	Acceptable BMI sample
Pan 14		No BMI sample was collected
Pan 15	diffuse spring	Acceptable BMI sample
Pan 16	diffuse spring	Acceptable BMI sample
Pan 17	Diffuse spring- Same fault as Pan16- (Ferns found) indicating stable flow)	Acceptable BMI sample
Pan 18	Near old mining camp- Highly Disturbed	No BMI sample was collected
Pan 19	Highly disturbed-	No BMI sample was collected
Pan 20	Highest conductivity; Basin spring; (Marked as a suspect sample)	2 Taxa → sample was removed
IES-047	Poplar spring	Acceptable BMI sample
IES-019	Tule Spring	Acceptable BMI sample

Table 12. CCA summary relating the structure of BMI communities and environmental variables.

```
Axes                                    1       2       3       4    Total inertia

Eigenvalues                    :      0.735   0.501   0.405   0.350           3.448
Species-environment correlations :    0.965   0.912   0.870   0.927
Cumulative percentage variance
   of species data             :       21.3    35.9    47.6    57.8
   of species-environment relation:    33.9    56.9    75.6    91.8

Sum of all          eigenvalues                                               3.448
Sum of all canonical  eigenvalues                                             2.171
```

Figure 27 and Figure 28 display the results of the CCA for the Panamint BMI. *Hyalella* (Tolerance

value of 8; Mandaville, 2002) was dominant in PAN 13 and IES-019 which exhibit the highest

water temperatures. High TDS and calcium concentrations provide a harsh environment for BMIs,

therefore, BMIs with high tolerance values were dominant in PAN 6 and PAN 7 as these springs

also have the highest TDS & Ca concentrations as shown in Appendix B (Timpano et al., 2010).

Springsnails (*Pyrgulopsis*) were dominant in mountain block springs with a temperate

environment, and moderate calcium concentration.
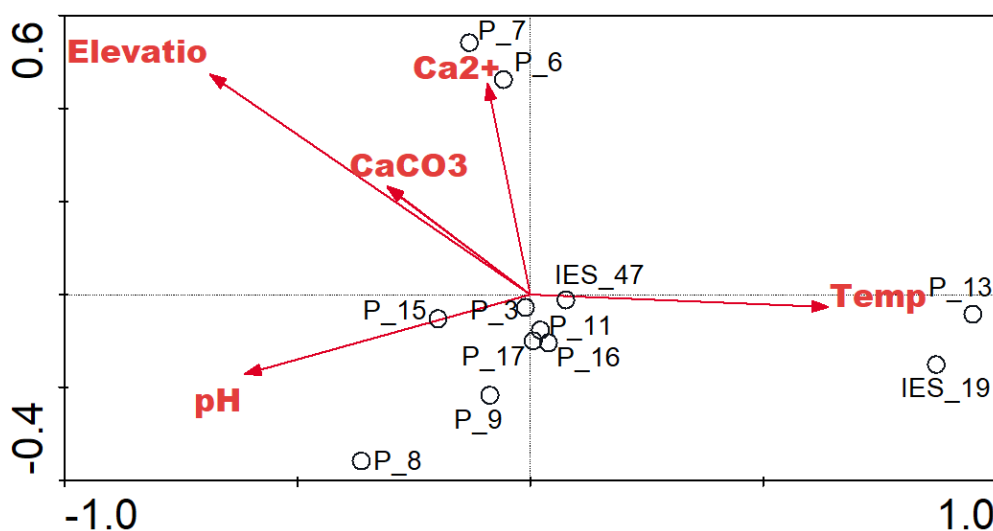
Figure 27. Canonical correspondence analysis biplot is showing the relationship between environmental variables and structure of BMI communities. Elevation, temperature, pH, Ca^{2+}, and $CaCO_3$ were statistically significant environmental metrics.
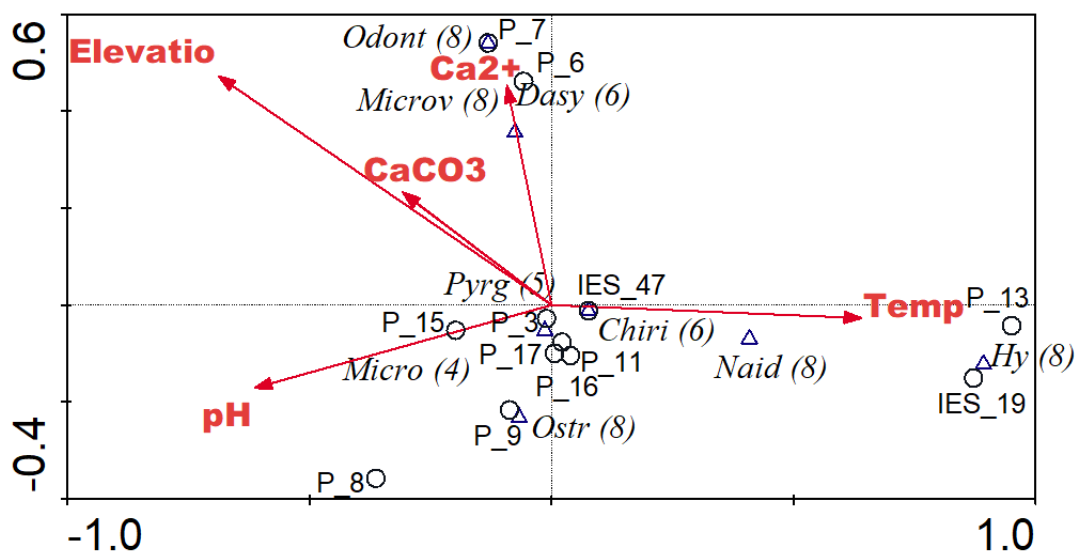
Figure 28. Canonical correspondence analysis triplot is showing the relationship between environmental variables and structure of BMI communities. Elevation, temperature, pH, Ca^{2+}, and $CaCo3$ were statistically significant environmental metrics. Species tolerance is shown in parenthesis.
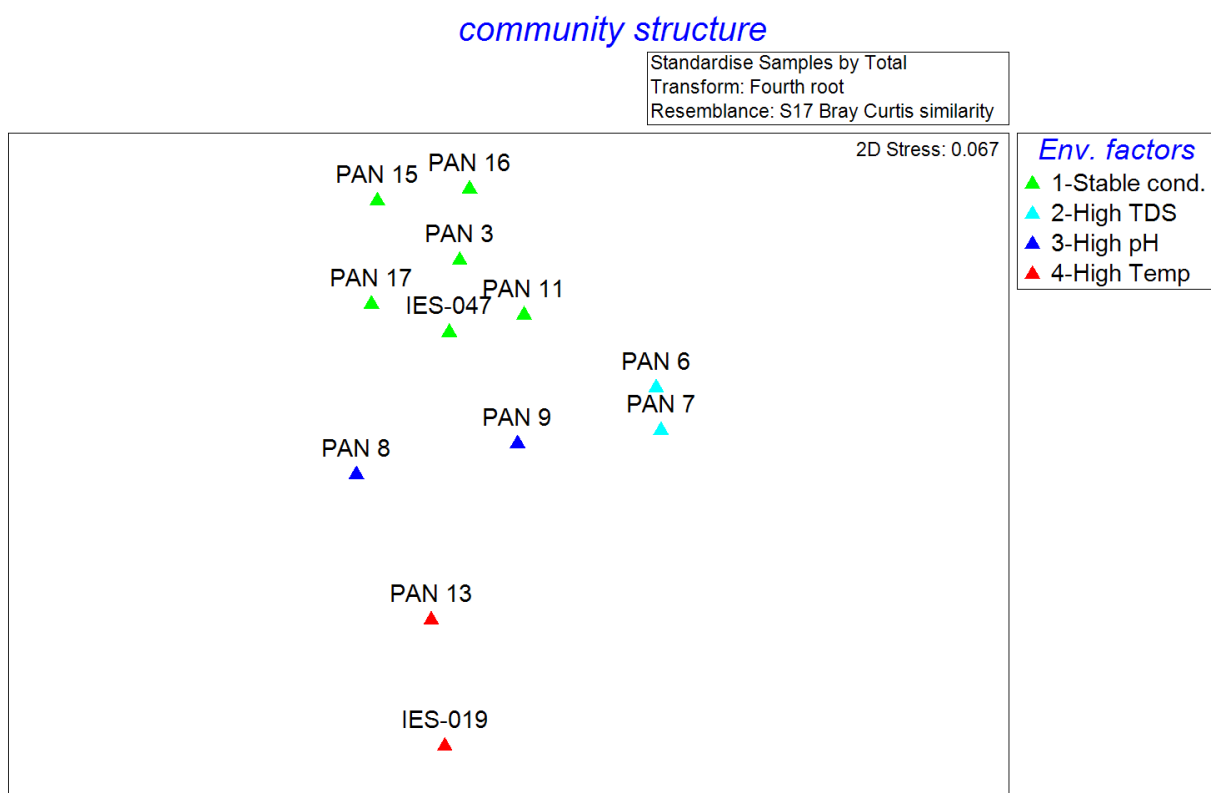
Figure 29. NMDS plot indicating the association between environmental factors and the structure of BMI communities in Panamint Range springs.

```
Global Test
Sample statistic (Global R): 0.986
Significance level of sample statistic: 0.1%
Number of permutations: 999 (Random sample from 13860)
Number of permuted statistics greater than or equal to Global R: 0

Pairwise Tests
                R  Significance       Possible        Actual  Number >=
Groups  Statistic       Level %  Permutations  Permutations   Observed
1, 4            1           3.6            28            28          1
1, 2        0.969           3.6            28            28          1
1, 3        0.969           3.6            28            28          1
4, 2            1          33.3             3             3          1
4, 3            1          33.3             3             3          1
2, 3            1          33.3             3             3          1
```

Table 13. ANOSIM comparing the structure of BMI communities in springs with a stable condition (group 1), highest TDS (Group 2 with TDS >1500 mg/lit), highest temperature (group 4 with temperature > 26 $^{\circ}$C), and highest pH (group 3 with pH > 8.5) to examine the strength of clustering between the groups established in the NMDS (Figure 29).

The relationship between environmental variables from geochemistry and BMI

community structure was examined using NMDS and ANOSIM. Figure 29 displays the NMDS results and indicates the associations between general geochemical factors and BMI community structure. The statistical outcomes of the ANOSIM are reported in Table 13. Both the NMDS stress value (0.067) and ANOSIM global R-value (0.98) indicate significant similarity between the BMI samples as they are clustered in Figure 29. As shown in Figure 29, BMI communities in moderate condition springs (green triangle) were tightly clustered, BMI communities in high-temperature springs (red triangles) clustered together and BMI communities in springs with high TDS (light blue triangles) were likewise clustered together.

The ANOSIM results confirm the strong clustering (high Global R-value = 0.98 and a significant sample statistic, P= 0.001) shown by the NMDS plot. Pairwise R-value between spring groups (1-stable condition or average mountain block springs in this setting, 2-highest TDS [>1500 mg/lit], 3-highest pH [> 8.5], and 4-highest temp [> 26ºC]) was close to 1, which indicates that the structure of communities is similar within each group, and each group has dissimilar BMI community structure relative to other groups. Differences between group one and other group's BMI communities were statistically significant (P < 5%).
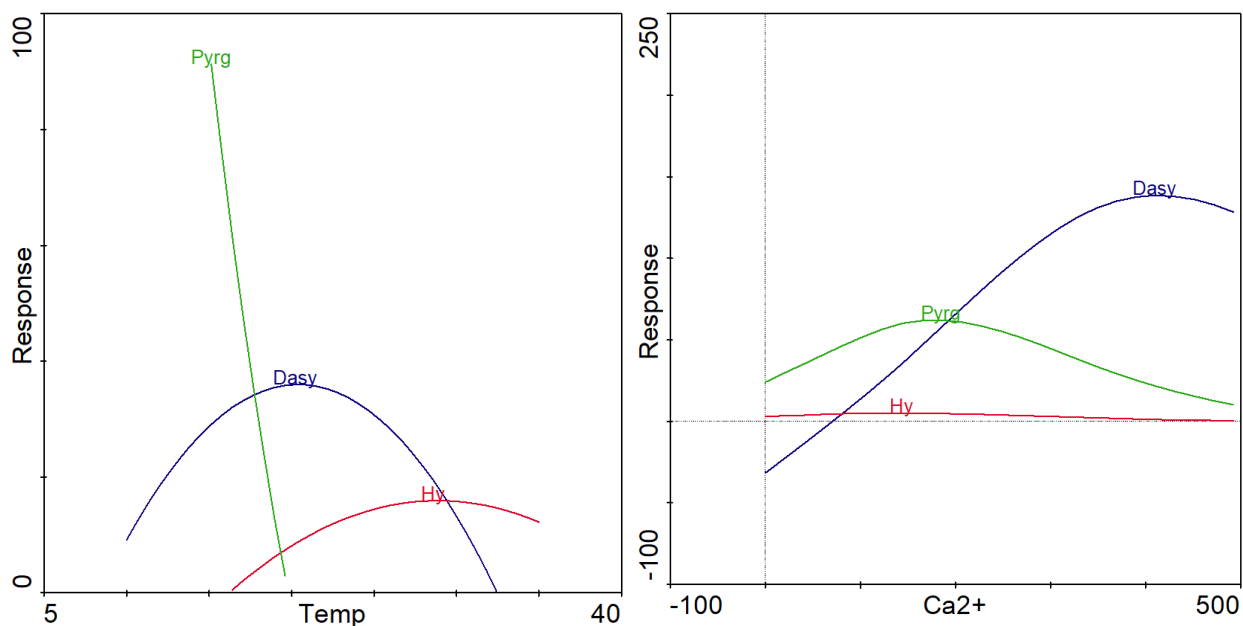
Figure 30. Species response curve is showing the relationship between the abundance value of *Pyrgulopsis* (Gastropod), *Dasyhelea* (Diptera), and *Hyalella* (Crustacea) and the gradient of an environmental variable (Ca^{2+} or temperature) in the Panamint Range springs.

Species response curves shown in Figure 30 demonstrate the BMI taxa response to a gradient of a particular environmental factor. Assuming an optimum abundance value for the BMI taxa along the environmental gradient, unimodal response curves calculated from a regression model to describe the environmental conditions in which a BMI taxon can be present or not (Leps and Smilauer, 2003). Figure 30 indicated that *Dasyhelea* (order: Diptera), with a tolerance value of 8 (Mandaville, 2002), tolerated a high concentration of calcium, while *Pyrgulopsis* (Springsnail) tolerated moderate concentration of calcium. According to the CCA Plot (Figure 28), *Hyalella* abundance was attributed to temperature, which was confirmed by the species response curve for temperature in Figure 30.

Microbiological Analysis

Removal of contaminated sequences

During data analysis of the Illumina sequences, it was determined that there were abnormalities in some of the microbial samples. When assessing community structure using non-

metric multi-dimensional scaling, some spring samples (liquid, filter, and sediment) were observed to differ substantially from the rest suggesting human microbial contamination may have occurred during field sampling or during the DNA extraction procedure. Spring samples were removed from further analysis if the combined percent abundance of the following genera was over 2%: *Lactobacillus, Staphylococcus, Streptococcus,* and *Escherichia-Shigella*. These genera that are often associated with humans (Ma et al., 2012; Rensburg et al., 2015; Lloyd-Price et al., 2016). The remaining spring samples exhibited little to no contamination from these genera. These genera were selected as contamination indicators as they have been reported to be common members of the human microbiome. Filter, liquid, and sediment samples contained contamination from *Escherichia-Shigella*, *Lactobacillus*, *Staphylococcus*, and *Streptococcus* and are indicated in Figure 31. Figure 31 also shows the sediment samples contaminated with the genus *Staphylococcus.* These patterns led to the removal of filter and liquid samples PAN1-F, PAN4-F, PAN4-L, PAN14-F, PAN14-L, PAN16-F, and PAN16-L and sediment samples PAN2-S1, PAN2-S2, PAN2-S3, PAN2-S4, PAN4-S1, PAN4-S2, PAN4-S4, PAN9-S3, PAN15-S3, PAN16-S1, PAN16-S4, and PAN17-S4 from statistical analysis.

Filter (F) and liquid (L) samples of springs.

Sediment (S) samples of springs

Genus
- Escherichia-Shigella
- Lactobacillus
- Staphylococcus
- Streptococcus
- Other
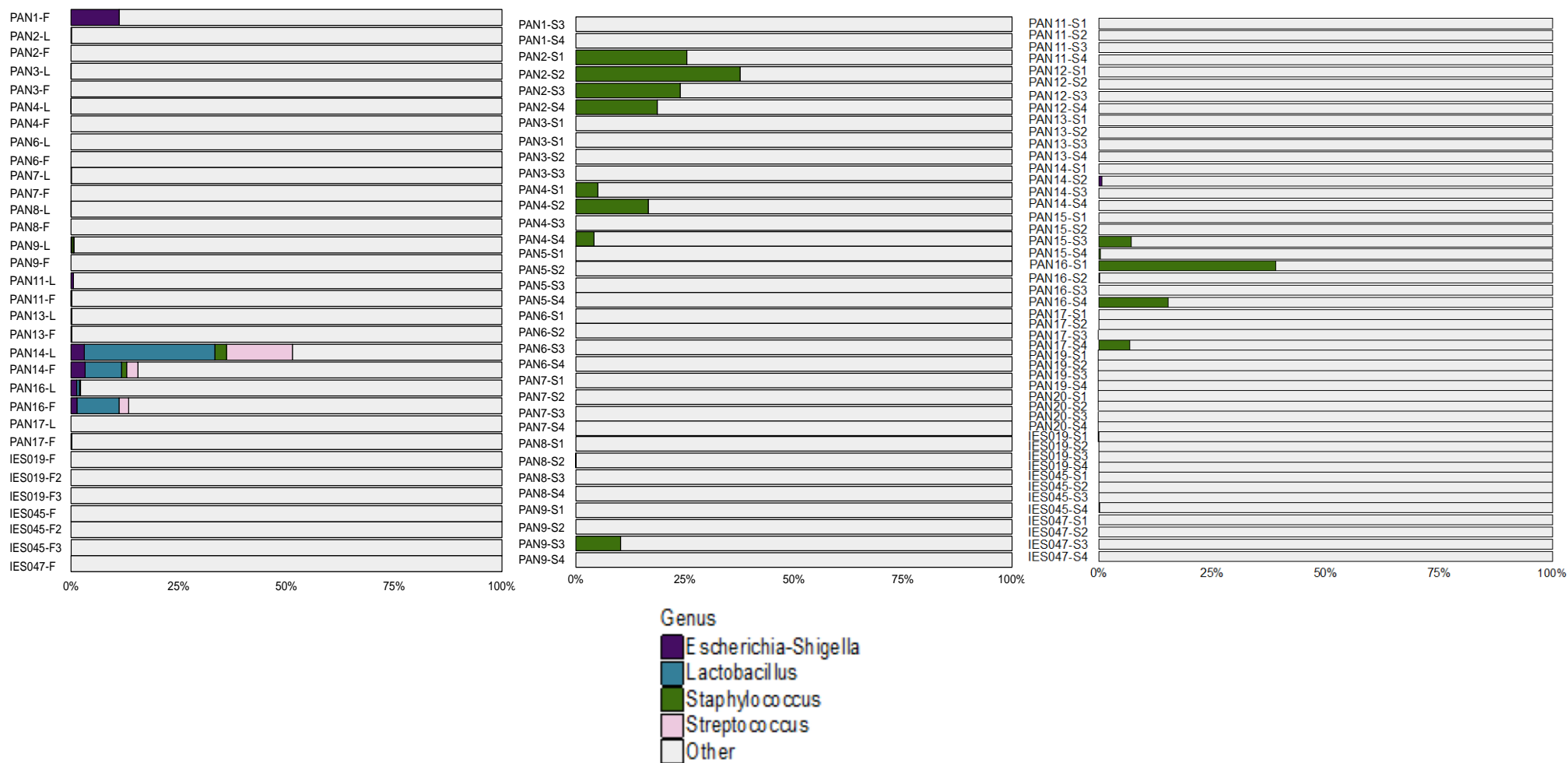
Figure 31. Percent abundance diagrams for samples influenced by human contamination.

Richness of microbial communities of Panamint desert springs

For 94 samples comprising 25 filter and liquid samples and 68 sediment samples, a total of 2,458,028 reads and 34,990 sequence variants were obtained through Illumina Sequencing. The average number of reads per sample was 26,149 reads. Alpha-diversity metrics demonstrated a wide range of observed sequence variants between filter, liquid, and sediment samples; however, both filter and liquid samples had higher alpha diversity values than sediment samples. Ranges for the number of observed sequence variants in filter and liquid samples was 330 to 1662 with an average of 1025 (Table 14). The range for sediment samples was 314 to 1404 with an average of 698 (Table 15; Table 16). PAN13-S4 was removed due to its low read abundance of 5073, which was not high enough for rarefying (set at 10,000 sequences). Shannon index in filter and liquid samples demonstrated a range of 5.44 to 6.82 with an average of 6.25 and in sediment samples a range of 3.44 to 6.73 and a range of 5.63. Ranges for inverse Simpson index in filter and liquid samples was 0.979 to 0.998 with an average of 0.994. The range for sediment samples was 0.749 to 0.998 with an average of 0.982.

Table 14. Alpha diversity metrics of filer (F) and liquid (L) samples.

Sample ID	Spring	Observed	Shannon	Invsimpson
PAN2.F	PAN2	1032	6.39	0.996
PAN2.L	PAN2	793	6.17	0.996
PAN3.F	PAN3	1289	6.49	0.996
PAN3.L	PAN3	1098	6.30	0.995
PAN6.F	PAN6	1174	6.57	0.998
PAN6.L	PAN6	837	6.15	0.996
PAN7.F	PAN7	1115	6.48	0.996
PAN7.L	PAN7	969	6.35	0.997
PAN8.F	PAN8	951	6.20	0.995
PAN8.L	PAN8	820	6.20	0.997
PAN9.F	PAN9	979	5.99	0.993
PAN9.L	PAN9	932	6.03	0.993
PAN11.F	PAN11	1430	6.82	0.998
PAN11.L	PAN11	330	5.55	0.995
PAN13.F	PAN13	1038	6.43	0.997
PAN13.L	PAN13	1662	6.57	0.995
PAN17.F	PAN17	1336	6.64	0.997
PAN17.L	PAN17	911	6.22	0.996
IES019.F	IES019	1124	6.43	0.996
IES019.F2	IES019	710	5.70	0.991
IES019.F3	IES019	726	5.65	0.990
IES045.F	IES045	1196	6.54	0.997
IES045.F2	IES045	1076	6.46	0.997
IES045.F3	IES045	1236	6.61	0.997
IES047.F	IES047	868	5.44	0.979

Table 15. Alpha diversity metrics of sediment (S) samples PAN1-PAN12.

Sample ID	Spring	Observed	Shannon	Invsimpson
PAN1.S3	PAN1	945	6.18	0.993
PAN1.S4	PAN1	695	5.84	0.992
PAN3.S1	PAN3	916	6.16	0.995
PAN3.S2	PAN3	574	5.80	0.995
PAN3.S3	PAN3	847	6.27	0.996
PAN3.S4	PAN3	686	5.65	0.989
PAN5.S1	PAN5	727	5.71	0.992
PAN5.S2	PAN5	459	4.88	0.945
PAN5.S3	PAN5	554	5.61	0.992
PAN5.S4	PAN5	449	4.37	0.902
PAN6.S1	PAN6	527	5.33	0.9867
PAN6.S2	PAN6	525	5.27	0.988
PAN6.S3	PAN6	510	5.26	0.989
PAN6.S4	PAN6	525	5.22	0.987
PAN7.S1	PAN7	917	6.24	0.996
PAN7.S2	PAN7	932	6.19	0.996
PAN7.S3	PAN7	768	5.78	0.991
PAN7.S4	PAN7	742	5.41	0.978
PAN8.S1	PAN8	487	4.92	0.956
PAN8.S2	PAN8	489	4.75	0.958
PAN8.S3	PAN8	435	5.03	0.975
PAN8.S4	PAN8	680	5.76	0.992
PAN9.S1	PAN9	1015	6.33	0.997
PAN9.S2	PAN9	564	5.23	0.981
PAN9.S4	PAN9	314	4.59	0.9797
PAN11.S1	PAN11	585	5.16	0.984
PAN11.S2	PAN11	618	5.25	0.979
PAN11.S3	PAN11	528	5.05	0.977
PAN11.S4	PAN11	317	4.93	0.987
PAN12.S1	PAN12	805	6.02	0.992
PAN12.S2	PAN12	591	6.04	0.997
PAN12.S3	PAN12	836	6.29	0.997
PAN12.S4	PAN12	1404	6.73	0.998

Table 16. Alpha diversity metrics of sediment (S) samples PAN13-PAN20, IES019, IES045, and IES047.

Sample ID	Spring	Observed	Shannon	Invsimpson
PAN13.S1	PAN13	665	5.71	0.992
PAN13.S2	PAN13	847	6.17	0.996
PAN13.S3	PAN13	904	6.18	0.996
PAN14.S1	PAN14	787	6.01	0.994
PAN14.S2	PAN14	796	5.86	0.992
PAN14.S3	PAN14	736	5.81	0.991
PAN14.S4	PAN14	496	3.44	0.749
PAN15.S1	PAN15	1117	6.50	0.997
PAN15.S2	PAN15	726	5.05	0.930
PAN15.S4	PAN15	702	5.13	0.957
PAN16.S2	PAN16	758	6.04	0.995
PAN16.S3	PAN16	675	5.95	0.995
PAN17.S1	PAN17	793	6.13	0.996
PAN17.S2	PAN17	789	6.11	0.994
PAN17.S3	PAN17	866	6.26	0.997
PAN19.S1	PAN19	591	5.39	0.988
PAN19.S2	PAN19	625	5.26	0.981
PAN19.S3	PAN19	680	5.41	0.987
PAN19.S4	PAN19	606	5.40	0.986
PAN20.S1	PAN20	742	5.81	0.993
PAN20.S2	PAN20	865	6.04	0.995
PAN20.S3	PAN20	901	5.93	0.993
PAN20.S4	PAN20	736	5.78	0.992
IES019.S1	IES019	705	5.80	0.993
IES019.S2	IES019	599	5.70	0.993
IES019.S3	IES019	455	5.49	0.992
IES019.S4	IES019	661	5.71	0.990
IES045.S1	IES045	760	6.01	0.996
IES045.S2	IES045	173	4.14	0.969
IES045.S3	IES045	505	5.26	0.988
IES045.S4	IES045	571	5.25	0.982
IES047.S1	IES047	1008	6.26	0.966
IES047.S2	IES047	789	6.11	0.996
IES047.S3	IES047	886	5.89	0.987
IES047.S4	IES047	976	6.34	0.997

Microbial diversity of desert springs in the Panamint Range

Phylum-level bar plots were generated for the planktonic and benthic communities using 16S rRNA genes from Illumina sequencing. Plots demonstrated 48 phyla dispersed across planktonic and benthic communities when taxa that are below 2% in the entire dataset are grouped together. The top five phyla that dominated planktonic communities as depicted by the filter and liquid samples included *Proteobacteria* (relative abundance 42%), *Bacteroidetes* (10%), *Planctomycetes* (5%), *Verrucomicrobia* (5%), and unclassified bacteria (4%). Benthic communities, represented by sediment samples, were dominated by *Proteobacteria* (41%), *Bacteroidetes* (8%), *Actinobacteria* (8%), *Planctomycetes* (6%), and *Firmicutes* (5%).

The planktonic communities from liquid and filter samples demonstrated consistency in community structure across most springs excluding IES-045 and IES-047 (Figure 32). These sequences were dominated by the phyla *Proteobacteria* (34%-58%), *Bacteroidetes* (1%-21%), and *Planctomycetes* (1%-17%). The planktonic samples also showed *Acidobacteria* (1%-6%), *Actinobacteria* (1%-18%), *Firmicutes* (1%-11%), *Verrucomicrobia* (1%-10%), unclassified bacteria (1%-8%), and *Chloroflexi* (1%-6%) which constituted large portions of their community structures. IES-045 was dominated by the phyla *Proteobacteria* (20%-22%), *Woesearchaeota* (15%-16%), *Parcubacteria* (13%-16%), unclassified bacteria (10%-13%), *Omnitrophica* (5%-10%), and *Peregrinibacteria* (7%-8%). IES-047 was dominated by *Proteobacteria* (65%) and *Bacteroidetes* (10%) but also showed a unique presence of *Gracilibacteria* (4%). While the planktonic communities from liquid and filter samples did principally demonstrate consistency in their structure, filter samples from PAN2, PAN3, PAN4, PAN6, PAN7, PAN11, and PAN17 showed increased presences of dark matter groups or understudied phyla. These included increases in *Woesearchaeota* (2%-17%), *Parcubacteria* (3%-9%), *Omnitrophica* (1%-7%), and

Peregrinibacteria (0%-1%).
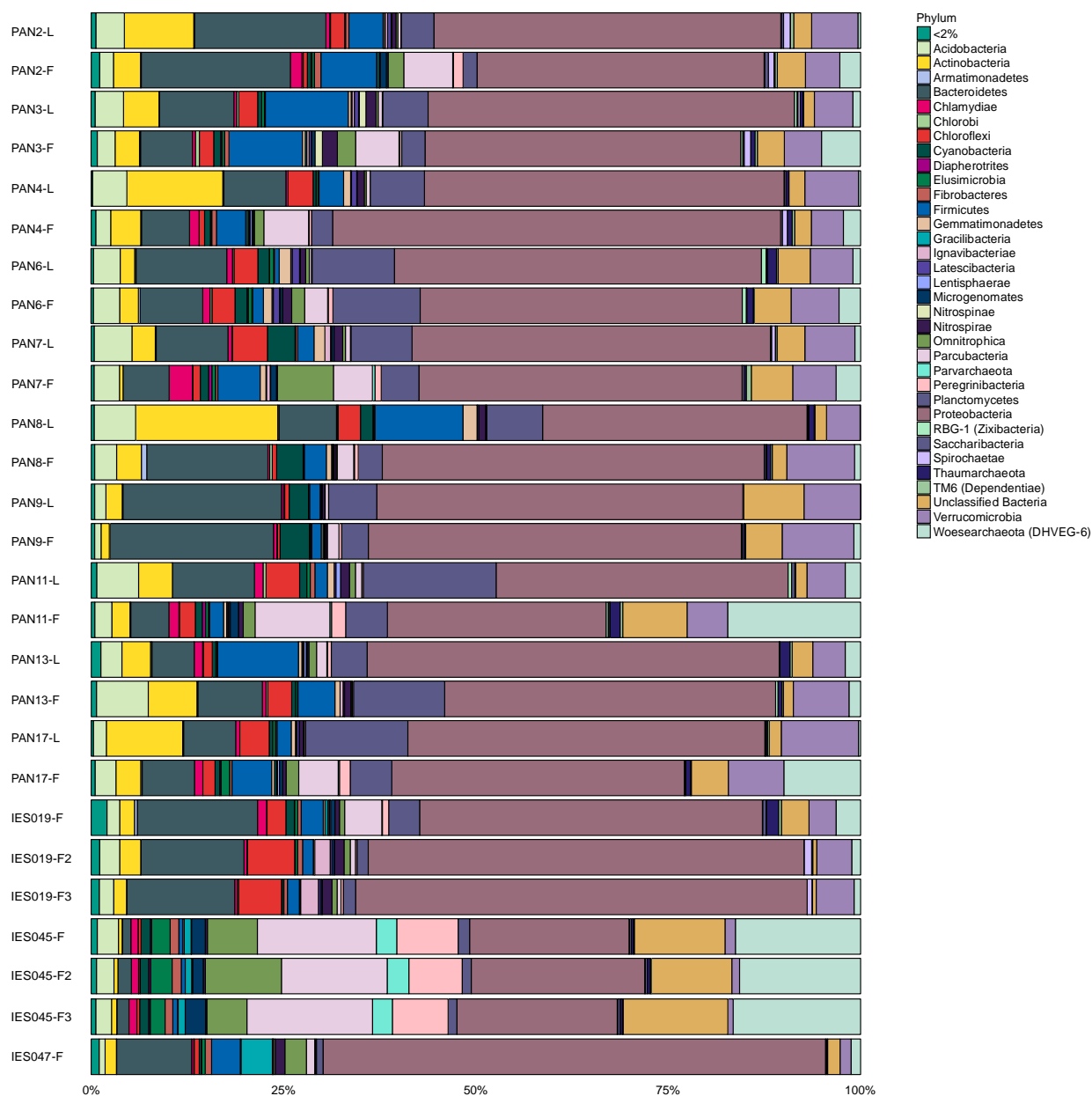
Figure 32. Percent abundance of microbial phyla present in filter (F) and liquid (L) samples of springs

The benthic communities were not as consistent across sediment samples and were thus

broken into six groups based off similar taxonomic groups (Figure 33 and Figure 34). It should

be noted that statistical analyses have not yet been performed to classify these groups, but the

phylum-level bar plots were compared to non-metric multidimensional scaling abundance data to

help guide the dictation of Group, A, B, C, D, E, and F.

Group A comprises PAN1, PAN12, PAN13, and PAN14. This group was dominated by *Proteobacteria* (19%-53%) but other prominent phyla include *Chloroflexi* (3%-8%), *Actinobacteria* (3%-5%), *Acidobacteria* (6%-12%), and *Bacteroidetes* (1%-6%). Group A also exhibited a composition of the phyla *Gemmatimonadetes* (0%-1%), *Nitrospirae* (2%-6%), *Thaumarchaeota* (1%-9%), and *Woesearchaeota* (0%-9%) that was elevated relative to the other groups. PAN14 differs from the other springs in this group due to a higher fraction of *Cyanobacteria* (1%-9%) and *Deferribacteres* (0%-2%) but was overall very similar to the other springs in Group A.

Group B consists of springs PAN6, PAN7, and PAN11. The phyla *Proteobacteria* (26%-63%), *Cyanobacteria* (1%-32%), *Bacteroidetes* (8%-30%), *Planctomycetes* (5%-10%), and *Verrucomicrobia* (4%-8%) dominate this group. PAN7 is from the other springs in this group as it has a higher percent abundance of *Gemmatimonadetes* (2%).

Group C consists of springs PAN3, PAN15, PAN16, and PAN17. The phyla *Proteobacteria* (29%-49%) and *Actinobacteria* (8%-31%) dominates this group. Other notable phyla include *Firmicutes* (1%-16%), *Planctomycetes* (4%-12%), *Acidobacteria* (2%-12%), *Chloroflexi* (3%-10%), *Bacteroidetes* (4%-9%), and *Verrucomicrobia* (1%-8%). There is also an increased presence of *Nitrospirae* (0%-3%) and *Thaumarchaeota* (0%-2%) in Group C.

PAN5 and PAN8 make up Group D. This group is dominated by *Proteobacteria* (25%-53%), *Actinobacteria* (3%-35%), and *Firmicutes* (3%-32%). Oher prominent phyla include *Bacteroidetes* (4%-8%), *Verrucomicrobia* (1%-8%), and *Planctomycetes* (2%-7%). PAN5 and PAN8 differ, as PAN5 had a higher percent abundance of Chloroflexi and PAN8 has a higher

percent abundance of Actinobacteria.

Group E comprises IES019 and IES047. The phyla *Proteobacteria* (19%-54%), *Bacteroidetes* (3%-26%), and *Chloroflexi* (6%-14%) dominated this group, and *Ignavibacteriae* (0%-4%) and *Spirochaetae* (0%-1%) exhibit an increased presence relative to the other groups. While the microbial structure is predominantly consistent across the two springs in Group E, there were notable differences. IES047 has a higher percent abundance of *Nitrospirae* (0%-3%) and *Nitrospinae* (0%-1%). IES019 has a higher percent abundance of *Omnitrophica* (0-1%).

Group F contains only PAN20 as the sediments samples form the spring are unique from the other springs. PAN20 is dominated by *Proteobacteria* (37%-42%), *Firmicutes* (6-14%), *Bacteroidetes* (7%-10%), and *Cyanobacteria* (6%-10%). PAN20 shows a unique presence of *Euryarchaeota* (1-5%), *Spirochaetae* (1%-2%), *Fibrobacteres* (1%), *Parcubacteria* (1%), and *Tenericutes* (0-1%).

PAN9, PAN19, and IES045 were not grouped as the samples within each spring do not demonstrate consistency. The benthic communities in PAN9 differ from one another. PAN9-S1 is dominated by *Proteobacteria* (49%) but other notable phyla include *Acidobacteria* (11%), *Planctomycetes* (9%), *Bacteroidetes* (5%), *Nitrospirae* (5%), and *Tectomicrobia* (1%). PAN9-S2 is dominated by *Proteobacteria* (44%), *Cyanobacteria* (24%), and *Bacteroidetes* (14%). PAN9-S3 is dominated by *Proteobacteria* (77%) and *Bacteroidetes* (17%).

The benthic communities in PAN19 also differ from one another. PAN19-S1 and PAN19-S4 were dominated by *Proteobacteria* (40%-43%) and *Cyanobacteria* (19%-21%), though other notable phyla include *Bacteroidetes* (8-10%) and *Planctomycetes* (9%). PAN19-SI and PAN-S4 also exhibit an increased presence of *Gemmatimonadetes* (2%) relative to the other

sediment samples. PAN19-S2 and PAN19-S3 were dominated by *Proteobacteria* (35%-41%), *Chloroflexi* (13%-26%), and *Actinobacteria* (8%-15%). PAN19-S2 and PAN-S3 also exhibit an increased presence of *Euryarchaeota* (1%-4%), *Firmicutes* (2%-3%), *Spirochaetae* (1%-3%), and *Zixibacteria* (0%-1%) relative to the other sediment samples.

IES045 exhibits consistency across samples as there is a high percent abundance of *Proteobacteria* (23%-46%) and *Bacteroidetes* (14%-29%). However, community trends are not consistent across the benthic communities. IES045-S1, IES045-S3, and IES045-S4 demonstrated the presence of *Actinobacteria* (1%-4%), *Cyanobacteria* (1%-4%), *Planctomycetes* (5%-8%), *Verrucomicrobia* (7%-15%), and unclassified bacteria (2%-5%). However, IES045-S1 includes a unique presence of *Chloroflexi* (3%), *Chlamydiae* (2%), and *Fibrobacteres* (1%). IES045-S3 and IES045-S4 exhibit a unique presence of FBP (0%-2%) and *Parcubacteria* (0%-1%). Alternatively, IES045-S2 is dominated by *Bacteroidetes* (29%), *Cyanobacteria* (36%), and *Proteobacteria* (23%).
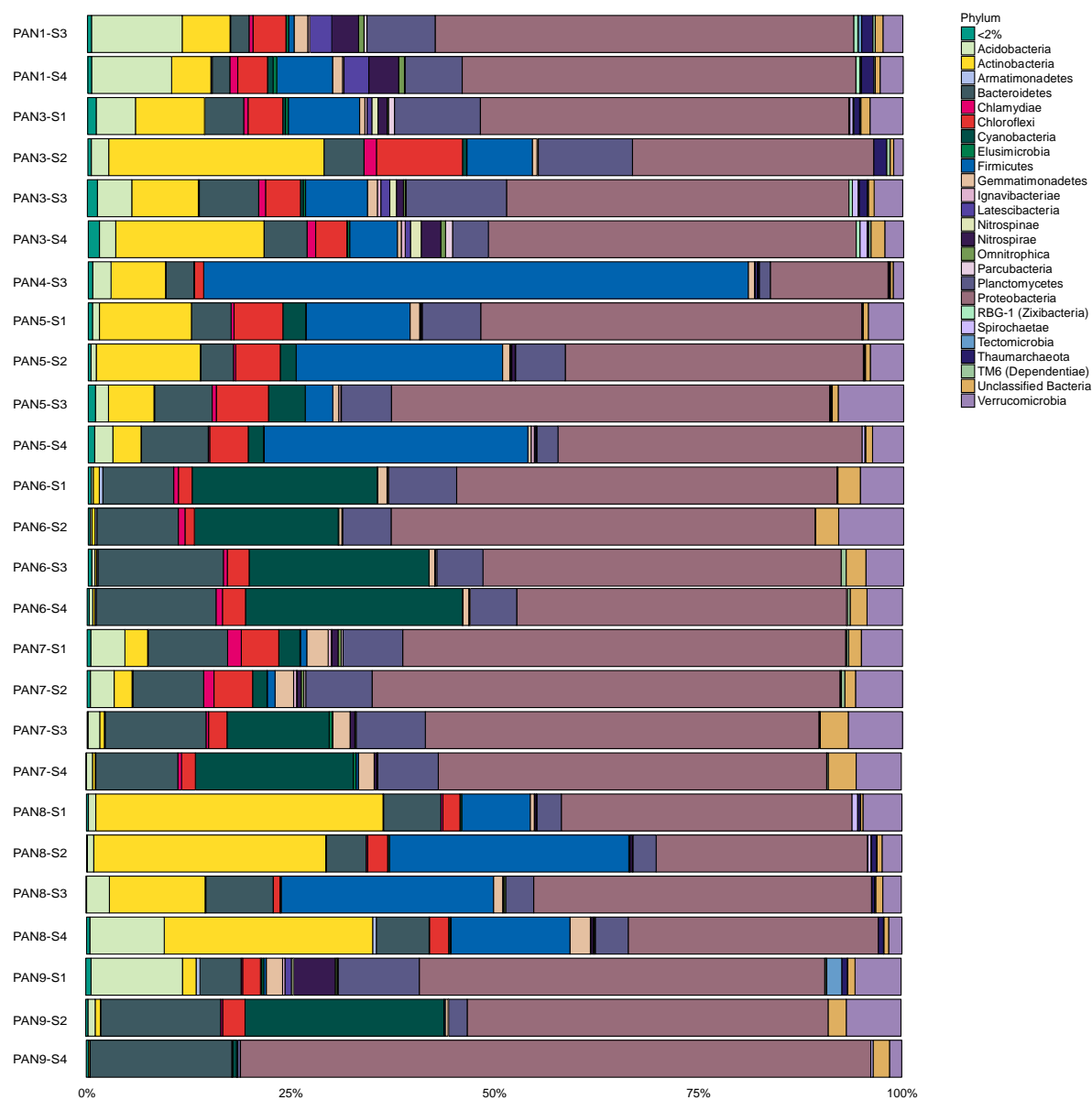
Figure 33. Percent abundance of microbial phyla present in sediment (S) samples of springs PAN1-PAN9
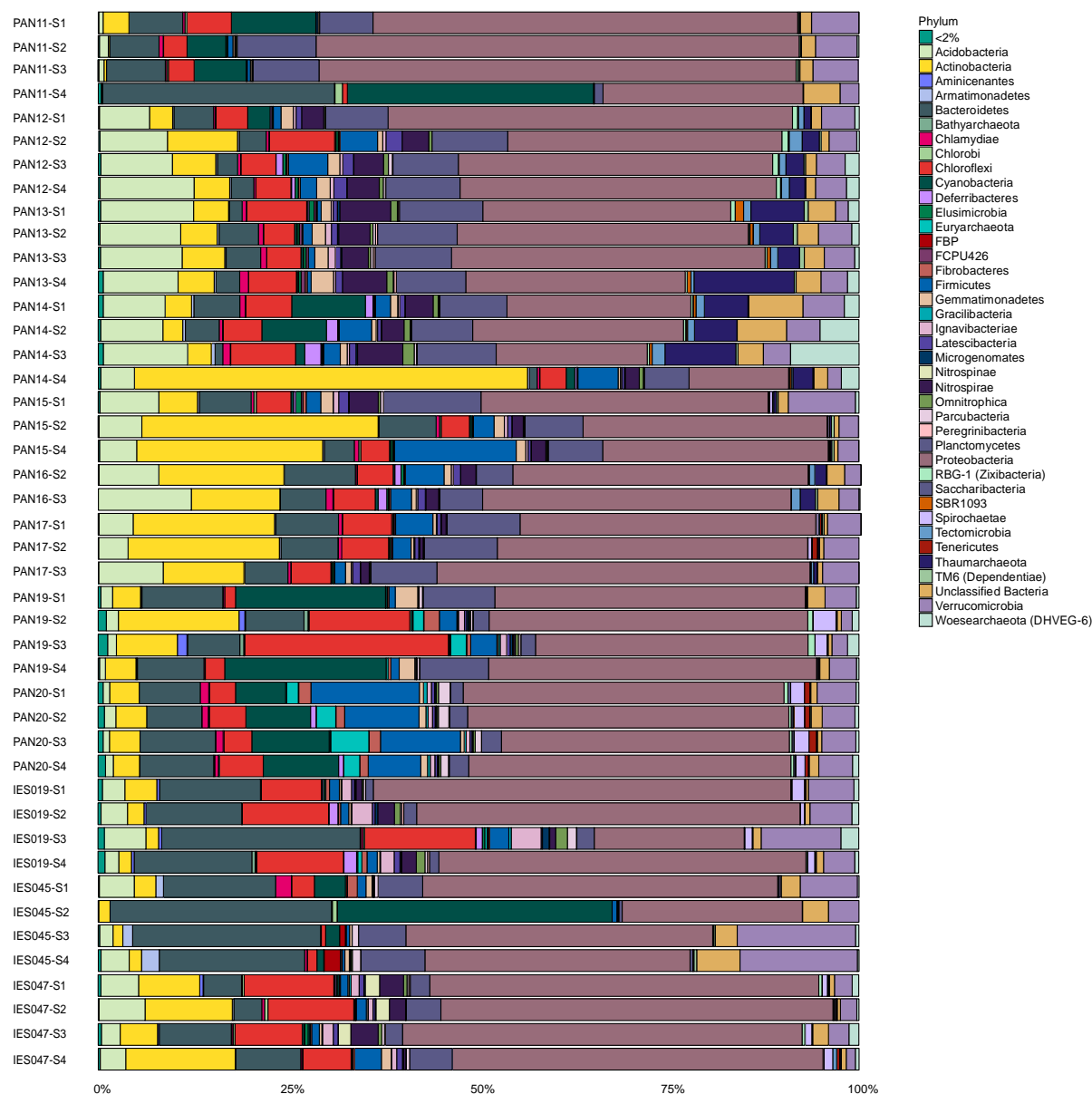
Figure 34. Percent abundance of microbial phyla present in sediment (S) samples of springs PAN11-PAN20, IES019, IES045, and IES047.

Environmental factors influencing microbial community structure

Non-metric multidimensional scaling (NMDS) was used to analyze correlations between hydrogeochemical parameters and microbial community structure for both planktonic and benthic communities. Microbial community structure in the filter and liquid samples are

significantly correlated to calcium carbonate, bicarbonate, elevation, temperature, chlorine, oxidation reduction potential, sodium, pH, dissolved oxygen, potassium, nitrate, and fluorine in the spring waters (r^2= 0.69, 0.69, 0.67, 0.56, 0.51, 0.49, 0.44, 0.33, 0.33, 0.31, 0.31, and 0.28 respectively; $P < 0.05$; Figure 35). Microbial communities in the sediment samples were structured statistically by sodium, chlorine, specific conductance, elevation, potassium, calcium carbonate, bicarbonate, oxidation reduction potential, strontium, hardness, temperature, nitrate, fluorine, calcium, sulfate, and pH in the spring waters (r^2= 0.79, 0.77, 0.56, 0.51, 0.50, 0.34, 0.34, 0.33, 0.28, 0.27, 0.26, 0.20, 0.19, 0.19, 0.16, and 0.16 respectively; $P < 0.05$; Figure 36).
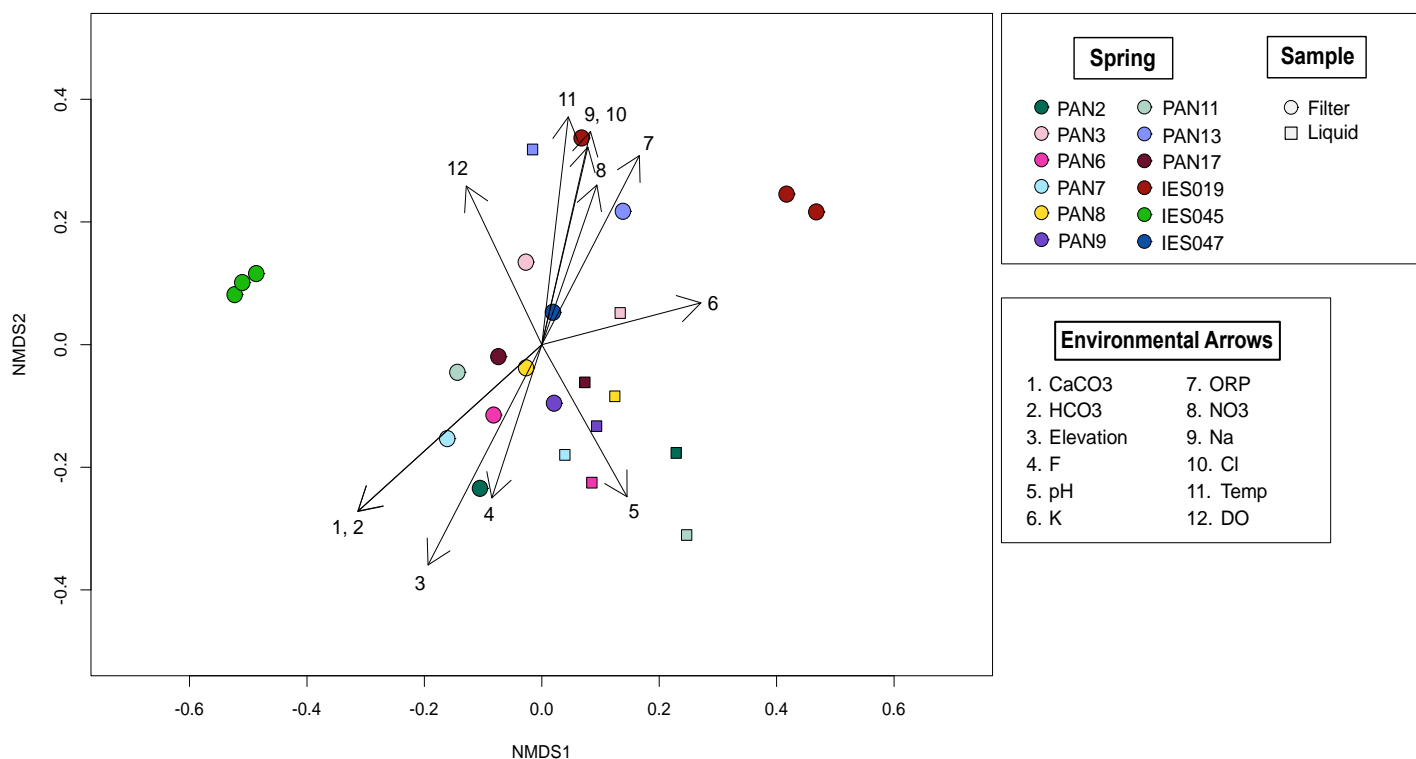
Figure 35. NMDS ordination of filter and liquid samples based on the Bray-Curtis dissimilarity of community composition (stress = 0.169).
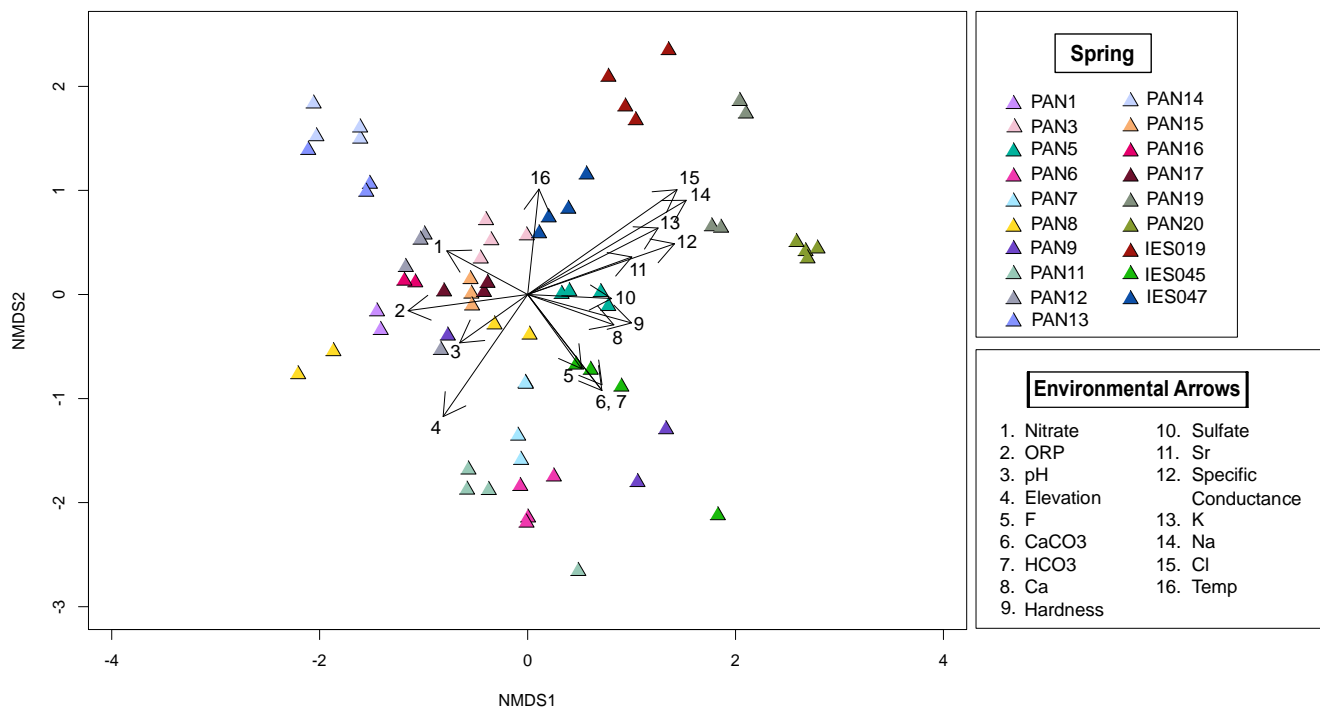
Figure 36. NMDS ordination of sediment samples based on the Bray-Curtis dissimilarity of community composition (stress = 0.177).

Conclusions

The characterization of groundwater dependent ecological communities reviewed in this study support the assertion that desert springs serve as biological oases for many macroscopic organisms and microbial communities. This study provides the first glimpse into BMI, bacterial, and archaeal diversity and community structure of desert springs in the Panamint Mountain Range and Death Valley, CA, as well as insight into which hydrogeochemical factors are related to shifts in their community structure. In both cases, despite being groups with very different biology, the community structures of the BMI and microbes sampled were dictated almost exclusively by TDS, elevation, and temperature.

Geochemical evolution increases relatively with increasing flowpath lengths and corresponding increases in temperature in these samples due to kinetic controls on solute dissolution within these aquifers. Longer flowpaths and residence times dictated by topography directly impact spring chemistry in this manner by increasing the amount of time that water is actively leaching geologic materials and appears to be creating diverging biologic communities as a result in this case.

BMI species at lower elevations (basin) showed a distribution of more tolerant organisms that were able to handle more chemically evolved spring waters with higher TDS, temperature, and pH values. Less tolerant species were found at high elevations, and are more sensitive to changes in groundwater sourcing (Zinger et al., 2011). The increases in Ca, CaCO3, and pH that shaped these elevation-dependent biologic communities also support the assertion that groundwater flow in the Panamint Range is reliant on the carbonate units within the mountain block. Microbial community consistency among filter and liquid samples also points to a consistent aquifer in the Panamint Range despite the wide variety of elevations in the springs sampled.

References

Auguet, J., E. Casamayor (2013). Partitioning of *Thaumarchaeota* populations along environmental gradients in high mountain lakes. *FEMS Microbiological Ecology*, 84, 154-164. doi: 10.1111/1574-6941.12047

Callahan, B., P. McMurdie, M. Rosen, A. Han, A. Johnson, & S. Holmes (2016). DADA2: High-resolution sample inference from Illumina amplicon data. *Nature Methods*, 13, 581-583.

Caporaso, J.G., J. Kuczynski, J. Sormbaugh, K. Bittinger, F. Bushman, E. Costello, … & R. Knight (2010). QIIME allows analysis of high-throughput community sequencing data. *Nature Methods*, 7, 355-366.

Clarke, K.R & R.N. Gorley (2006). Primer v6: User Manual/Tutorial.PRIMER-E Ltd. Publisher.

Hill, M.O., & H.G. Gauch Jr. (1980). Detrended correspondence analysis: an improved ordination technique. In: van der Maarel E. (eds) *Classification and Ordination. Advances in vegetation science*, vol 2. Springer, Dordrecht

Kamp G. (1995). The hydrogeology of springs in relation to the biodiversity of spring fauna: a review. *Journal of the Kansas Entomological Society*, 68, 4-17.

Katoh, K., & D. Standley (2013). MAFT multiple sequence alignment software version 7: improvements in performance and usability. *Molecular Biological Evolution*, 30, 772-780.

Kløve, B., P. Ala-aho, G. Bertand, Z. Boukalova, A. Erturk, N. Goldsheider, J. Ilmonenen, …& A. Winderlund (2011). Groundwater dependent ecosystems. Part I: Hydroecological status and trends. *Environmental Science & Policy*, 14, 770-781.

Kløve, B., P. Ala-aho, G. Bertand, J.J. Gurdak, H. Kupfersberger, J. Kvӗrner, ...& M. Pulido-Velazquez (2014). Climate change impacts on groundwater dependent ecosystems. *Journal of Hydrology,* 518, 250-266.

Lloyd-Prince, J., G. Abu-Ali, C. Huttenhower (2016). The heathy human microbiome. *Genome Medicine*, 8,1-11.

Ma, B., L. Forney, & J. Ravel (2012). The vaginal microbiome: rethinking health and diseases. *Annual Review of Microbiology*, 66, 371-389.

Madigan, M., J. Martinko, P. Dunlap, & D. Clark (2005). *Brock Biology of Microorganisms*, Benjamin Cummings, (11).

Mallory, M.L., P.J. Blancher, P.J. Weatherhead, & D.K. McNichol (1994). Presence or absence of fish as a cue to macroinvertebrate abundance in boreal wetlands. *Hydrobiologica*, 279/280, 345-351.

Mandaville, S.M. (2002). Benthic macroinvertebrates in freshwaters- taxa tolerance values, metrics and protocols. *Project H-1 Soil & Water Conservation Society of Metro Halifax*, http://chebucto.ns.ca/Science/SWCS/SWCS.html

McMurdie, P., and S. Holmes (2013). Phyloseq: and R package for reproducible interactive analysis and graphic of microbiome census data. PLoS One, 8, 1217.

Mermillond-Blondin, F., J-P. Gaudet, M. Gerino, G. Desrosier, & M. Creuze des Chatelliers (2003). Influence of macroinvertebrates on physio-chemical and microbial processes in hyporheic sediments. *Hydrological Processes*, 17, 779-794.

Minchin, P.R. (1987). An evaluation of the relative robustness of techniques for ecological ordination. *Vegetatio*, 69, 89-107.

Resh, V., D. Rosenberg, & A. Wiens (1983). Emergence of Cadddisflies (Trichoptera) from Eroding and Non-Eroding Shorelines of Southern Indian Lake, Manitoba, Canada. *The Canadian Entomologist, 115*(12), 1563-1572. doi:10.4039/Ent1151563-12

Rensburg, J., H. Lin, X. Gao, E. Toh, K. Fortney, S. Ellinger, … & S. Spinola (2015). The human skin microbiome associates with the outcome of and is influenced by bacterial infection. *mBio*, 6, 1-13.

Okanen, J., R. Kindt, P. Legendre, B. O'Hara, G. Simpson, P. Solymos, H. Wagner (2009). Community ecology package-VEGAN. *R package*, 2.2-1.

Probst, A., T. Weinmaier, K. Raymann, A. Perras, J. Emerson, T. Rattei, G. Wanner, A. Kling, … & C. Moissl-Eichinger (2014). Biology of a widespread uncultivated archaeon that contributes to carbon fixation in the subsurface. *Nature Communications*, 5, 1-13. doi: 10.1038/ncomms6497

Sada, D. W., & Lutz, A. D. (2016). Environmental characteristics of Great Basin and Mojave Desert spring systems. *Desert Research Institute, Division of Hydrologic Sciences*.

Sherr, E. & B. Sherr (1988). Roles of microbes in pelagic food webs: A revised concept. *Limnology and Oceanography*, 33(5), 1225-1227.

Springer, A., L. Stevens, D. Anderson, R. Parnell, D. Kreamer, L. Levin, & S. Flora (2008). A comprehensive springs classification system: Integrating geomorphic, hydrogeochemical, and ecological criteria. *Aridland springs in North America: ecology and conservation*, 49-75.

ter Braak, C.J.F. & P.F.M. Verdonschot (1995) Canonical correspondence analysis and related multivariate methods in aquatic ecology. *Aquatic Sciences*, 57: 255. doi:10.1007/BF00877430

Timpano, A.J., S.H. Schonholtz, C.E. Zipper, D.J. Soucek (2010). Isolating effects of total dissolved solids on aquatic life in central Appalachian coalfield streams. *Proceedings from the America Society of Mining and Reclamation*, 1284-1302.

Vinson, M. and C.W. Hawkins 1996. Effects of sampling area and subsampling procedures on comparison of taxa richness among streams. *Journal of the North American Benthological Society*, 15, 392-399.

Thomas, J.M., A.H. Welch, & M.D. Dettinger (1996). Geochemistry and isotope hydrology of representative aquifers in the Great Basin region of Nevada, Utah, and adjacent states. U.S. Geological Survey Professional Paper 1409-C.

Wickman, H. (2009). Ggplot2: elegant graphics for data analysis. *Springer*: New York.

Zinger, L., A. Gobet, & T. Pommiers (2011). Two decades of describing the unseen majority of aquatic microbial diversity. *Molecular Ecology*, 21, 1878-1896. doi:10.1111/j.1365-294X.2011.05362.x

CONCLUSIONS AND FUTURE WORK

In this thesis, a conceptual model for hydrologic flow within the Panamint Range was proposed based on geochemical analyses. This model is a heterogeneous topography-driven groundwater flow model through the mountain block of the Panamint Range, although it may be intercepted by faulting in Lower Warm Spring Canyon and along the mountain front. The first chapter identified the source of mountain block recharge among these springs as spring snowmelts with some rain influence. Springs in the basins, however, are likely receiving mountain system recharge that sources water from flow through the mountain block, as well as alluvial storage and allows for exchange in the basin with basin brines.

The second chapter highlighted the importance of the dolomite units in the Panamint Range because distinctive gypsum-driven dedolomitization trends in the geochemistry indicate preferential flow through dolomitic units. Several groundwater residence times within the mountain block were also determined using a multi-tracer approach and range between 67 and1800 years. These relatively young residence times suggest that flow to the Panamint Range mountain block springs may accordingly be sensitive to climate change that may reduce the snowpack because they are not supported by any other sources of recharge or exchange. Finally, a flow continuum between Hanaupah Canyon and Tule Spring was identified using the strontium analyses from the Hanaupah Spring complex to Tule Spring in the basin.

The final chapter was a collaborative chapter characterizing the ecological communities supported by spring flow in the Panamint Range. This includes both microbial and benthic macroinvertebrate analyses and shows that community structure in this region is dictated primarily by kinetic geochemical evolution. There was also little overall variance in community structure within the mountain block, further supporting similar flow conditions to the majority of the springs sampled.

Future work on the springs in the Panamint Range should include the sampling of the remaining spring emergences that were not reached in this study. The rough terrain on the Panamint range has greatly limited the amount of work done in this mountain block flow system in the past, but there is still much to characterize within these mountains. Precipitation data and snowpack estimations are also substantial data gaps and a greater time series of stable isotope data across the range and estimations of precipitation quantities would improve flow modeling in these springs dramatically. Further investigation into the Hanaupah Canyon Fault and its impact on groundwater flow would likewise improve interpretations on the difference in springs surrounding this canyon relative to the larger Panamint Range spring dataset. Finally, further work on estimating the impact that brines have on the basin springs in the Panamint Range would also greatly improve groundwater modeling and residence time estimates for these cases receiving multiple sources of water along the mountain front.

In conclusion, the Panamint Range represents a geologically complex region in the United States with a heterogeneous topography-driven groundwater flow model. This system supports freshwater springs which in turn support diverse life that respond to the geochemistry provided by this groundwater flow. This system depends on seasonal snowpack to fuel groundwater flow through the mountain block and the rate of turnover for the majority of these waters ranges between 67 and 1800 years with some exceptions. For this reason, climate change leaves this system especially vulnerable to dramatic changes in groundwater flow and mandates the continuation of careful landscape conservation in the area if these spring ecosystems are to be preserved.

APPENDIX A

This Appendix displays all of the stable isotope data referenced in this study from published and unpublished sources. All sources are referenced by origin and application.

Owens Valley LMWL				
Location	δ ^{2}H	δ ^{18}O	Sampling Period	Corresponding Citation
Lone Pine	-89	-12	October 1985	Friedman et al. 1992
Lone Pine	-60	-7	April 1986	Friedman et al. 1992
Lone Pine	-119	-16	October 1986	Friedman et al. 1992
Lone Pine	-30	-3	April 1987	Friedman et al. 1992
Inyokern	-106	-14	October 1986	Friedman et al. 1992
Inyokern	-37	-3	April 1987	Friedman et al. 1992
Bishop	-27	-4	Summer 1991	Friedman 2002
Bishop	-107	-14	Winter 1992	Friedman 2002
Bishop	-108	-13	Winter 1993	Friedman 2002
Bishop	-109	-15	Winter 1994	Friedman 2002

Death Valley LMWL, Friedman 2002				
	Dantes View		Furnace Creek	
Sampling Period	δ ^{2}H	δ ^{18}O	δ ^{2}H	δ ^{18}O
Summer 1991	-40	-5.7	-18	0
Winter 1991	-103	-14.5	-75	-10
Summer 1992	-68	-8.2	-69	-8
Winter 1992	-97	-13.7	-71	-9
Winter 1994	-108	-14.1	-51	-4

Spring Mountains LMWL, Ingraham et al. (1991)	
δ 2H	δ ^{18}O
-116	-16
-103	-14
-89	-12
-75	-10
-61	-8
-48	-6
-34	-4
-20	-2

Full Citations

Friedman, I., G.I. Smith, J.D. Gleason, A. Wardern, & J.M. Harris (1992). Stable Isotope Composition of Waters in Southeastern California 1. Modern Precipitation. *Journal of Geophysical Research*, 97(D5), 5795-5812.

Friedman, I., G.I. Smith, C.A. Johnson, & R.J. Moscati (2002). Stable isotope compositions of waters in the Great Basin, United States 2. Modern precipitation. *Journal of Geophysical Research*, 107(D19), 4401. https://doi.org/10.1029/2001JD000566

Ingraham, N.L., B.F. Lyles, R.L. Jacobson, & J.W. Hess (1991). Stable isotopic study of precipitation and spring discharge in southern Nevada. *Journal of Hydrology*, 125, 243-258.

IES Project Data (unpublished); Spring Mountain Springs

Sampling Date	δ^2H	$\delta^{18}O$	Spring name
Mar-16	-87	-12	Mountain Spring
Mar-16	-88	-12	Potosi/BSA Spring
Mar-16	-93	-13	Cave Spring
Mar-16	-93	-13	Kiup Spring
Mar-16	-95	-13	Horse Spring
Mar-16	-99	-14	Buck Spring
Mar-16	-92	-13	Grapevine/Nye Spring
Mar-16	-92	-13	Grapevine Spring 2
Dec-16	-88	-12	Potosi/BSA Spring
Dec-16	-94	-13	Kiup Spring
Mar-17	-88	-12	Potosi Spring
Mar-17	-94	-13	Cave Spring
Mar-17	-94	-13	Kiup Spring
Mar-17	-97	-14	Buck Spring
Mar-17	-92	-13	Grapevine Spring

IES Project Data (unpublished); Sierra Nevada Springs

Sampling Date	δ^2H	$\delta^{18}O$	Spring name
Mar-16	-120	-16	Lubkin Canyon Spring 1
Mar-16	-124	-17	Indian Spring (Lone Pine)
Mar-16	-121	-16	Lone Pine Creek Complex
Mar-16	-123	-17	Hogback Creek A.
Mar-16	-127	-17	Boron Spring B
Mar-16	-117	-15	Reinhackle Spring
Mar-16	-123	-17	Boron Spring A
Mar-16	-117	-16	Grover Anton Spring
Mar-16	-124	-17	Red Mountain Spring
Mar-16	-125	-16	Big Pine Spring
Mar-16	-132	-18	Sharps Meadow
Mar-16	-131	-18	Elderberry Canyon Spring
Mar-16	-117	-15	Birchim Spring B
May-16	-134	-18	Wells Meadow A
May-16	-132	-18	Wells Meadow B
May-16	-132	-18	Unnamed Pine Creek Spring
May-16	-126	-17	McMurray Meadow Spring A
May-16	-127	-17	North Fuller Spring A
May-16	-119	-16	North Harry Birch Spring
May-16	-120	-16	South Harry Birch Spring
Dec-16	-130	-17	Elderberry Canyon Spring
Mar-17	-121	-16	Lubken Canyon Spring 1
Mar-17	-122	-16	Hogback Ck. A
Mar-17	-115	-14	Reinhackle Spring
Mar-17	-124	-16	Boron Spring A
Mar-17	-115	-16	Grover Anton Spring
Mar-17	-123	-17	Red Mountain Spring
Mar-17	-129	-18	Elderberry Canyon Spring
Mar-17	-117	-15	Birchim Spring B
Mar-17	-132	-18	Wells Meadow B
Mar-17	-117	-16	North Harry Birch
Mar-17	-120	-16	South Harry Birch

APPENDIX B

General geochemistry of all springs sampled

Spring Name	Date	ID	Elevation (m)	Specific Conductance (mS/cm)	pH	Temperature (°C)	TDS (ppm)	ORP (mV)	DO (mg/L)	DO (%)
Jail Spring	5/24/2017	PAN 1	2434	226.9	7.98	9	147.9	157.1	9	78.4
Thorndike Spring	5/25/2017	PAN 2	2337	382.1	7.66	9.8	247.65	-63.1	4.93	43.2
Unnamed Panamint Spring E	5/26/2017	PAN 3	963	970	8.31	18.8	650.5	-10.1	7.14	78.4
Unnamed Panamint Spring F	5/26/2017	PAN 4	803			19.4				
Wheel Spring	5/26/2017	PAN 5	748	777	8.3	22.6	507	-11.9	7.64	91.2
High Noon Spring	5/27/2017	PAN 6	1419	2234	7.94	17.3	1449	45.4	6.06	64
Apron Spring	5/27/2017	PAN 7	1606	2743	8.11	17.7	1781	24.1	8.07	87
Main Hanaupah Spring #2	5/28/2017	PAN 8	1265	265.4	8.54	15.1	172.9	18.5	9.08	90
Main Hanaupah Spring #1	5/28/2017	PAN 9	1258	406.5	8.46	20.5	263.9	41.6	6.1	71.4
Hanaupah Canyon	5/28/2017	PAN 10	1184	301.7	8.27	16.1	196.3	29	8.84	89.9
South Hanaupah Spring #3	5/28/2017	PAN 11	1154	708	7.99	16.1	461.5	25	7.8	79.3
Wilson Spring	5/29/2017	PAN 12	1195	943	8.34	20.4	617.5	172.5	7.84	91.6
Lower Warm Spring A	5/30/2017	PAN 13	755	654	7.64	34.4	422.5	-11.5	4.58	65
Lower Warm Spring B	5/30/2017	PAN 14	760	667	7.82	34.3	429	74.6	4.48	63.5
Uppermost Spring	5/31/2017	PAN 15	1633	796	8.45	16.5	455	109.1	7.59	77.8
Limekiln Spring	6/1/2017	PAN 16	1223	765	8.13	19.4	494	53.08	8.01	92.4
Unnamed Panamint Spring C	6/1/2017	PAN 17	1206	747	7.99	16.5	475	22.8	4.88	50.2
Surprise Canyon	6/1/2017	PAN 18	818	793	8.6	21.6	513.5	-1.4	8.35	95
Warm Sulfur Spring	6/1/2017	PAN 19	318	3791	7.86	32	2463.5	14.5	4.17	58.2
Post Office Spring	6/2/2017	PAN 20	321	8922	7.72	18.7	5798	-107.5	2.8	32.1
Poplar Spring	3/13/2017	IES-047	1225	1070	7.4	17.7	695.5	15.9	0.39	4.7
Tule Spring	3/14/2017	IES-019	-77	3181	7.35	27.4	2073.5	33.3	1.1	12
Upper Emigrant Spring	5/19/2016	IES-045	1231	931	7.13	19.8	604.5	39.9	52.8	4.75

Note: all concentrations shown in mg/L

| Spring Name | Date | ID | Cations and [Detection Limit]. | | | | | | Anions and [Detection Limit]. | | | | | | Alkalinity | Bicarbonate | |
| | | | Ca2+ | Fe2+ | Mg2+ | K+ | Na+ | Sr2+ | Br- | Cl- | F- | NO3- | PO43- | SO42- | CaCO3 | HCO3- | Si |
			[0.05]	[0.02]	[0.05]	[0.05]	[0.05]	[0.005]	[0.1]	[1.0]	[0.1]	[0.1]	[0.5]	[1.0]	[5]	[5]	[0.05]
Jail Spring	5/24/2017	PAN 1	59.9		5.66	2.42	9.24	0.173	0	3.28				67	130	158	16.1
Thorndike Spring	5/25/2017	PAN 2	62.8	0.051	3.88	2.61	14.4	0.279	0	7.44		0.16		8.28	190	231	13.1
Unnamed Panamint Spring E	5/26/2017	PAN 3	146		41.1	5.62	35.1	0.811	0.2	30.9	0.19			347	211	258	28.5
Unnamed Panamint Spring F	5/26/2017	PAN 4	125		41.7	5.78	35.6	0.8	0.19	32.5	0.14			352	156	191	26.2
Wheel Spring	5/26/2017	PAN 5	27.2	0.312	58.9	3.7	36.3	0.561	0.24	53.9	3.38			168	137	167	14.3
High Noon Spring	5/27/2017	PAN 6	352		136	8.63	39.7	3	0	21.5	2.1			1180	216	263	35.2
Apron Spring	5/27/2017	PAN 7	359		232	9	33.9	1.44	0	18.3	2.83			1510	286	349	38.8
Main Hanaupah Spring #2	5/28/2017	PAN 8	35.4		11.1	1.44	4.42	0.108	0	1.63	0.28	0.27		28.8	110	134	16.8
Main Hanaupah Spring #1	5/28/2017	PAN 9	51.9		10.4	1.76	19.4	0.219	0	6.95	1.67	0.3		49.2	156	191	27.4
Hanaupah Canyon	5/28/2017	PAN 10	37.3		12.1	1.27	6.23	0.145	0	1.87	0.68	0.48		32.8	128	156	19.7
South Hanaupah Spring #3	5/28/2017	PAN 11	95.6		28.9	3.18	15.4	0.517	0	6.7	0.8	1.82		137	247	302	37.2
Wilson Spring	5/29/2017	PAN 12	91.1		67.9	2.59	16.1	1.06	0	11.7	0.24	0.12		282	222	271	20.6
Lower Warm Spring A	5/30/2017	PAN 13	64		21.4	3.21	33.5	0.81	0.13	25.9	0.55	2.54		179	107	130	34.2
Lower Warm Spring B	5/30/2017	PAN 14	64.2		21.6	3.26	33.9	0.806	0.11	25.8	0.54	3.53		177	105	128	32.8
Uppermost Spring	5/31/2017	PAN 15	40.2	0.02	72.6	2.85	23	1.85		12.9		1.58	2	41	397	485	32.7
Limekiln Spring	6/1/2017	PAN 16	89.4		40.5	3.9	11.6	0.46		8.35	0.97	0.45		214	184	224	21.3
Unnamed Panamint Spring C	6/1/2017	PAN 17	92.9		39.9	3.84	11.3	0.451		7.57	1.19			204	210	257	20.7
Surprise Canyon	6/1/2017	PAN 18	84.9		45.9	5.22	14	0.507		9.39	1.24			250	164	191	21
Warm Sulfur Spring	6/1/2017	PAN 19	85		45.8	28.4	575	0.862	1.27	873	1.87			354	147	179	27
Post Office Spring	6/2/2017	PAN 20	720		202	59.9	1170	8.78	2.21	1520	0.86			2420	440	537	34.7
Poplar Spring	3/13/2017	IES-047	190	0.829	58.6	9.21	58.3	1.68	0.17	23.9	0.89			503	267	326	32.2
Tule Spring	3/14/2017	IES-019	105		68.3	9.42	487	2.23	0.144	998				143	89	109	27.5
Upper Emigrant Spring	5/19/2016	IES-045	77.4		58.4	1.07	50.3	0.889		38.8	0.38	0.31		108	356	435	23.1